AtkinsRéalis

TECHNICAL JOURNAL

Engineering a better future for our planet and its people

Volume 6 | Issue 1 | 2024

Special Section: Global Technology Centre's transportation capabilities

CHRIS HENDY

Editor-in-Chief
AtkinsRéalis
Technical Journal

AtkinsRéalis Fellow,
Professional Head of
Bridge Engineering
and Transportation
Technical Director

BHARAT GALA

CEO, Global Technology
Centre (GTC)

Foreword

Welcome to the latest edition of our AtkinsRéalis Technical Journal, established to showcase the fantastic depth and breadth of our expertise and excellence across a wide range of disciplines. This edition features some of the work we have been doing in structural engineering, nuclear engineering and water and environment, and has a special feature on the work of our colleagues in our Global Technology Centre (GTC) within the transportation sector.

In improving societal health, safety and well-being, we have studied the health effects and nuisance caused by railway noise and proposed possible mitigations. We have carried out hydrologic and hydraulic design of a flood gate closure structure to prevent flooding of the western part of the City of Lumberton during extreme storms. And we have carried out design and testing within the nuclear sector to verify that precisely placed refractory components within Low Activity Waste (LAW) Melters will not shift during transport.

In reducing carbon in our designs and improving the resilience of new assets, we have proposed a methodology for design using basalt reinforcing bars in concrete, rather than conventional steel reinforcement, and demonstrated that there are often carbon reduction benefits. We have designed the first UK Level Crossings using Overlay Axle counters, providing increased economy and improved service performance over existing traditional practice using directional treadles and track circuits. And we have made proposals for further improvements in travel demand forecasting practice, focusing on the Absolute Model Applied Incrementally (AMAI) approach and the UK's Transport Appraisal Guidance (TAG).

In extending the life of existing assets, we have led research and development aimed at eliminating unplanned closures of bridges and vastly reducing maintenance and strengthening costs by developing new technologies to determine much-improved condition data without the need for intrusive investigations. We have also used non-linear structural analysis to demonstrate that a historic steel and wrought iron railway bridge was safe to remain in service without restrictions to current train operations.

The above examples provide only a glimpse into the wealth of innovation that AtkinsRéalis creates day to day and we hope you enjoy the selection of technical papers included in this edition as much as we have enjoyed compiling them.

Editor-in-chief

Chris Hendy
FREng MA (Cantab)
CEng FICE Eur Ing
Technical Director; Fellow;
Professional Head of Bridge Engineering
UK – Transportation UK
Epsom, UK

Production Team

Dorothy Gartner
MLIS
Sr Librarian
Office of the COO, Group Quality & Knowledge Management
Montreal, Canada

Samantha Morley
CAPM
Project Controls Analyst I
US – Operational Services
Omaha, NE, USA

Cheryl Law
MEng CEng MICE
Associate Director
UK – Infrastructure UK
Epsom, UK

About the Cover

Upgrade of the Belaugh Lane Level Crossing, Norfolk, UK.
A first-ever UK level crossing with an axle counter overlay system.

2024 Editorial Board Members

Ramy Azar
PhD Eng.
VP, Engineering & Chief Technology Officer – Power Grids; Fellow
Canada – Power & Renewables
Montreal, Canada

Vinod Batta
PhD P.Eng.
VP, Market Lead, Power & Renewables; Fellow
Canada – Power & Renewables
Vancouver, Canada

Donna Huey
GISP
SVP, Chief Digital Officer; Fellow
US – Business Development, Digital
Orlando, FL, USA

Mufeed Odeh
PhD PE
Sr Engineer IV
US – TPO Water Engineering
Raleigh, NC, USA

Jill Hayden
PhD FIET
Technical Director; Fellow (Intelligent Mobility & Smart Technologies)
UK – Transportation UK
Manchester, UK

Tracey Radford
BSc MSc CGeol FGS
Practice Manager, Geotech Network Chair
UK – Infrastructure UK & Ireland
Epsom, UK

Dr. Santhosh Kumar M (Outgoing)
PhD CEng MIET
Technical Director, GDC and Atkins Fellow of Digital
Office of the COO – Global Technology Center
Bangalore, India

Roger Cruickshank
BEng
Regional Market Director – Transportation; Fellow
AMEA – Middle-East – Transportation
Dubai, UAE

Kan Pang
BEng CEng
Director – Highways, Transportation & Infrastructure
AMEA – Asia – Transportation & Water
Hong Kong, China

Samuel Fradd
Technology Manager
UK – Transportation UK
Epsom, UK

Contents

Structural Engineering

01: Basalt FRP as Embedded Reinforcement and its Embodied Carbon Comparison Against Steel RC 9

02: Advancements in Bridges Non-Destructive Testing: National Highways' "Structures Moonshot" 43

Water and Environment

03: Nuisance and Health Impacts of Railway Noise 79

04: Hydrologic and Hydraulic Design of the West Lumberton Flood Gate, Lumberton, NC 105

Nuclear Engineering

05: Safe Transportation of LAW Melter in Support of Hanford Cleanup 139

Feature Section on the Global Technology Centre (GTC)

Transportation

06: Principles of Absolute Model Applied Incrementally (AMAI) in Travel Demand Forecasting 153

07: Overlay Axle Counter Automatic Half Barrier Crossing 173

08: Assessment of River Mersey Steel Truss Bridge Using Non-Linear Finite Element Analysis 193

Chandan Gowda
Engineer
Transporation UK
Epsom, UK

Chris Hendy
Technical Director
Transportation UK
Epsom, UK

Structural Engineering

01: Basalt FRP as Embedded Reinforcement and its Embodied Carbon Comparison Against Steel RC

Abstract

The urgent need to limit global temperature rise to well below 2.0˚C above pre-industrial levels (UNFCC, 2015), and the need to reduce the greenhouse Gas (GHG) emissions especially from manufacturing and construction industry, calls for immediate actions. One of the steps to achieve this involves introducing new sustainable materials in construction. The current work explores the performance of basalt fibre reinforced polymer (BFRP) as internal reinforcement for concrete beams and compares its performance against conventional steel reinforced beams. Basalt is an emerging sustainable material with low embodied carbon. It has advantages over other fibre reinforced polymers, such as carbon, glass and aramid, and also over steel as it is a natural material. The performance is assessed in terms of: serviceability limit state (SLS) - crack width and deflection; ultimate limit state (ULS) - moment of resistance and shear resistance; embodied carbon dioxide emissions and manufacturing cost.

Based on the investigation described in this paper, a BFRP reinforced concrete beam results in considerable savings in embodied carbon emissions compared to a steel reinforced concrete beam with given performance requirements. However, the cost of BFRP reinforced beams is currently higher than that for ordinary carbon steel but is lower than that for stainless steel where durability is the key design criterion.

KEYWORDS

Basalt FRP; Sustainable Construction; Embodied carbon emissions

LIST OF NOTATIONS

f_{ftd}	design tensile strength of FRP reinforcement
γ_{FRP}	partial factor for FRP reinforcing material
$f_{ftk,100a}$	long-term tensile strength of FRP reinforcement
C_t	long term strength reduction factor for environmental conditions
C_c	long term strength reduction factor to account for temperature
C_e	long term strength reduction factor for creep
f_{tk0}	tensile strength of FRP reinforcement at the rupture strain ε_{ftk0}
$\tau_{Rdc,min}$	minimum shear stress resistance allowing to avoid a detailed verification for shear (average shear stress over a cross section)
γc	partial factor for concrete
f_{ck}	characteristic concrete cylinder compressive strength
E_{fR}	design value of modulus of elasticity of FRP-reinforcement
d_{dg}	size parameter describing the crack and the failure zone roughness taking account of concrete type and its aggregate properties
E_s	design value of modulus of elasticity of ordinary reinforcing steel
D	effective depth of cross section
$\tau_{Rd,sy}$	shear resistance of steel RC beam
ρ_w	steel shear reinforcement ratio
f_{ywd}	design yield strength of shear reinforcement
$\tau_{Rd,f}$	shear resistance of a member with FRP reinforcement
$\tau_{Rd,c}$	shear resistance of a member without shear reinforcement
f_{fwRd}	design tensile strength of FRP shear reinforcement
f_{cd}	design value of concrete compressive strength
ρ_l	longitudinal reinforcement ratio
γ_v	partial factor for shear and punching resistance without shear reinforcement
φ	diameter of the reinforcement

1. Introduction

The manufacturing and construction industry is responsible for 12.7% of total GHG emissions in 2019 (Ritchie, Roser and Rosado, 2020). The buildings and construction sector contributed to 39% of total energy and process related CO_2 emissions in 2018 (International Energy Agency. and Global Alliance for Buildings and Construction., 2019), 11% resulting from manufacturing building materials and products. The emissions based on individual sector is presented in Figure 1a. The requirement to limit greenhouse gas (GHG) emissions and to limit the temperature increment below 2.0˚C (UNFCC, 2015) calls for the civil engineering community to take immediate action towards sustainable solutions. Hence, it is vital for the construction sector to concentrate towards sustainable development.

FIGURE 1

(a) GHG emissions

- All sectors

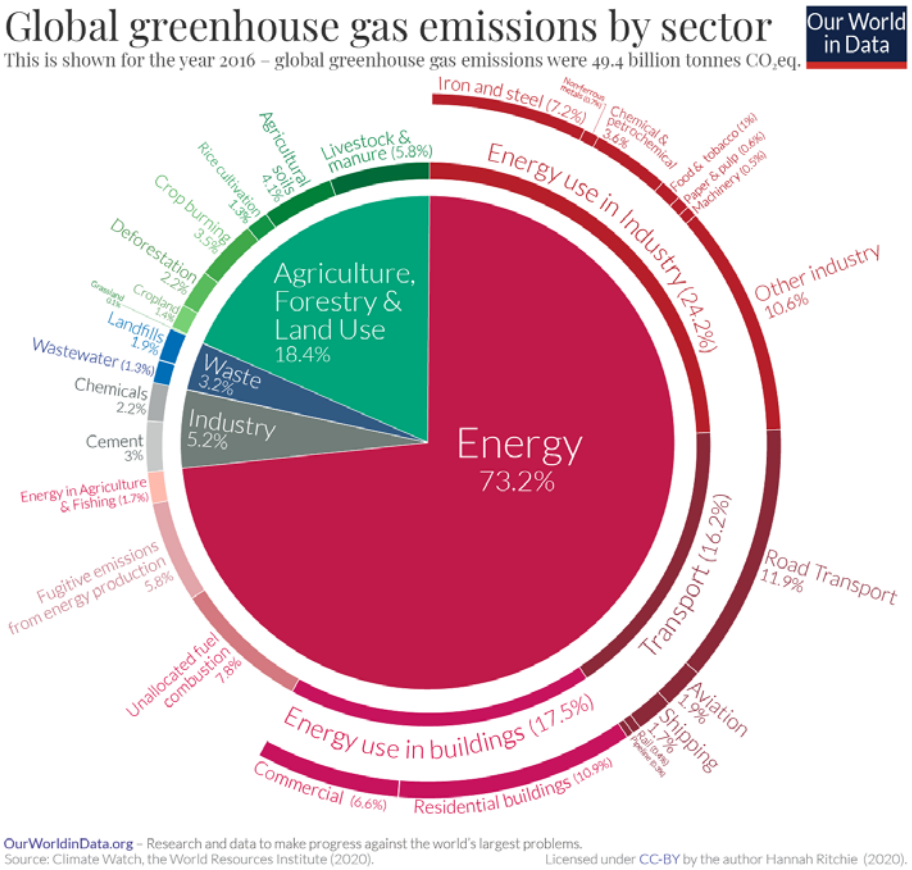

FIGURE 1

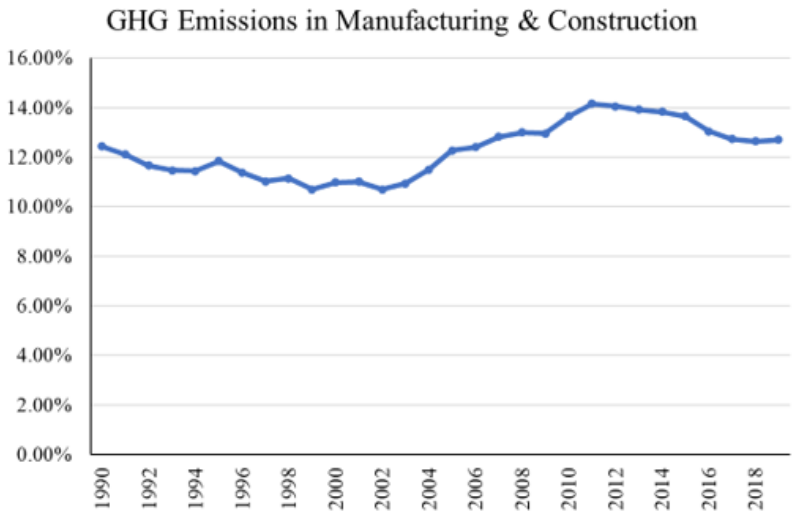

(b) GHG emissions - Manufacturing & construction, (Ritchie, Roser and Rosado, 2020)

The application of fibre reinforced polymers (FRP) like carbon, glass and aramid to strengthening of concrete structures has risen in the past decade. FRPs have many advantages over conventional materials, such as high strength, high stiffness and resistance to corrosion and chemical attack. These FRPs are man-made and there is a need for naturally sustainable materials to curb the emissions. One such sustainable material is basalt, which is a volcanic material fitting into the FRP family. Hence the current investigation explores this application and its performance against conventional steel reinforced concrete beams. The typical stress-strain diagrams of FRP materials are presented in Figure 2, including basalt, with steel shown for comparison.

FIGURE 2

Uni-axial stress-strain diagram for steel and fibre reinforced polymers

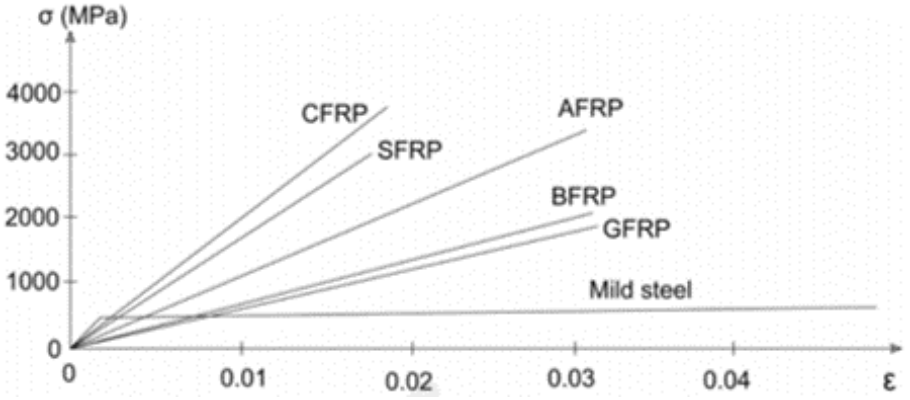

Steel reinforced concrete bridges often deteriorate because of direct exposure to harsh environmental conditions such as freeze-thaw cycles, wet-dry cycles, de-icing chemicals, and traffic loads all of which result in corrosion of steel reinforcement. Due to their non-corroding nature, FRP reinforcing bars help improve the durability of bridge decks and reduce maintenance and repair costs.

Basalt fibre has higher or comparable modulus of elasticity and tensile strength with glass fibre. In addition to good mechanical properties, basalt has a high chemical and thermal stability, good thermal insulation, electrical and sound properties (Technobasalt, 2004). The thermal insulation is three times greater than asbestos. Due to these good insulating properties, it can be used for fire protection. Furthermore, basalt has ten times better electrical characteristic insulation than glass fibres. It also has better chemical resistance, particularly in alkaline environment (Urbanski, Lapko and Garbacz, 2013). BFRP bars are an alternative to conventional steel reinforced concrete members in corrosive environments.

2. Literature Review

2.1 LITERATURE

The experimental performance of basalt FRP as internal reinforcement for transportation infrastructure was explored in Patnaik, (2009). Moment resistances were found to be in very good agreement with the analytical prediction according to ACI440.1R-06, (2006) with a ductile behaviour. Banibayat & Patnaik, (2015) carried out tests on basalt FRP bars by applying sustained loads in alkaline solution at an elevated temperature to accelerate and understand the long-term creep behaviour. The creep coefficients were determined to be 18% for 50-year service life and 28% for 5-year service life, and the one-million-hour creep coefficient was estimated to be 13%.

Patnaik & Banibayat, (2012) investigated the mechanical properties of BFRP bars to check if they are suitable for reinforced concrete applications. The tests confirmed high average tensile strength, acceptable rupture strain and average elasticity comparable with glass FRP bars. Serbescu et al., (2014) explored performance of basalt FRP bars for 1000 hours in different alkaline environments (pH7, pH9 and pH13) and multiple temperatures (20˚C, 40˚C and 60˚C) to understand the long-term durability performance. Temperature was found to be the parameter most affecting the degradation process and the lowest strength retention of 69% was observed for bars in pH solution at 60˚C for 5000 hours. Similar investigation on mechanical properties was also carried out in Elgabbas et al., (2013) and Elgabbas et al., (2015).

Urbanski et al., (2013) and Lapko & Urbański, (2015) performed experimental tests with basalt as internal reinforcement and a hybrid combination of basalt and steel reinforcements, to study the effect of reinforcement ratio on flexural behaviour. Beams with only BFRP had better performance with high reinforcement ratios. The hybrid combination had reduced deflection, reduced crack widths and increased load carrying capacity (10%). The results were validated by theoretical calculations and also involved application of digital image correlation (DIC) to better understand the cracking process of BFRP reinforced beams.

Bond durability of basalt FRP bars embedded in normal and aggressive environments is investigated in Hassan et al., (2016), Vincent et al., (2013) and Mehany et al., (2022). Ribbed BFRP bars in flexural behaviour of concrete beams is explored in Elgabbas et al., (2017) and experimental testing of concrete bridge deck slabs under concentrated loads is investigated in Elgabbas et al., (2016).

2.2 PROPERTIES AND DESIGN STANDARDS

Table 1 shows the comparison of properties of basalt and steel. The tensile strength of basalt is almost 3 – 3.5 times higher than the yield strength of steel and the ultimate strain is almost 10 times lower. The modulus of elasticity is one third of steel E_s resulting in higher deflection and crack width, and the thermal coefficient is two thirds of steel, meaning the expansion or contraction of basalt due to temperature variation is low.

TABLE 1

Mechanical properties of basalt and steel

Property	Steel	Basalt FRP	Units
Density	7500	2800	kg/m^3
Tensile strength, f	450 – 550 (f_{sy})	1600 – 1750 (f_u)	MPa
Modulus of elasticity, E	200	60 – 75	GPa
Ultimate strain, ε_u	0.200	0.025 – 0.028	-
Thermal coefficient, α	12 X 10^{-6}	8 X 10^{-6}	/°C
Electrical resistivity, K	10^{-7}	10^3 - 10^6	Ωm

f_{sy} = yield strength, f_u = ultimate strength

Standard codes are not available for design nor for the strengthening of reinforced concrete elements with basalt. ACI440.1R-06 (Guide for the Design and construction of structural concrete reinforced with FRP bars, American Concrete Institute) and CAN/CSA C806-12 (Design and construction of building structures with fibre reinforced polymers, January 2012) are few of the first codes to develop design guidelines for carbon and glass FRPs. fib bulletin 14 (Externally bonded FRP reinforcement for RC structures, July 2011) and fib bulletin 40 (FRP reinforcement in RC structures, September 2007) provide design guidelines for carbon as well as glass FRPs. More recently fib has also published fib bulletin 90 on externally applied FRP reinforcement for concrete structures (May 2019). The new Eurocode 2, EN 1992-1-1 (2023) includes Annex J for strengthening of existing concrete structures with CFRP, and Annex R for design as embedded FRP reinforcement with carbon and glass FRP. As the mechanical properties and the durability of basalt is very similar to glass, existing standards for glass FRP can be used.

3. Material and Geometric Properties

The investigation in this paper involves three beams with a cross section of 300mm x 200mm with steel (Beam 1) and BFRP (Beam 2 and 3) as the internal longitudinal reinforcements. These beams were selected because of the availability of test results published in Elgabbas et al., (2017). Beam 1 (steel) and Beam 2 (BFRP) have the same reinforcement ratio, where as Beam 3 has an increased BFRP reinforcement ratio (additional longitudinal bar in the bottom face). All beams are 2700mm long and are as shown in Figure 3.

FIGURE 3

Beam sectional properties

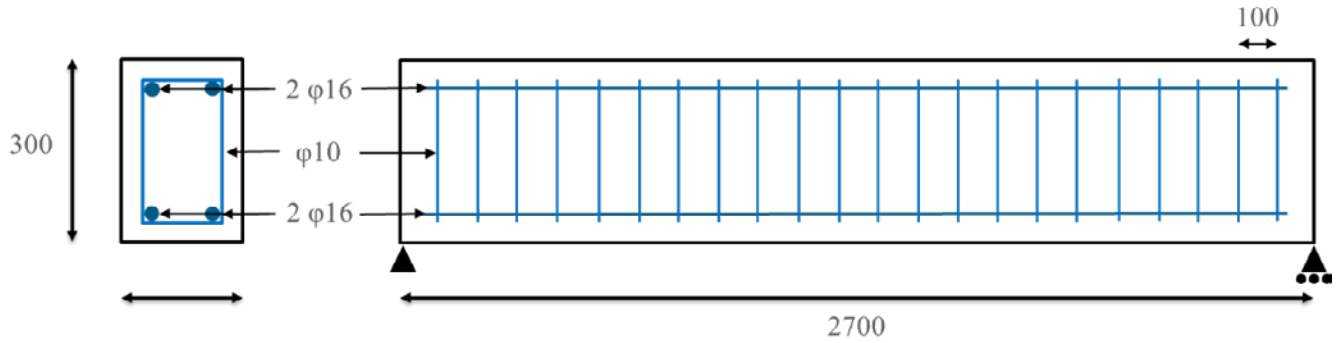

(a) Longitudinal section

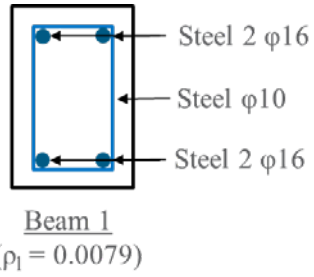

(b) Beam 1: Steel 2φ

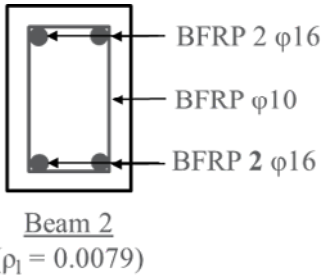

(c) Beam 2: BFRP 2φ

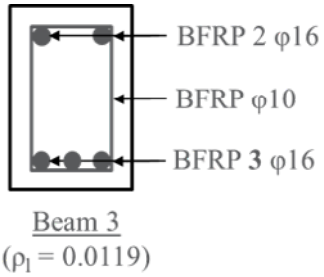

(d) Beam 3: BFRP 3φ

The concrete has a compressive strength, f_{cm} = 44.7 MPa, modulus of elasticity, E_c = 34.5 GPa and a tensile strength, f_t = 3.13 MPa. The steel, 15M has a yield value, f_{sy} = 450 MPa, modulus of elasticity, E_s = 200 GPa and yield strain, ε_y = 0.002, and the BFRP has a tensile strength, f_{ft} = 1724 MPa, modulus of elasticity, E_f = 64.80 GPa and ultimate strain, ε_{fy} = 0.0266. The material properties are experimentally tested and adopted from the literature review (Elgabbas, Ahmed and Benmokrane, 2017).

Standards for the design and assessment of basalt fibre reinforced polymer are not currently available due to limited investigation of their behaviour. However, basalt FRP is similar to glass FRP in terms of mechanical properties and durability. The new generation Eurocode 2 (2023) includes the design details for carbon and glass FRP as internal reinforcement in Annex R and for strengthening of concrete structures in Annex J. Hence, Eurocode 2 has been used in this work to explore the performance of BFRP reinforced beams. The geometric and material properties are adopted from the reference , Elgabbas, Ahmed and Benmokrane (2017) for ease of comparison with the analytical results, as well as to assess the predictive performance of the new generation Eurocode 2 (2023) on FRP materials.

4. Performance of BFRP

4.1 INTRODUCTION

This section describes the performance of basalt FRP at the serviceability limit state and ultimate limit state in terms of crack width, deflection, moment of resistance and shear resistance.

4.2 SERVICEABILITY LIMIT STATE (SLS)

4.2.1 Crack Width

Wider crack widths are permitted for BFRP than steel reinforcement due to the fact that BFRP does not corrode. The conventional reinforced Beam 1 (2φ steel) has a limiting moment of 35.0kNm for an SLS crack width limit of 0.3mm. Beam 2 with BFRP reinforcement has a limiting moment of 22.8kNm for an SLS crack width limit of 0.4mm (higher limit for FRP materials). The limiting moment of Beam 2 (2φ BFRP) is reduced to 65% of Beam 1 at the crack width limit due to the lower modulus of elasticity of the BFRP, which is one third of steel E_s. Hence, Beam 3 (3φ BFRP) with an increased reinforcement ratio results in a higher limiting moment of 31.6kNm at the crack width limit of 0.4mm, closer to Beam 1 (steel). Table 2 shows the crack width values of the three beams at varying moment values.

TABLE 2

Comparison of crack width values of all beams

Beam 1 (Steel 2φ)		Beam 2 (BFRP 2φ)			Beam 3 (BFRP 3φ)		
Moment (kNm)	CW (mm)	Moment (kNm)	CW (mm)	Diff. wrt. Beam 1	Moment (kNm)	CW (mm)	Diff. wrt. Beam 1
12.43	0.000	12.50	0.000	-	12.50	0.008	-
15.00	0.031	15.00	0.097	-	15.00	0.052	-
20.00	0.098	20.00	0.292	+ 198%	20.00	0.157	+ 60%
30.00	0.234	**22.80**	**0.400**	-	27.28	0.310	-
35.00	**0.301**	27.28	0.576	-	**31.63**	**0.401**	-
36.99	0.328	35.00	0.881	+ 169%	36.99	0.513	+ 56%
43.73	0.419	41.26	1.122	-	41.26	0.603	-
-	-	-	-	-	60.41	1.000	-

The evolution of crack width against flexural moment is presented in Figure 4a, and its comparison against experimental results in Figure 4b. The analytical results are comparable but not in good agreement with the experimental results. The experimental results show a lower stiffness in the initial zone, and an increase at the end. An abnormal dip is also observed in the central zone in BFRP beams.

FIGURE 4

Crack width evolution of all beams

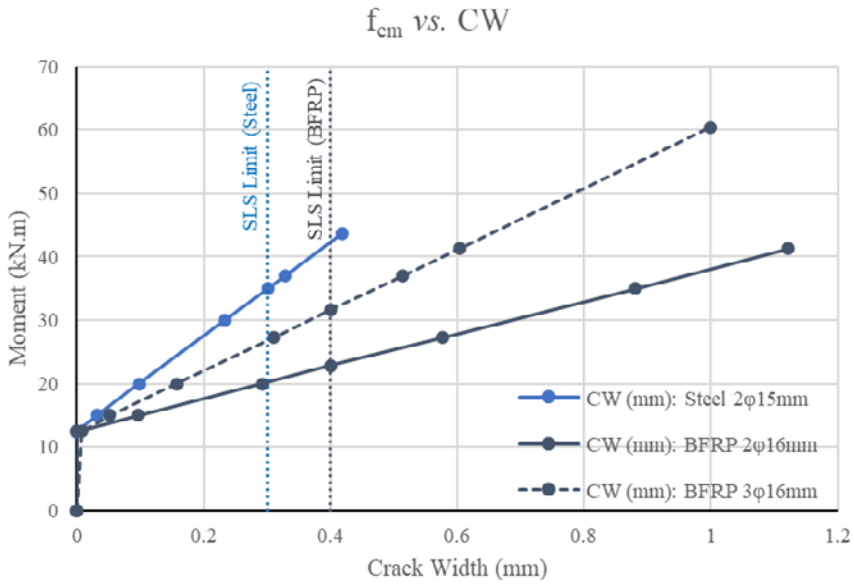

(a) Analytical results

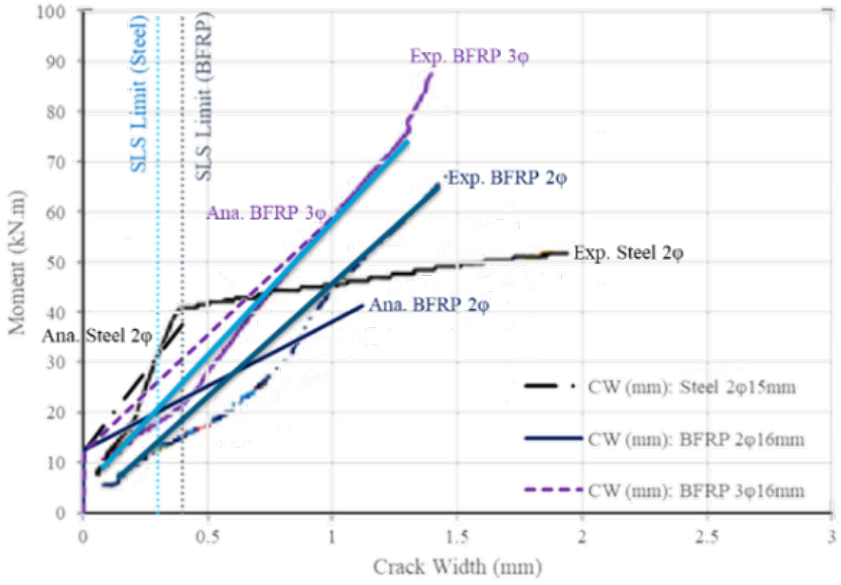

(b) Comparison with experimental results, (Elgabbas et al., 2017)

4.2.2 Deflection

Figure 5 shows the moment vs. deflection of all three beams. Beam 1 (steel 2φ) has a stiffer response after cracking moment. Whereas, BFRP beams have higher deflection after cracking as the effective cracked section in resisting the applied force is reduced due to a lower modular ratio.

FIGURE 5

Deflection vs. moment

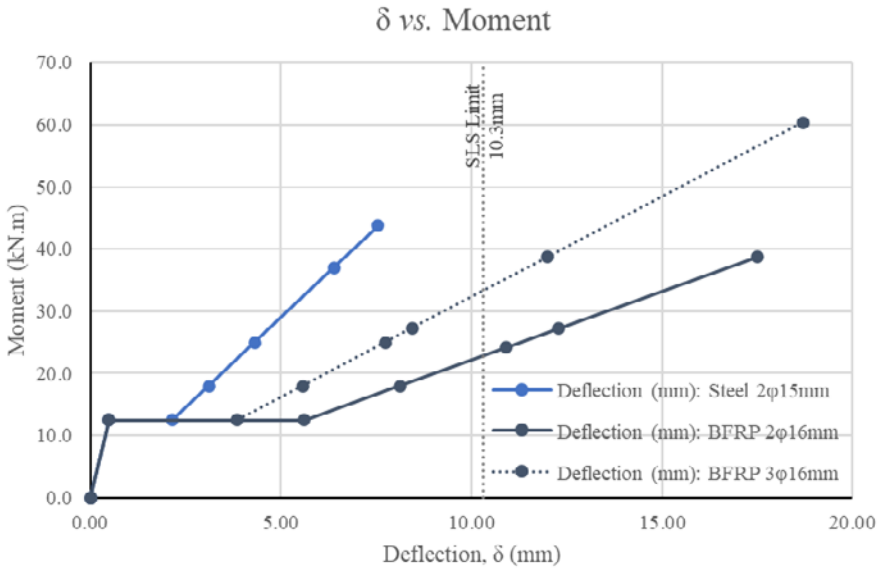

(a) Analytical results

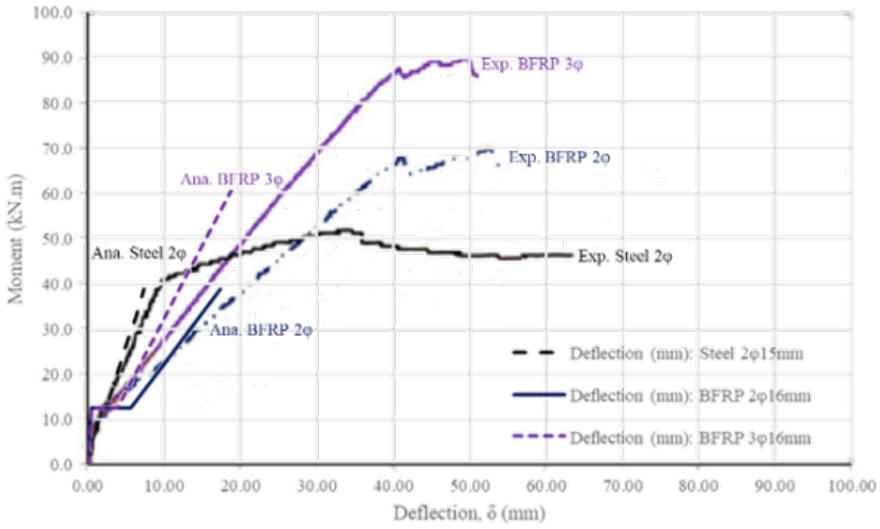

(b) Comparison with experimental results, (Elgabbas et al., 2017)

The analytical results are in agreement with the experimental results. If the experimental results are cleaned for noise (initial adjustments), the results will improve further. The values of deflection at different moments are tabulated in Table 3.

TABLE 3

Comparison of deflection

Beam 1 (Steel 2φ)		Beam 2 (BFRP 2φ)			Beam 3 (BFRP 3φ)		
Moment (kNm)	**Deflection (mm)**	**Moment (kNm)**	**Deflection (mm)**	**Diff. wrt. Beam 1**	**Moment (kNm)**	**Deflection (mm)**	**Diff. wrt. Beam 1**
12.44	0.487	12.44	0.487	-	12.44	0.487	-
12.44	2.147	12.44	5.613	162%	12.44	3.933	83%
18.00	3.108	18.00	8.124	162%	18.00	5.569	-
25.00	4.317	25.00	11.284	162%	25.00	7.907	83%
36.99	6.387	27.27	12.285	-	27.28	8.628	-
43.73	7.551	38.75	17.490	-	38.75	12.25	83%
-	-	-	-	-	60.29	19.07	-

4.3 ULTIMATE LIMIT STATE (ULS)

4.3.1 Moment of Resistance

The moment of resistance for Beams 1, 2 and 3 are derived for multiple compressive strengths of concrete and are presented in Figure 6a. Beam 1 (Steel 2φ) has moment of resistance 37.0kNm and Beam 2 (BFRP 2φ) has a resistance of 27.2kNm, 26% lower than Beam 1. Beam 3 (BFRP 3φ) has a resistance of 39.76kNm, 7.4% higher than Beam 1 for concrete with compressive strength of 44.7MPa.

FIGURE 6

Moment of resistance against compressive strength

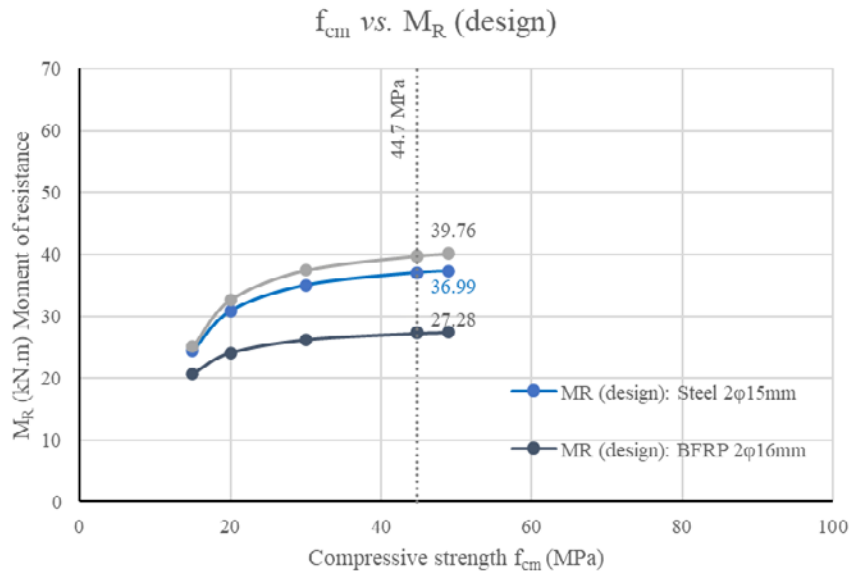

(a) Analytical results

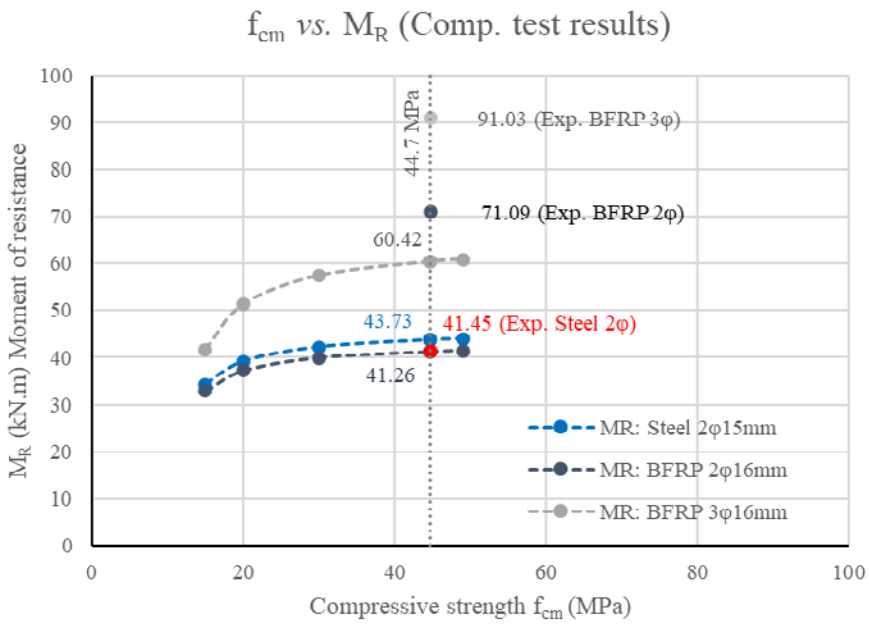

(b) Analytical and experimental results

Comparing the analytical results without material partial factors with experimental results, Beam 1 with steel reinforcement is found to be close to the experimental value as expected: 43.73kNm (analytical) and 41.45kNm (experimental). Beam 2 has a difference of 72.3% with 41.26kNm (analytical) and 71.09kNm (experimental), and Beam 3 has 50.6% difference with 60.42kNm (analytical) and 91.03kNm (experimental). The higher difference in analytical and experimental values of basalt reinforced beams is due to the reduced tensile strength which is derived from Eurocode 2 (2023). Despite the tensile strength of basalt FRP being four times higher than steel, the characteristic (and design) value includes multiple influence factors for temperature, service life and environmental attack, reducing the characteristic value to 24.5% of its ultimate tensile strength according to Equation 1. If we consider the material safety factor, then the design value further reduces to 16.3% of its ultimate tensile strength according to Equation 2.

$$f_{ftd} = \frac{f_{ftk,100a}}{\gamma_{FRP}} \qquad \text{Equation 1}$$

$$f_{ftk,100a} = C_t C_C C_e f_{ftk0} \qquad \text{Equation 2}$$

C_t = influence factor for temperature
C_c = influence factor for service life
C_e = influence factor for environmental attack

FIGURE 7

Design stress-strain diagram for FRP reinforcement (Eurocode 2 (2023))

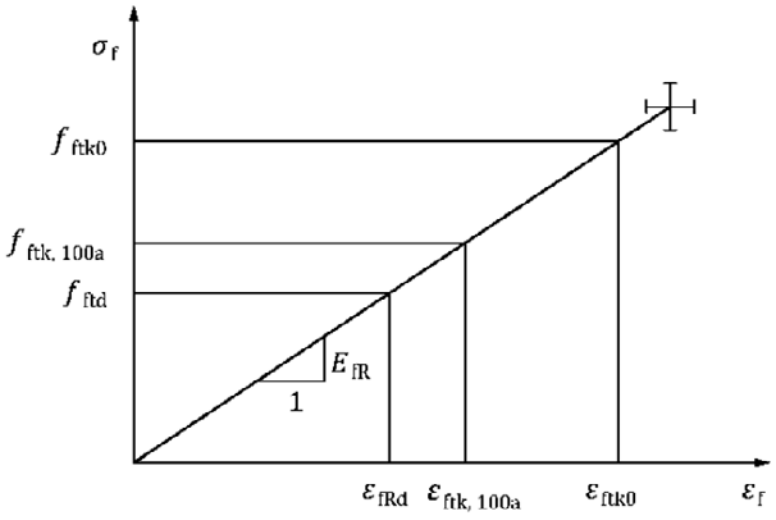

Analysing the impact on moment of resistance by excluding influence factors on temperature, service life and environmental attack, and material partial factors is shown in Figure 8. In BFRP Beam 2 (2φ), the analytical value is 102% higher than the experimental value and in BFRP Beam 3 (3φ), the analytical value is 109% higher than the experimental value. On an average there is an increase in moment of resistance by more than 100% when influence factors and material safety factors are excluded, and an under prediction in moment of resistance when considering them. This shows the importance and requirement of further investigations in analytical FRP formulations.

FIGURE 8

BFRP beam performance excluding influence factors

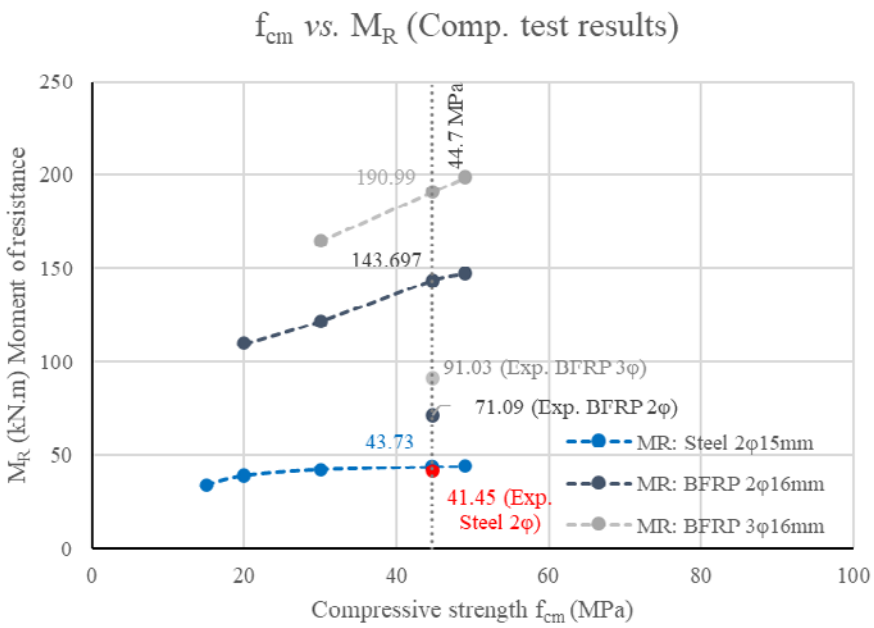

4.3.2 Shear Resistance

The minimum shear resistance ($\tau_{Rdc,min}$) of beams with basalt FRP reinforcement is calculated using Equation 3, from Annex R Eurocode 2 (2023). It is dependent on the concrete properties and the modular ratio (modulus of elasticity between BFRP and steel) inside the square root. As a result, BFRP reinforced beams will always result in lower minimum shear resistance than steel reinforced beams as the basalt FRP modulus of elasticity, E_{fR}, is lower than steel, E_s, as shown in Figure 10.

$$\tau_{Rdc,min} = \frac{11}{\gamma_v}\sqrt{\frac{f_{ck}}{f_{tk0}}\frac{E_{fR}}{E_s}\frac{d_{dg}}{d}} \qquad \text{Equation 3}$$

E_{fR} = design value of modulus of elasticity of FRP reinforcement
d_{dg} = aggregate size

FIGURE 9

Minimum shear resistance, $\tau_{Rd,cmin}$

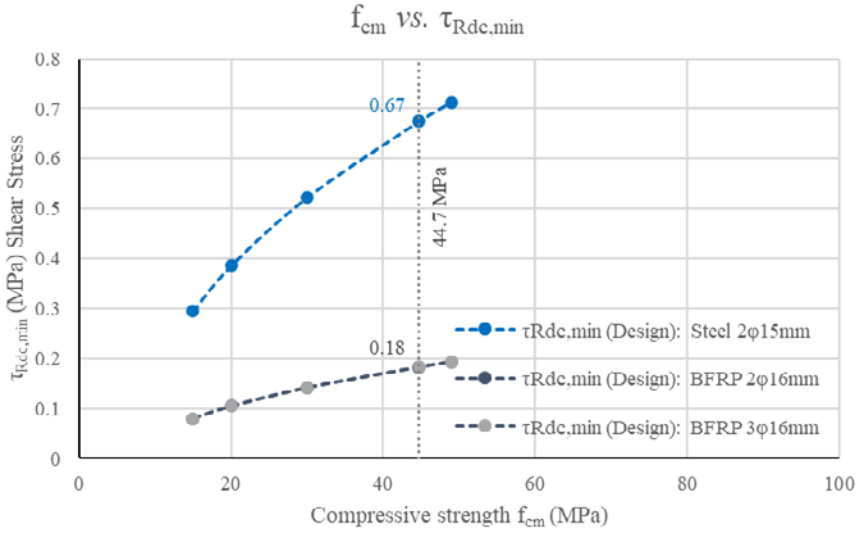

The shear resistance of Beam 1 is evaluated according to Equation 4, which considers only the contribution of steel reinforcement. In the case of basalt Beams 2 and 3, it is calculated according to Equation 5 considering the contribution of both concrete ($\tau_{Rd,c}$) and the FRP. Despite this, BFRP reinforced beams result in lower shear resistance due to the strain limitation imposed on FRP materials (Equation 7). The shear resistances of Beams 1, 2 and 3 are shown in Figure 10, and the values are presented in Table 4.

$$\tau_{Rd,sy} = \rho_w f_{ywd} \cot\theta \qquad \text{Equation 4}$$

$$\tau_{Rd,f} = \tau_{Rd,c} + \rho_w f_{fwRd} \cot\theta \leq 0.17 f_{cd} \qquad \text{Equation 5}$$

$$\tau_{Rd,c} = \frac{0.66}{\gamma_v}\left(100\rho_l f_{ck}\frac{d_{dg}}{d}\right)^{\frac{1}{3}} \geq \tau_{Rdc,min} \qquad \text{Equation 6}$$

$$f_{fwRd} = \frac{f_{fwk,100a}}{\gamma_{FRP}} \leq \varepsilon_{fwRd} E_{fwR} \qquad \text{Equation 7}$$

$\tau_{Rd,sy}$ = shear resistance of steel RC beam
ρ_w = steel shear reinforcement ratio = $A_{sw}/(b_w * s)$
ρ_l = longitudinal reinforcement ratio
γ_v = partial factor for shear and punching resistance without shear reinforcement

TABLE 4

Shear values of Beams 1, 2 and 3

Beam 1 (Steel 2φ)		Beam 2 (BFRP 2φ)			Beam 3 (BFRP 3φ)		
Moment (kNm)	$\tau_{Rd,s}$ (MPa)	Moment (kNm)	$\tau_{Rd,f}$ (MPa)	Diff. wrt. Beam 1	Moment (kNm)	$\tau_{Rd,f}$ (MPa)	Diff. wrt. Beam 1
15.00	3.073	15.00	1.471	-52%	15.00	1.506	-51%
20.00	3.073	20.00	1.519	-51%	20.00	1.561	-49%
30.00	3.073	30.00	1.585	-48%	30.00	1.637	-47%
44.70	3.073	44.70	1.651	-46%	44.70	1.714	-44%
49.00	3.073	49.00	1.667	-46%	49.00	1.731	-44%

FIGURE 10

Shear resistance

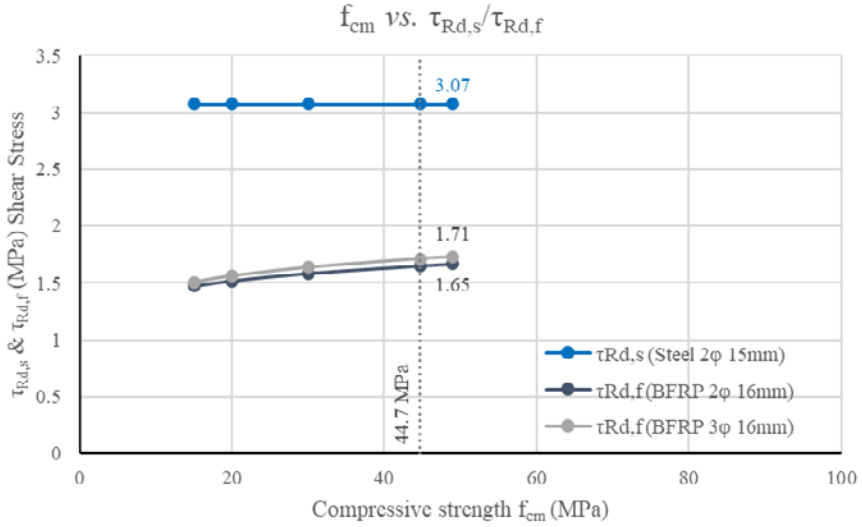

(a) Analytical results, $\tau_{Rd,s}$ & $\tau_{Rd,f}$

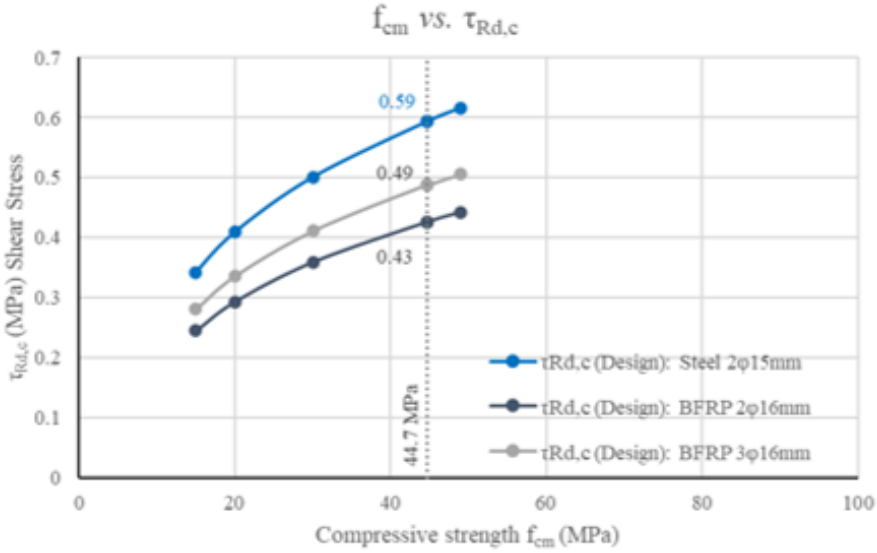

(b) Analytical results, $\tau_{Rd,c}$

5. Embodied Carbon Emissions and Manufacturing Cost

5.1 INTRODUCTION

In this section, embodied carbon emissions and average cost of manufacturing an RC beam and basalt reinforced beam in the U.K. are investigated and reviewed. The life cycle of any material consists of five stages: product, construction process, use, end of life and beyond the life cycle, as shown in Figure 11. The figure suggests that the majority of embodied carbon emissions are concentrated in Stage A which includes raw material supply, transport, and manufacturing, accounting for 55% of the total embodied carbon. Stage B and Stage C with 'use' and 'end of life' accounts for 45% of the total embodied carbon emissions, which may be typical for steel- reinforced concrete structures but is likely to be an overestimate for basalt reinforced concrete structures due to their improved durability. It is clear therefore that the choice of material type can have a significant impact on embodied carbon emissions in both Stage A and B.

FIGURE 11

Life cycle stages, Institution of Structural Engineers (IStructE, 2020)

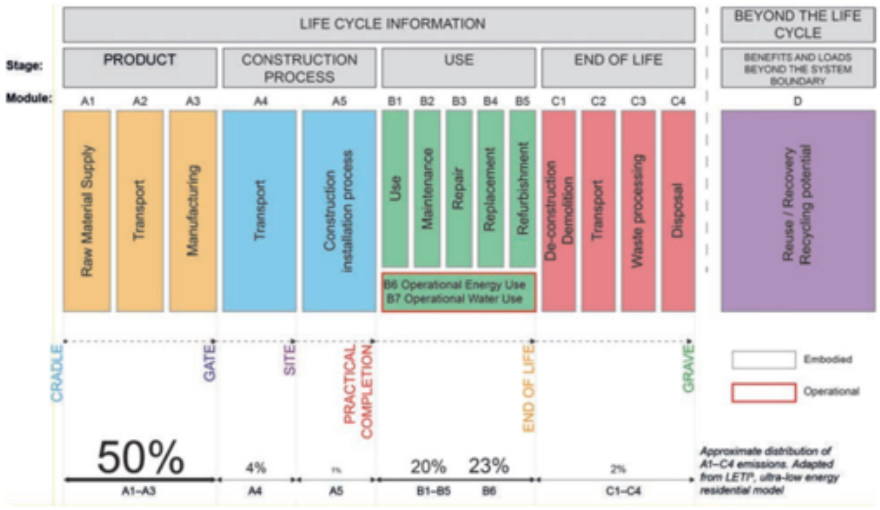

5.2 EMBODIED CARBON EMISSIONS

The embodied carbon emission calculations for each beam are subdivided into two categories: embodied carbon values with recycled steel (5.2.1) and embodied carbon values with normal steel (5.2.2). According to the ICE database (Institution of Civil Engineers, 2023), the embodied carbon of recycled steel is 0.980 $EcCO_2$/kg, and that of normal steel is 1.200 $EcCO_2$/kg. Concrete has an average value of 0.103 $EcCO_2$/kg, and according to reference (Pavlović et al., 2022) BFRP has 22% lower $EcCO_2$/kg than recycled steel leading to 0.764 $EcCO_2$/kg.

It should be noted that different basalt FRP producers have different environmental product declarations (EPD) based on the availability of raw materials, transportation, manufacturing method and delivery which results in varying embodied carbon values. Hence, based on the reference (Pavlović et al., 2022) the value of 0.764 $EcCO_2$/kg will be adopted in the current calculations as being representative for the U.K.

5.2.1 Embodied Carbon Calculations with Recycled Steel, 0.980 $EcCO_2$/kg

Table 5 shows the embodied carbon values of all the beams, and the performance of BFRP beams (Beams 2 & 3) assessed against the steel RC beam (Beam 1).

Beam 2 with similar reinforcement ratio as Beam 1 has lower performance across all criteria. Whereas, Beam 3 with increased BFRP reinforcement ratio has better performance than Beam 1 in moment of resistance and almost matches the crack width limit with a difference of 10%. In shear resistance, both the BFRP beams have lower values due to the reasons described in Section 4.3.2. Generally, FRP materials are weaker in shear as the fibres are not effective in the transverse direction, resulting in reduced dowel action and aggregate interlock. This results in wider and deeper diagonal cracks leading to early failure of the element. Additionally, unlike steel, a yield plateau is not available in FRPs as they are linear elastic materials (Figure 2).

TABLE 5

Embodied carbon emission calculations considering recycled steel (0.980 $EcCO_2$/kg)

	Beam 1 (Steel 2φ)		Beam 2 (BFRP 2φ)		Beam 3 (BFRP 3φ)	
Description	**Embodied Carbon (kg)**	**Percentage embodied carbon**	**Embodied Carbon (kg)**	**Percentage embodied carbon**	**Embodied Carbon (kg)**	**Percentage embodied carbon**
Concrete embodied carbon	39.12	57.67%	39.12	87.28%	39.12	86.65%
Basalt FRP embodied carbon	-	-	5.70	12.72%	6.03	13.35%
Steel embodied carbon	28.71	42.33%	-	-	-	-
Total embodied carbon	67.84	100%	44.83	100%	45.66	100%
Difference in embodied carbon wrt. steel RC beam	-	-	**23.01**	**33.92%**	**22.18**	**32.70%**
	Resistance		**Resistance**	**Difference from steel (%)**	**Resistance**	**Differerence from steel (%)**
Moment of resistance (kNm)	36.99		27.22	-26.42%	39.67	7.25%
Shear resistance, τ_{Rdc} (MPa)	0.62	-	0.43	-31.32%	0.49	-21.38%
Shear resistance, $\tau_{Rd,s}$ & $\tau_{Rd,f}$ (MPa)	3.07	-	1.65	-46.27%	1.71	-44.24%
Moment at crack width SLS limit	34.92	-	22.70	-34.99%	31.59	-9.54%
Moment at deflection SLS limit	36.99*	-	24.00	-35.12%	35.00	-5.38%

Deflection limit = Span/250 (EN 1992-1-1, 2004) = 10.8mm, *moment of resistance attained at 6.3mm

Table 6 shows the results of varying the embodied carbon emissions for different concrete strengths (lower and higher). Lowering the embodied carbon of concrete results in a higher percentage of BFRP and therefore higher embodied carbon savings are observed and vice versa.

TABLE 6

Embodied carbon emissions for different concrete with recycled steel values

Concrete, $EcCO_2$/kg	Beam 1 (Steel 2φ), kg	Beam 2* (BFRP 2φ), Percentage savings $EcCO_2e$	Beam 3 (BFRP 3φ), Percentage savings $EcCO_2e$
0.063	52.64	43.71%	43.09%
0.103	67.84	33.92%	33.44%
0.161	89.87	25.60%	25.24%

*performance does not match or exceed Beam 1 (Steel 2φ) performance

Table 7 presents the differences in embodied carbon values of basalt reinforced beams matching the specific performance of the steel RC beam. The results show that the basalt FRP material has very good performance in terms of all criterias resulting in significant embodied carbon savings.

TABLE 7

Comparison of embodied carbon matching recycled steel values

Description	Steel beam	Steel $EcCO_2e$ (kg)	Equivalent BFRP $EcCo_2e$ (kg)	Savings in $EcCO_2e$ (kg)	Embodied carbon percentage savings	Remarks (wrt steel beam 1)
Moment of resistance (kNm)	36.99	26.69	5.87	**22.84**	**33.67%**	Increasing longitudinal BFRP bars to 2.8
Shear resistance, τ_{Rdc} (MPa)	0.62	26.69	8.40	**20.31**	**29.94%**	Increasing longitudinal BFRP bars to 6.3
Shear resistance, $\tau_{Rd,s}$ & $\tau_{Rd,f}$ (MPa)	3.07	26.69	8.72	**22.39**	**29.47%**	Reduce stirrup spacing to 80mm
Moment at crack width SLS limit	34.92	26.69	6.32	**22.39**	**33.01%**	Increasing longitudinal BFRP bars to 3.4

Concrete embodied carbon emission for the current beam is 39.12 kg

5.2.2 Embodied Carbon Calculations with Ordinary Carbon Steel, 1.200 $EcCO_2$/kg

The embodied carbon emissions of beams with ordinary carbon steel is presented in Table 8, and Table 9 compares embodied carbon emissions for different concrete strengths.

TABLE 8

Embodied carbon emission calculations considering ordinary carbon steel (1.200 $EcCO_2$/kg)

	Beam 1 (Steel 2φ)		Beam 2 (BFRP 2φ)		Beam 3 (BFRP 3φ)	
Description	**Embodied Carbon (kg)**	**Percentage embodied carbon**	**Embodied Carbon (kg)**	**Percentage embodied carbon**	**Embodied Carbon (kg)**	**Percentage embodied carbon**
Concrete embodied carbon	39.12	52.67%	39.12	87.28%	39.12	86.65%
Basalt FRP embodied carbon	-	-	5.70	12.72%	6.03	13.35%
Steel embodied carbon	35.16	47.33%	-	-	-	-
	74.28	**100%**	**44.83**	**100%**	**45.15**	**100%**
Embodied carbon savings	-	-	**29.45**	**39.65%**	**29.13**	**39.21%**

The BFRP reinforced Beam 2 with similar reinforcement ratio of steel RC beam, has lower performance as expected. Whereas, Beam 3 with increased reinforcement ratio has better performance in moment of resistance and crack width as in the case of the BFRP beam compared with the recycled steel beam.

TABLE 9

Embodied carbon emissions for different concrete strengths with ordinary carbon steel values

Concrete, $EcCO_2$/kg	Beam 1 (Steel 2φ), kg	Beam 2* (BFRP 2φ), Percentage savings $EcCO_2e$	Beam 3 (BFRP 3φ), Percentage savings $EcCO_2e$
0.063	59.09	49.85%	49.30%
0.103	74.28	39.65%	39.21%
0.161	96.31	30.58%	30.24%

*performance does not match or exceed Beam 1 (Steel 2φ)

The performance of BFRP reinforced beams with ordinary carbon steel has better performance and embodied carbon savings, as recycled steel has lower embodied carbon emissions. These results are vital as all the steel requirement in the U.K. can not be fulfilled by recycled steel.

5.3 COST

The cost of manufacturing a steel RC beam and a BFRP beam is shown in Table 10. Concrete has an average cost of £175/m3 in the U.K., steel reinforcing bars cost an average of £1400/tonne and basalt FRP bar varies for different diameters. An average value of £2.27 for a metre of 10mm diameter bar was obtained from a manufacturer. This value was used to estimate the cost of 16mm diameter bar by multiplying by the area ratio (leading to £5.81/m).

TABLE 10

Comparison of manufacturing costs

	Beam 1 (Steel 2φ)		Beam 2 (BFRP 2φ)		Beam 3 (BFRP 3φ)	
Element	**Material**	**Cost (£)**	**Material**	**Cost (£)**	**Material**	**Cost (£)**
Concrete	Concrete	27.74	Concrete	27.70	Concrete	27.74
Longitudinal reinf. (bottom)	Steel	10.49	BFRP	34.87	BFRP	52.30
Longitudinal reinf. (top)	Steel	10.49	BFRP	34.87	BFRP	34.87
Stirrups	Steel	17.16	BFRP	61.29	BFRP	61.29
Total cost (additional cost wrt. beam 1)		**65.83 (-)**		**158.72 (141%)**		**176.15 (167%)**

As seen from the above table, the cost of manufacturing a basalt FRP reinforced beam (Beams 2 & 3) is 2.4 and 2.7 times respectively more expensive than a steel reinforced beam. More usage of basalt FRP rebars and innovative manufacturing techniques is likely to significantly reduce the cost of BFRP bars in future. However, if the BFRP reinforced beam is compared against an equivalent stainless steel reinforced beam, then the cost of the basalt reinforced beam is lower.

6. Conclusions

Basalt FRP bars are promising high strength linear elastic materials, which can be used as internal reinforcement in concrete structures. They are natural polymers which are sustainable and eco-friendly with respect to other FRPs like carbon, glass and aramid. As described in section 1, BFRP has been explored in a small number of R&D investigations, including long term effects.

Based on the current investigation the following conclusions are obtained:

- In terms of crack width, the basalt reinforced Beam 3 with higher reinforcement ratio meets the required crack width limits at approximately the same applied moment as the steel reinforced Beam 1.
- Basalt reinforced Beam 3 also matches the moment of resistance of steel reinforced Beam 1.
- Both the basalt reinforced beams have higher deflection than the steel reinforced beam due to the lower modulus of elasticity.
- The basalt reinforced beams have lower shear resistance than the steel reinforced beams because the contribution to the shear resistance from the BFRP longitudinal bars is much lower than that from the steel longitudinal bars due to their lower modulus of elasticity.
- Eurocode 2 makes reasonable predictions of strength for BFRP reinforced elements through the introduction of several factors for environment, temperature and age. The design tensile strength is underestimated due to conservative assumptions necessitated by a lack of long term data on material behaviour for basalt. If material factor and influence factors are eliminated for short-term assessment, there is over prediction (e.g., moment of resistance).

- Significant savings (an average 30%) in embodied carbon emissions are achieved by using basalt reinforcement with respect to recycled steel reinforcement. The embodied carbon emission savings increases even more (an average 39%), when it is compared against normal steel reinforcement.
- The cost of manufacturing a BFRP beam is currently high compared to a beam with ordinary carbon steel due to the costs associated with the production of the basalt reinforcements, but is lower than compared to a beam with stainless steel reinforcement for situations where durability is the key design criterion.

Overall, the performance of BFRP Beam 3 with higher reinforcement ratio matches the conventional steel reinforced beam in terms of moment of resistance and almost with the crack width requirements. The embodied carbon emissions are around 30% lower when using basalt reinforcement in place of steel reinforcement. The embodied carbon savings presented in the current investigation is for a beam of small size; the savings will be significant if basalt FRP is explored in large scale construction. More manufacturing will lead to reduced costs in the future, and the combination of embodied carbon savings together with cost is likely to eventually lead to an effective sustainable solution.

References

[1] ACI440.1R-06 (2006) *Guide for the Design and Construction of Structural Concrete Reinforced with FRP Bars*.

[2] Banibayat, P. and Patnaik, A. (2015) 'Creep Rupture Performance of Basalt Fiber reinforced Polymer Bars', *Journal of Aerospace Engineering*, 28(3). Available at: https://doi.org/10.1061/(asce)as.1943-5525.0000391.

[3] Elgabbas, F., Ahmed, E. and Benmokrane, B. (2013) 'Basalt FRP reinforcing bars for concrete structures', in *Fourth Asia-Pacific Conference on FRP in Structures (APFIS 2013)*, pp. 11–13.

[4] Elgabbas, F., Ahmed, E.A. and Benmokrane, B. (2015) 'Physical and mechanical characteristics of new basalt-FRP bars for reinforcing concrete structures', *Construction and Building Materials*, 95, pp. 623–635. Available at: https://doi.org/10.1016/j.conbuildmat.2015.07.036.

[5] Elgabbas, F., Ahmed, E.A. and Benmokrane, B. (2016) 'Experimental Testing of Concrete Bridge-Deck Slabs Reinforced with Basalt-FRP Reinforcing Bars under Concentrated Loads', *Journal of Bridge Engineering*, 21(7). Available at: https://doi.org/10.1061/(asce)be.1943-5592.0000892.

[6] Elgabbas, F., Ahmed, E.A. and Benmokrane, B. (2017) 'Flexural Behavior of Concrete Beams Reinforced with Ribbed Basalt-FRP Bars under Static Loads', *Journal of Composites for Construction*, 21(3). Available at: https://doi.org/10.1061/(asce)cc.1943-5614.0000752.

[7] EN 1992-1-1 (2004) 'EN 1992-1-1: Eurocode 2: Design of concrete structures - Part 1-1: General rules and rules for buildings'.

[8] EN 1992-1-1 (2023) 'EN 1992-1-1: Eurocode 2: Design of concrete structures - Part 1-1: General rules and rules for buildings'.

[9] Hassan, M. et al. (2016) 'Bond durability of basalt-fiber reinforced-polymer (BFRP) bars embedded in concrete in aggressive environments', *Composites Part B: Engineering*, 106, pp. 262–272. Available at: https://doi.org/10.1016/j.compositesb.2016.09.039.

[10] Institution of Civil Engineers (2023) *Embodied Carbon - The ICE Database, ICE*.

[11] Institution of Structural Engineers (IStructE) (2020) *How to calculate embodied carbon*.

[12] International Energy Agency. and Global Alliance for Buildings and Construction. (2019) *2019 global status report for buildings and construction*. International Energy Agency.

[13] Lapko, A. and Urbański, M. (2015) 'Experimental and theoretical analysis of deflections of concrete beams reinforced with basalt rebar', *Archives of Civil and Mechanical Engineering*, 15(1), pp. 223–230. Available at: https://doi.org/10.1016/j.acme.2014.03.008.

[14] Mehany, S. et al. (2022) 'Bond-dependent coefficient and cracking behavior of lightweight self-consolidating concrete (LWSCC) beams reinforced with glass- and basalt-FRP bars', *Construction and Building Materials*, 329. Available at: https://doi.org/10.1016/j.conbuildmat.2022.127130.

[15] Patnaik, A. (2009) *Applications of Basalt Fibre Reinforced Polymer (BFRP) Reinforcement for Transportation Infrastructure*.

[16] Patnaik, A. and Banibayat, P. (2012) 'Mechanical Properties of Basalt Fiber Reinforced Polymer Bars Manufactured Using a Wet Layup Method', *International Review of Civil Engineering (IRECE)*, 3(5). Available at: https://www.researchgate.net/publication/275893770.

[17] Pavlović, A. et al. (2022) 'Sustainability of alternative reinforcement for concrete structures: Life cycle assessment of basalt FRP bars', *Construction and Building Materials*, 334. Available at: https://doi.org/10.1016/j.conbuildmat.2022.127424.

[18] Ritchie, H., Roser, M. and Rosado, P. (2020) *CO2 and Greenhouse Gas Emissions, Published online at OurWorldInData.org*.

[19] Serbescu, A., Guadagnini, M. and Pilakoutas, K. (2014) 'Mechanical Characterization of Basalt FRP Rebars and Long-Term Strength Predictive Model', *Journal of Composites for Construction*, 19(2). Available at: https://doi.org/10.1061/(ASCE)CC.1943-5614.

[20] Technobasalt (2004) *Technobasalt: Basalt Rebar*.

[21] UNFCC, U.N. (2015) PARIS AGREEMENT.

[22] Urbanski, M., Lapko, A. and Garbacz, A. (2013) 'Investigation on concrete beams reinforced with basalt rebars as an effective alternative of conventional R/C structures', in *Procedia Engineering*. Elsevier Ltd, pp. 1183–1191. Available at: https://doi.org/10.1016/j.proeng.2013.04.149.

[23] Vincent, P., Ahmed, E.A. and Benmokrane, B. (2013) 'Characterization of Basalt Fiber reinforced Polymer (BFRP) Reinforcing Bars for Concrete Structures', in *3rd Specialty Conference on Material Engineering & Applied Mechanics*, p. MEC-1111-MEC-111-10. Available at: https://www.researchgate.net/publication/258839905.


PROTECT
THE BUILT
WORLD

Chris Mundell
Technical Director
Transportation UK
Bristol, UK

Chris Hendy
Technical Director
Transportation UK
Epsom, UK

Tom Argyle
Principal Engineer
Transportation UK
Epsom, UK

Colin George
National Highways, UK

Structural Engineering

02: Advancements in Bridges Non-Destructive Testing: National Highways' "Structures Moonshot"

Abstract

The "Structures Moonshot" project, initiated by National Highways and led by Atkins (now AtkinsRéalis), Jacobs, and supported by VSL, advances non-destructive testing (NDT) for highway structures, with a focus on post-tensioned bridges and half joints. Launched in late 2022 and continuing, its vision to revolutionise asset management for vulnerable bridges, enabling better and more efficient data collection, leading to self-monitoring and self-diagnosis for National Highways' most critical structures.

The project comprises two phases; The first involves testing high Technology Readiness Level (TRL) NDT technologies on bridge sections from the dismantled A14 Huntingdon Viaduct. These are compared with the as-found physical conditions after hydro-demolition. The goal is to evaluate current NDT methodologies, identify areas for improvement, and enhance efficiencies in deployment.

The second phase centers on developing low TRL NDT technologies tailored for post-tensioned bridges. This includes the use of guided wave technology, with the aims of enabling direct tendon deterioration measurements without intrusive inspections.

Through the collaborative efforts involving National Highways, AtkinsRéalis, Jacobs, VSL and the NDT supply chain engaged with the project, this work is leading to a better understanding of how we can determine the condition of post-tensioned bridges and half joints. The project will also provide valuable insights for future bridge inspections and structure maintenance works, enabling the development of clear training and guidance on optimal NDT deployment. This in turn will improve our overall asset management practices, ultimately leading to better safety of our structures and those using and maintaining them, and reducing disruption on our road networks.

KEYWORDS

Non-destructive testing; Highways; Bridges, Post-tensioned; Half joints; Asset management

1. Introduction

1.1 CHALLENGE

Within the transport infrastructure sector, all asset owners face an ongoing challenge to both inspect, maintain and operate their asset stock, whilst maintaining the highest levels of customer service possible. These two drivers are interlinked; to provide a reliable level of service, the assets need to be well maintained and well-managed. However, this is becoming increasingly difficult; key UK bridge owner National Highways estimated that by the end of the decade, 57% of their bridge stock will be over 50 years old. This is coupled with increasing levels of traffic in terms of magnitude and vehicle weights, meaning our structures are under more stress but are also more difficult to inspect and repair due to the disruption associated with road and lane closures. Whether a closure to inspect, maintain or repair a structure is planned or unplanned, the public and political impact can be substantial. For example, after routine inspections of the A52 Clifton Bridge in Nottingham, UK uncovered significant deterioration of post-tensioning strands at one location, the bridge was closed as a precautionary measure. This emergency closure led to a spike in congestion and traffic that made it the most congested city in the world during this time (BBC News, 2020).

1.2 MOONSHOT VISION

To face this challenge, National Highways have instigated a research programme they are calling their Structures 'Moonshot'. The underlying ambition of this is to maximise the benefits from advances in technology (e.g. new technologies, Artificial Intelligence and Machine Learning) to facilitate new and improved asset management approaches. The ultimate goal is to better understand the condition of our structures and facilitate interventions before deterioration has progressed to the point where major works are required.

By applying new and developing technology, the goal is to transform the management of our structures through accessing, piloting, deploying and upscaling technology. Improvements in processes and ways of working will impact on:

- **Safety:** minimising human intervention and improve road user safety.
- **Efficiency:** Reducing costs from planned and unplanned closures and enabling more proactive maintenance.
- **Availability:** minimising disruption to users and improving road user satisfaction.
- **Sustainability:** Reducing congestion and delivering more sustainable and less intrusive asset management approaches.

1.3 POST TENSIONING AND HALF JOINT FOCUS

National Highways' ambitious Moonshot project aims to consider all of the typically 'high risk' features associated with bridge structures, including post tensioning, half joints, hinge decks, scour and fatigue. In the first phase of this project, the team are investigating new approaches associated with internal post tensioning and half joints, of which there are approximately 1200 and 420 respectively within National Highways' jurisdiction in the UK (AtkinsRéalis, 2023).

2. Specific Challenges and Approaches for Post Tensioned Bridges

2.1 INSPECTION CHALLENGES

Both post-tensioned bridges and those with half joints provide a challenge for asset maintainers to inspect, assess and maintain. For post-tensioned bridges, this is primarily due to the primary load-bearing element typically being located within grouted ducts within the concrete volume and therefore inaccessible to most forms of inspection. For half joints, whilst the external facade of the joint can usually be inspected, the condition of the critical reinforcement along the joint length is often equally difficult to inspect without intrusive and damaging inspection.

The issue of inaccessibility is exacerbated when coupled with poor workmanship, poor detailing for water management or inferior construction techniques and materials. This can leave the tendons or half joints exposed to deterioration even in more recently-constructed structures. Whilst the failure of a half joint is usually a more ductile failure mode, failure of individual post tensioning strands can be progressive without any external warning signs and, in the worst case scenario, lead to brittle and catastrophic collapse of structures.

2.2 TYPICAL DEFECTS FOR POST TENSIONING SYSTEMS

Ultimately, failure of a stressing system occurs if either the load within the system increases to an extent that it exceeds the limits of the undamaged strands or, more likely, when corrosion reduces the strand strength through section loss (Fisk & Armitage, 2019), whereupon failure is often brittle in nature. Many early post-tensioned bridges simply relied on infill concrete being placed around the stressed tendons to provide corrosion protection, but this has been found to offer very poor protection against water ingress. To give better protection against corrosion, post-tensioning strands are typically encased in a duct (either metallic or PVC), with the duct usually infilled with grout to prevent the ingress of moisture and/or chlorides.

However, poor detailing, poor quality workmanship or inferior grouting materials can lead to a number of defects that may be present from construction:

- Voids within the ducts (most likely at high-points within the system).
- Bleed water accumulating during grout curing.
- Galvanic reactions from soft grout surrounding hard grout (Fisk & Armitage, 2019).
- Incorrect placement of ducting leading to low cover.
- Poor detailing of bridge joints, waterproofing or anchorage cappings.

Each of the above defects in isolation may not necessarily lead to deterioration of the post-tensioning system, however in combination with each other and through general degradation of the structure, they are likely to lead to deterioration. These defects can occur in any post-tensioned bridge, but pre-cast, post-tensioned segmental structures are of the greatest concern due to increased numbers of transverse joints - potential inlets for water and chlorides (WSP, 2017).

2.3 CURRENT APPROACHES TO DETERMINING CONDITION

Determining the condition of internal post-tensioning systems is a process that is complex and often requires a mix of approaches, led by skilled and experienced engineers and specialists. In essence, this can be simplified to:

- Optical inspection methods for surface-level indications of post-tensioning deterioration.
- Numerical Modelling, often including Finite Element Analysis (FEA).
- Non-Destructive Testing (NDT).
- Destructive/Intrusive Testing.

Each approach has its own advantages and limitations, with current technologies unable provide a single non-destructive method for determining all required information for assessing a structure. Therefore, they must all be used to some extent, requiring an understanding of the appropriateness of each, and where it can be relied upon.

3. Post Tensioned Bridge Moonshot - Scope

3.1 PRECEDING WORK

Following the closure of the A52 Clifton Bridge described in Section 1.1, National Highways formed a 'Tiger Team' to review their approach to managing post tensioned bridges. This included reviewing assurance processes, the relevant standards and their adoption, post tensioned experience and capabilities both internally and within the industry, risk management and the approach to inspection, data gathering and structural health monitoring. The latter aspect included a literature study on global approaches to data gathering, and in particular – a study on global approaches to NDT and the associated technologies (AtkinsRéalis, 2020). This concluded there does not yet exist a clear technology that provides a bridge owner a comprehensive understanding of the internal condition; All of the systems available have inherent flaws, limitations and inaccuracies. A combination of approaches - including visual, numerical, NDT and intrusive inspections – all still have their place within the current best practice maintenance strategy. However, there is likely a benefit to be achieved with reviewing the current usage of individual technologies, and how they can be used in parallel to better effect.

Building on the Tiger Team work, the first phase of the post-tensioned Structures Moonshot was commissioned to articulate the challenge noted in Section 1.1 of this paper and investigate the approaches that might be developed to meet these objectives. The project team - led by this paper's authors – undertook a global engagement process to appropriate institutions and sectors that might face similar challenges, and may have solutions or are undertaking research and development in a related field. This was undertaken through a 'Call for Ideas' challenge statement, which was issued to a broad range of potential research partners. This included engineering and NDT bodies and institutions, but also sought to reach out to potentially compatible institutions and companies within aeronautical, biomedical, agricultural, heavy civils (e.g. nuclear) and mining sectors.

The aim was to uncover technologies, approaches or low TRL ideas that would enable the determination of:

1. Identification if the conditions for corrosion exist, and how severe they are.
2. Identification if corrosion is actually occurring.
3. Identification if corrosion has occurred, and if so quantification of deterioration.

The statements are of increasing value to asset owners, but equally increasing in difficulty to achieve with any certainty. The aim was to identify technologies that either were already at a high enough TRL that they could be trialed and their effectiveness reviewed, or else be invested in to develop these ideas or concepts to a point at which they can be trialed and reviewed (i.e. very low TRL technologies).

Submissions were assessed and scored using a weighted scoring mechanism that considered TRL, evidence of experience in the relevant field, application of the technology (i.e. which of the three criteria above would it meet), cost and duration to develop, cost to deploy at scale and ease of applicability at scale.

At this point in the project, the A14 Huntingdon Viaduct – a post-tensioned rail bridge – was in the process of being demolished as part of a larger infrastructure scheme. The structure contained both post tensioning and half joints, with previous assessments and structural health monitoring pointing to defects in both. As will be described later in this paper, through a separate investigation led by AECOM, National Highways were able to secure three large samples of the structure to augment the scope of the moonshot project. Consequently, in addition to investing in low-TRL research, the project scope was expanded to include testing the effectiveness and applicability of higher TRL NDT technologies that are not yet in common usage.

The testing recommendations are presented in Table 1 below. The technologies selected included a number of higher TRL applications for trials, including; those from the agricultural sector, typically used for determining the composition of soil, high-accuracy optical strain and displacement measurements, creation of 'chloride maps' of surfaces using ground penetrating radar (GPR) and application of ultrasonic waves along the exposed tendon ends for short-distance condition mapping.

The lower TRL technologies included a guided wave application developed by Omnia, who – together with research partners Vallen Systeme – are well experienced in the field of acoustic monitoring techniques. Sentec's proposals included harnessing their specialisms in electronics and signal transmission to measure electrical transmission along tendons for fault finding, in addition to a variant on guided wave measurements, applied via thermal or electromagnetic means to the tendon through a surrounding concrete medium.

TABLE 1

Moonshot Testing Recommendations (AtkinsRéalis, 2020)

Technology	Lead Organisation	Application
Hyperspectral imagery, gas monitoring (FTIR) and portable X-Ray (pTRX)	Royal Agricultural University (RAU)	A14 Trials
Digital Image Correlation (DIC)	AtkinsRéalis	A14 Trials
GPR Chloride Mapping	Bridgology	A14 Trials
Anchorage guided wave	Mistras	A14 Trials
Direct Impedance	Sentec	R&D Programme
Guided Wave	Sentec	R&D Programme
Guided Wave	Omnia	R&D Programme

3.2 PHASE 2 COMMISSIONING AND SCOPE

The first phase of the Moonshot project ended with a report recommending the trials noted above in mid 2021. In late 2022, the second phase of National Highways' Structures Moonshot was commissioned through its Specialist Professional and Technical Services (SPaTS), and funded by National Highways' designated funds for Innovation and Modernisation Fund.

The project was awarded to a Joint Venture of AtkinsRéalis and Jacobs (AJJV), with the AJJV team including contractors VSL to be the Main Works Contractor, handling the management of the site activities through the project.

The main scope of this phase of the Moonshot project is split into two distinct activities; Testing of the low-TRL technologies of Omnia and Sentec (Section 4 below), and; mobilising a site compound to enable the a suite of NDT to be undertaken (including those noted in Table 1 above) on the recovered samples from the A14 (Section 5 below).

4. Research and Development studies

4.1 AIMS OF THE TRIALS

As part of the Moonshot project, National Highways were committed to investing in promising technologies that might enable the identification of tendon condition in existing post tensioned structures. The aim of this aspect of the project is to take early TRL technologies and ideas, and develop them to such a position that they can be deployed in a trial capacity on live structures (i.e. TRL 5). It should be noted that whilst the research is carefully assessed for alignment with the overall project goals, the investment is not linked to ownership of any developed technologies or the associated Intellectual Property (IP). National Highways are seeking the betterment of the industry through the application of new technology, rather than developing new capabilities.

Each of the R&D programmes has been split into a number of distinct phases or work packages. These are initially desk-based, using Finite Element Modelling (FEM) and small-scale testing to demonstrate the viability of the approach and the concepts involved. Follow on programmes include larger-scale testing to prove the FEM concepts, and introduce some of the real-world complexities that make these structures such a challenge to investigate. The final investment phase is to enable the construction of a prototype system that can be trialed in real-world application.

Funding and investment through the work packages/phases is dependent on a gated assessment approach. At each milestone, the project team (including National Highways and the AJJV team) review the progress to date, and the findings and outcomes compared to expectations. This provides the project team the opportunity to help steer the technology development at critical junctures, or in the case that the development is not deemed to be yielding the value required, potentially pivot to new avenues or technology investments.

4.2 SENTEC RESEARCH PROPOSALS

Technology and product developers Sentec (part of the Xylem group) supplied a number of potential NDT solutions to the Moonshot 'call for ideas', building on their experience of developing innovative sensors and smart metering for gas, water and electricity sectors. Two proposals were identified that would attempt to tackle the most challenging aspect – determining how much corrosion has occurred within a tendon. These were direct impedance measurement and Radio frequency (RF) coupled guided ultrasound.

For the RF coupled guided ultrasound involves the remote induction of a temperature gradient within the tendon via pulsed radio frequency. The induced temperature gradient is used to generate a high-power guided ultrasonic wave within the tendon, which is then measured by multiple receivers along the length of a section (from the surface of the concrete).

FIGURE 1

Sentec RF Coupled Guided Ultrasound

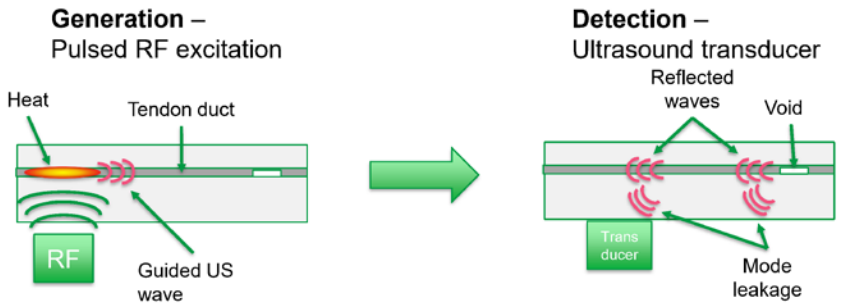

4.2.1 Progress to date – Direct Impedance

At the time of writing, the direct impedance methodology has been proven through a series of small scale tests and numerical modelling. Validated and compared against numerical modelling, the team constructed a 1m long grouted line, which was then injected with an 80 MHz bandwidth pulse, which was drilled with a 1cm hole (simulating a defect). The system was able to measure a demonstrable difference and change in signal between wet and dry conditions.

Demonstrating initial promise, the system does currently have a number of limitations and assumptions. These are namely;

- Changes in condition are best measured as variations from a baseline, and as such generation of a baseline is required for optimum results.
- A direct electrical connection to the duct and strands is required to induce the signal into the system (with potential to use a current loop to couple a signal into the strand remotely at a later date).
- Instances of connections between the tendon and metallic ducts, and further connections between duct and reinforcement will lead to a 'short' in the circuit and currently prevents further interpretation of the signal at this point.

4.2.2 Progress to date – RF Coupled Guided Ultrasound

The initial approach for this methodology was to attempt to induce a guided wave using an RF source, however it was determined through the course of the research that for situations where a duct is metallic, the power was predominantly absorbed by the duct. As such, the technology developed to trialing near field coupling via a magnetic field induced by a coil.

With the revised methodology, the Sentec team were able to induce and detect a generated ultrasound signal from a standoff of 300mm. Through numerical studies, this was progressed to observing wave propagation through water-filled voids within a duct, with a number of possible mechanisms for detecting and measuring the void.

4.2.3 Omnia Research Proposal

Omnia Integrity is a company specialising in non-intrusive methods for asset inspections, with a focus on wave mechanics (guided wave and acoustic emission). The proposal team included partners with ARCES (Bologna University) and Vallen Systeme, specialists in guided wave mechanics and acoustic emission inspections respectively.

The Omnia proposal harnesses their teams' expertise in acoustic monitoring, and utilizing the same apparatus, to induce guided waves that can assess condition in addition to detecting wire breaks.

4.2.4 Progress to date

The Omnia-headed team have been commissioned to undertake two phases of development to date; a numerical study with small scale testing, and; larger scale testing to validate numerical concepts and theory.

The initial phase of finite element modelling involved incremental increases in modelling complexity, moving from detecting responses in a 2D, single plain bar through to a 3D-modelled concrete-encased 7-wire wound strand. At each stage of testing, the team have been careful to test multiple frequencies and wave forms and ensure full understanding of the wave propagation and the associated response before moving onto subsequent stages, including identification of defect patterns such as breaks or section loss. The technology has shown promise that defects within grouted tendons can be identified up to a range of (currently) approximately 4m when utilising an excitation source connected directly to a strand.

At the time of writing, Omnia are undertaking large scale testing to validate the numerical studies, having constructed a 9m beam with stressed tendons encased in concrete. A number of 'windows' have been cast into the beam to allow the connection of excitation devices, in addition to control defects to be detected by the system. Trials are ongoing, with positive results indicating that the hypotheses of the numerical studies are borne out in practical application.

4.3 NEXT STEPS

Next steps for these technologies have been mapped out, but each technology must next be evaluated on its own merits and assessed with respect to those criteria set out in the initial moonshot 'call for ideas'. Likelihood of successful development through to a deployable technology will be key considerations, along with scalability and impact; to secure further investment the project team must be satisfied that a suitable return on investment will be achieved in the form of a high-impact technology that will lead to a step change in current asset management approaches.

5. Non-Destructive Testing – Technology Appraisal Trials

5.1 AIMS OF THE TRIAL

As discussed in previous sections, through preceding work, National Highways have secured a number of sections of the A14 Huntingdon Viaduct - including two sections with half joints – with the intention of undertaking blind trials of various forms of higher-TRL NDT technologies. The overall approach is to deploy these technologies across the three sections, followed by controlled hydrodemolition of the sections and extraction of key features (e.g. PT ducts and anchorages). By comparing the NDT results with as-found condition, the project team will be able to determine the effectiveness of various technologies and identify particular strengths and limitations. These findings will be used to develop improved approaches and process maps for asset investigations, laying different technologies together to complement each other and respond to the specific challenges faced on a structure-by-structure basis.

The trial does not just consider technology – gathering good data is a combination of people, process and technology; Having the appropriate equipment for a situation can be rendered ineffective if it is deployed in a sub-optimal arrangement, or used by insufficiently trained teams. This study therefore captures what 'best practice' looks like, and also includes duplication of specific pieces of equipment to attempt to distinguish differences in quality through different applications.

Finally, through the reach of the Phase 1 'call for ideas', the trials have included a number of cross-sector technologies. In particular, as will be detailed later in this paper, technologies from the agriculture sector – typically used for soil composition analysis – have been adopted.

5.2 SAMPLE DETAILS & HISTORY

The A14 Huntingdon Railway Viaduct (HRV) was constructed in 1975, carrying four lanes of traffic over six spans and crossing both local distributor roads and the East Coast Main Line (rail link). In December 2019, new routes were opened which rendered the structure obsolete.

FIGURE 2

A14 Huntingdon Railway Viaduct (HRV)

The main span consists of a main drop-in span formed of simply-supported precast beams (with transverse post tensioning and an in-situ deck slab), supported on longitudinally post-tensioned cantilever sections. The support and articulation for the precast main span elements are via half joints at the end of the precast cantilevers.

Over the course of 20 years, the structure has been subject to a number of detailed structural assessments, supported by testing and continuous monitoring (e.g. via Acoustic Emission Monitoring, or AEM). Due to a low assessed capacity and observed increases in re-entrant cracking of the half joints, a number of repair and remedial measures have been carried out, including regrouting of PT ducts and providing a secondary support structure to negate the risk of sudden half-joint failure. It should be noted that over the course of the 20 year period of AEM, a total of 52 wire breaks were recorded within the PT ducts, with a number concentrated in the section of the structure that was removed as part of this project and identified as 'Sample 3' (AECOM, 2021). In 2020, during the demolition of the full structure, three number samples were removed by wire cutting from the north monolith, as shown in Figure 3.

FIGURE 3

Moonshot Samples removed from the A14 HRV

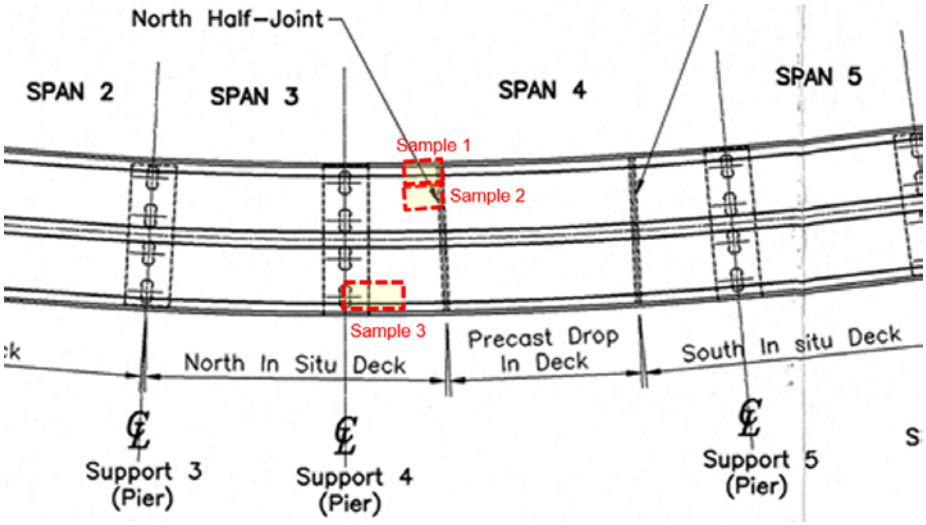

Samples 1 and 2 have been extracted from the end of the cantilever, being two adjacent sections containing half joints and PT ducts. The PT ducts all terminate within either the half joint nibs or immediately behind within the full-height section of the structure, meaning that all PT ducts within these samples also contain anchorages (5 number in sample 1, 8 number in Sample 2). The samples vary in size between 2m to 3m in length and width, weighing 16 and 24 tonnes respectively. Sample 1, being the outermost section, also includes the parapet beam support and a patterned finish to the external-facing elevation.

Sample 3 has been removed from the opposite side of the same cantilever monolith, starting at the pier support diaphragm and extending 6m along the cantilever section, being 4m tall at the highest (diaphragm) end. The section has been taken from part of the outermost cell, and as such contains part of the top and bottom flanges of the cell, along with the web. The external façade of the web is patterned and contains a diagonal nib to support the parapet beam (as per Sample 1). This section contains 7 number PT strands, of which one terminates within the section web. Images of the 3 samples are shown in Figure 4.

FIGURE 4

(Left to right) A14 HRV Samples 1, 2 and 3

5.3 NDT TECHNOLOGIES AND OPEN INVITE

The initial plan included engaging with some of the industries most established NDT suppliers to provide a suite of NDT techniques. This included optical/spectral inspections, electromagnetic sensors, mechanical wave induction and electrochemical tests. Testing providers initially included VSL (also acting at the main works contractors) Bridgology, Mistras, CTS, Allied Associates and the Royal Agricultural University (RAU). Many of the techniques were commonplace; Ground penetrating radar (GPR), covermeter surveys, ultrasonic tomography, half cell potential surveys and impact echo, but a number were also less common; Hyperspectral imagery, FTIR gas monitoring, magnetic flux leakage, chloride mapping via GPR and ultrasonic guided wave testing.

In addition to the planned NDT providers and technologies, the project team undertook a further 'call for ideas' from the wider industry (akin to the phase 1 moonshot call out). This was specifically seeking to understand if additional technologies and approaches had come to the market since the first phase, or had been missed in the first instance. Using National Highways' competitions page, coupled with social media outlets, the project and the opportunity to engage was opened up for several weeks while testing progressed. During this time, a number of new technologies and testing providers were brought into the project. This included Screening Eagle, bringing the latest Proseq sensors, HausBots, deploying their climbing robot, reinforcement scanning specialists Hilti and Muon tomography specialists GScan. The full list of providers, technologies and equipment deployed through the NDT phase is included in Table 2 below.

TABLE 2

Test Types, equipment used and NDT specialists engaged

Test Type	Equipment Used	Provider
Dust Sampling	-	VSL, Bridgology
Hammer Tapping	-	CTS
Cover meter Survey	Elcometer 331 Cover Meter	CTS
Electrical Resistivity	Proceq Resipod	CTS
GPR	Proceq GP8000	VSL, Bridgology
GPR	Proceq GP8800	Screening Eagle
GPR	Proseq GP8000	Screening Eagle
Joint Fracture Evaluation	-	Screening Eagle
Ultrasonic Pulse Echo	Proseq PD8050	Screening Eagle
Impact Echo	Proseq PI8000	Mistras
Anchorage Guided Wave	Mistras Proprietary Equipment	Mistras
Acoustic Emissions	Mistras Proprietary Equipment	Mistras
FTIR Gas Monitoring	Gasmet GT5000 Terra Portable Gas Analyser	RAU
Hyperspectral Imaging	Hyperspectral Camera	University of Bristol
Field Spectroradiometry	Spectral Evolution RS3500	Pro-Lite Technology
Raman spectroscopy	Wasatch Photonics Raman Spectrometer	Pro-Lite Technology
Gamma Ray spectroscopy	ImiTec ARARM Gamma Ray Sensor	RAU
pXRF	ThermoFisher Niton XL3t GOLDD+ analyser	RAU
Ultrasonics (Concrete)	ELOP	Allied Associates
GPR	GSSI Flex NT	Allied Associates
GPR	GSSI Structure Scan Mini XT	Allied Associates
Half-cell potential survey	Proseq Profometer Corrosion	Screening Eagle
Visual Inspection	Hausbots 1080p/30x optical zoom	HausBots, VTC
Cover meter Survey	Proseq Profometer PM8000	HausBots, VTC
GPR	Proseq GP8000	HausBots, VTC
Half-cell potential survey	Proceq Profometer Corrosion TBC	HausBots, VTC
Magnetic Flux Leakage	IFDB Proprietary Equipment	IFDB
Muon Tomography	GScan Proprietary Equipment	Gscan
UT Testing (Tendons)	Mistras Proprietary Equipment	Mistras
Cover meter Survey	Hilti PS300	Hilti
Cover meter Survey	Hilti PS1000	Hilti
Concrete carbonation tests	-	CTS
Half-cell potential survey	Proceq Profometer Corrosion	CTS

5.4 OUTCOME FOCUSED SPECIFICATION

The intention for each form of NDT is that it builds on the overall dataset which will allow structural condition to be appraised. Furthermore, the project team acknowledge that in the majority of cases, the most advantageous use of each form of NDT is best identified by the technology provider.

Based on the above requirements, the project specification produced for the NDT was primarily defined by outcomes, rather than prescriptive approaches. A hierarchy of data value was established, identifying the types of defects or data measured and their relative value (see Table 4). Leveraging this, it was the requirement that the technology providers themselves confirm the deployment methodology and which of the desired outcomes noted in Table 3 that they hoped to meet. Note that Table 4 include observations relevant to both PT tendons and those associated with half joints (noted as 'HJ' in Table 3).

With the nature of this project being aspirational, each provider was challenged to aim to achieve the maximum level of data and interpretation possible, even where the confidence of the data gathered may be lower. To capture this, the specification allows for individual tests to differentiate between when there are strong indications that defects are present, or conversely where there may only be a suggestion of potential for defects or the conditions for deterioration. As such, when capturing data from surveys, where defects are identified, these are coupled with a 'Level of Confidence' indication by the testing provider, scored as high, medium or low depending on the definition of the observation and potential for misinterpretation.

Finally, to enable a holistic review of the NDT data and actual condition data post-demolition, a detailed co-ordinate and referencing system has been established, catering for the different types of NDT and how they will capture data. This includes a 3D local co-ordinate system for each sample, individual identification of sample faces, duct numbering and chainage system and strand and wire numbering. Each NDT provider provides their findings in a standardised format where appropriate, allowing the project team to consolidate defects and findings and look for trends and linked observations.

TABLE 3

Hierarchy of NDT Testing and Relative Value of Observations

Ref	Description	Applicability		Value
		HJ	PT	
1	**Locating and identifying physical properties**			
1.1	Locate the strands and/or the reinforcement (approximate)	✓	✓	
1.2	Identify the sizes of the strand and/or reinforcement	✓	✓	
1.3	Identify the duct type		✓	
1.4	Map all strands and reinforcement (accurate)	✓	✓	
1.5	Identify chemical and physical properties of the materials	✓	✓	
2	**Conditions for corrosion**			
2.1	Locate the absence of duct grouting		✓	
2.2	Identify areas where reinforcement is at high risk of corrosion	✓	✓	
2.3	Identify areas where tendons are at high risk of corrosion		✓	
3	**Indications of damage**			Increasing Value of NDT Data
3.1	Identify discontinuities in reinforcement or prestressing steel	✓	✓	
3.2	Identify plastic deformations in reinforcement	✓		
3.3	Measurement of surface cracking at re-entrant corners	✓		
3.4	Measurement of cracking along length of re-entrant corners	✓		
4	**Pinpoint location and quantify magnitude of deterioration**			
4.1	Corrosion locations	✓	✓	
4.2	Magnitude and shape of section loss from corrosion at each location	✓	✓	
4.3	Wire break locations		✓	
4.4	Number of wire breaks at each location		✓	
5	**Other detectable behaviours**			
5.1	Bond slip between steel and concrete		✓	
5.2	Re-anchoring of strands		✓	

5.5 NDT KEY OUTCOMES TO DATE

At the time of writing, detailed NDT findings are still pending, however an initial collaboration session with the NDT providers has yielded outline results and initial findings as noted within this Section.

5.5.1 Half Cell Resistivity

Detailed electro-potential readings, dust sampling and chloride content testing carried out immediately prior to demolition (of the samples) are yet to be provided, however initial resistivity testing of the exposed faces results have typically been found to show low likelihood of deterioration in the near surface reinforcement and concrete, with some areas of hotspots, such as the re-entrant corners of the half joints of Samples 1 and 2.

5.5.2 Ultrasonic Pulse Echo

Ultrasonic Pulse Echo testing has been independently undertaken by a number of NDT providers, including Mistras, Screening Eagle and Allied Associates. Focus of testing has been on Sample 3 where the suspected wire breaks are located. This testing has identified a number of suspected voids within the tendon ducts, particularly within the web of the sample, as shown by Figure 5 below. This would indicate that at several points along the length of the tendons there is a lack of grout within the ducts, which would in turn provide an elevated risk of tendon deterioration.

FIGURE 5

Ultrasonic Pulse Echo testing examples

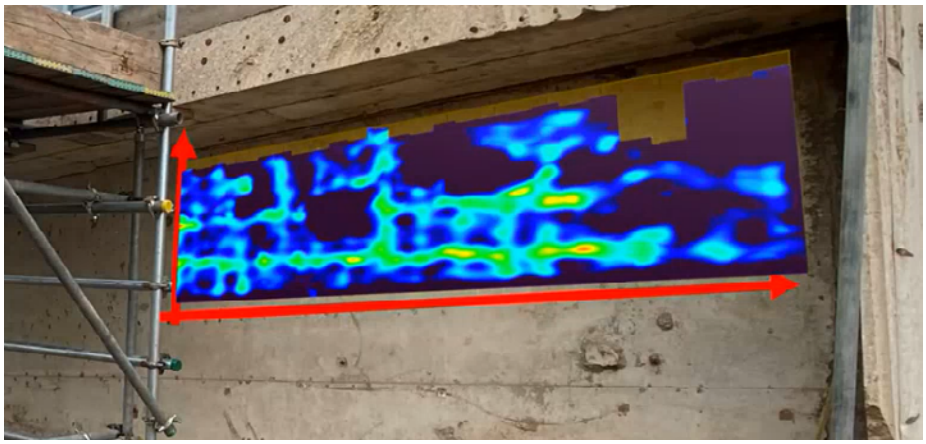

5.5.3 Impact Echo

Similar to the ultrasonic tomography, impact echo testing has focused on Sample 3 for the most part, and has again found a number of areas where there are strong indications that there is voiding within the sample and the ducts at a number of locations.

5.5.4 Ultrasonic Testing of Wires

Using a probe mounted to the exposed ends of the strands, a signal is induced to the individual wires within the tendons, with Mistras proprietary software analysing the signal for approximately 1m along the length of the tendon. As shown in Figure 6, the system has identified a number of tendons where there is a strong indication of corrosion along the length tested, although this test is limited to those locations where the tendon end can be cleanly accessed.

FIGURE 6

Ultrasonic tendon testing example data.

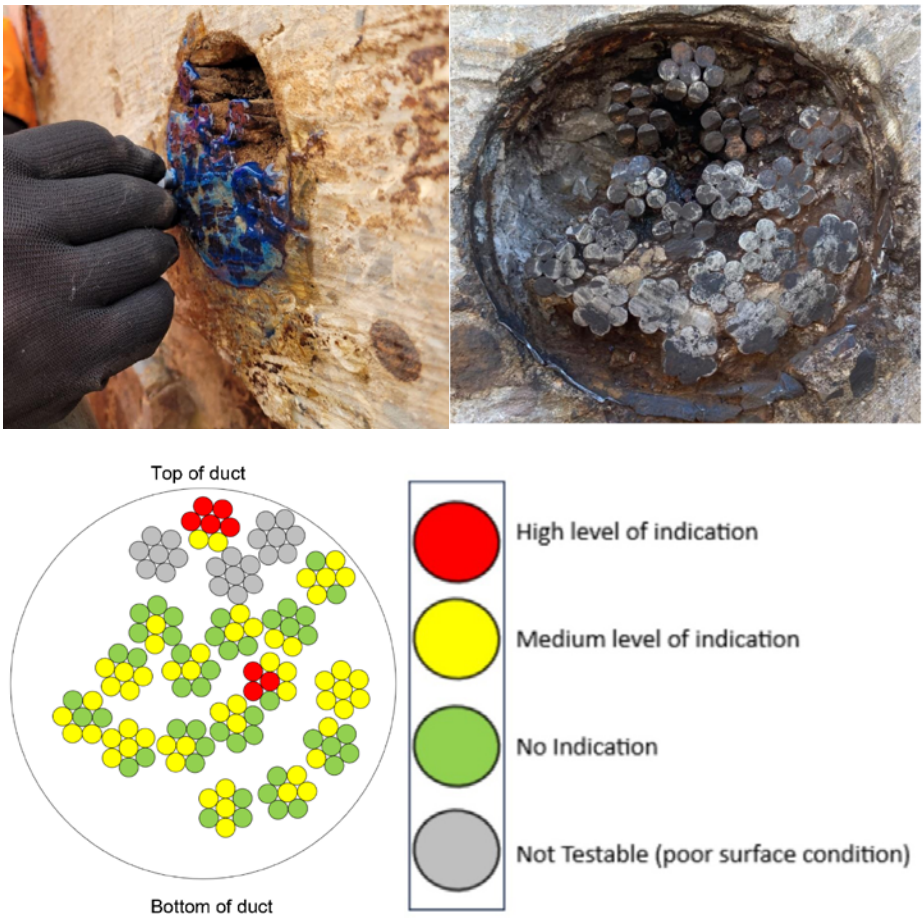

5.5.5 Acoustic Emission Testing

AEM is normally a passive system that is installed to measure potential tendon breaks over time; for the purposes of these NDT tests, a number of sensors were installed along the length of the samples, with signals induced by a 13cm spring loaded centre punch and a Schmidt hammer. The system measures signal attenuation and amplitude along the length of the sample, looking for breaks and potential indicators for wire breaks.

5.5.6 Ground Penetrating Radar (GPR)

GPR has been undertaken using a number of different devices and by a number of different providers, producing detailed coverage of all samples. Although a relatively simple and quick test to undertake, the latest GPR systems have proved effective at locating reinforcement and PT ducts, with multiple scans unlocking 3D images.

This technology has been effectively paired with the ultrasonic pulse echo technology, with both complementing the other in detecting voids and moisture. Following the workshop noted above, further tests were commissioned to attempt to use GPR to specifically identify duct deterioration; results from these tests are pending.

FIGURE 7

GPR testing data

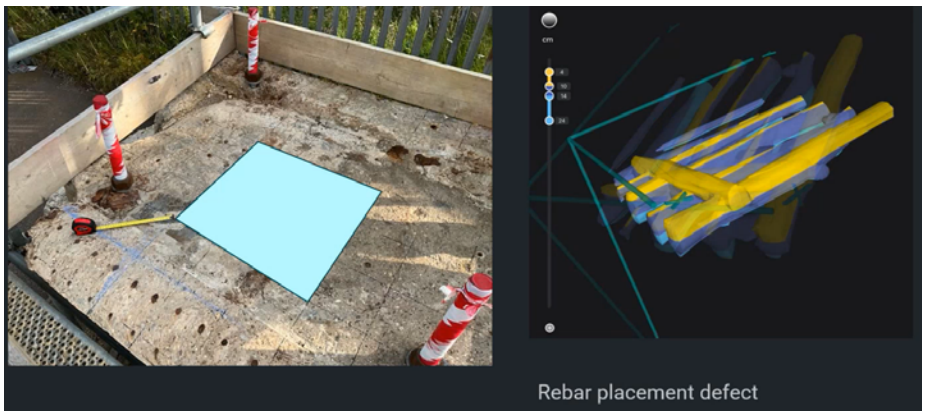

5.5.7 Portable X-Ray Fluorescence (pXRF)

pXRF is a technique used to identifying elemental composition within a sample, and can be applied via a hand-held device directly to a surface. The technique can detect many different impurities in the materials (e.g. sulfur, silicon or zinc), but the team focused on identifying corrosion accelerants such as chlorides, which were found to be most abundant in the duct areas. High concentrations of Sulphur were also identified specifically in the duct areas, which is also currently being reviewed further.

FIGURE 8

pXRF Data Capture and Chlorine Ion Detection

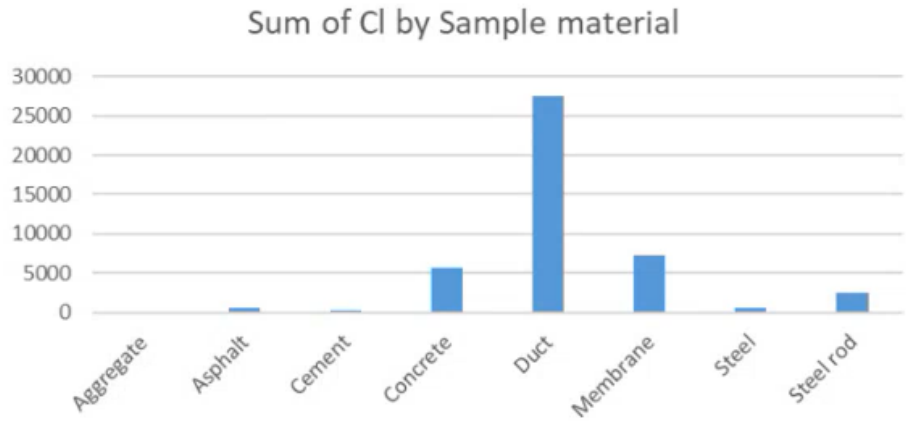

5.5.8 Fourier Transform Infra-Red (FTIR) Spectroscopy

FTIR Spectroscopy is a gas-sampling approach which uses a Gasmet device through two different applications; either a chamber attached to the surface of the samples, which is sealed and made a vacuum (or as close as possible), or via a 'sniffer' which can be inserted into bore holes and cracks. The device then analyses the gases to identify specific variances in gases that are being emitted directly by the sample (compared against baseline readings).

In the case of the moonshot tests, over a 10 minute timeframe, there were increases in Methane, Carbon Monoxide and Carbon Dioxide. Methane in particular was measured consistently across all of the samples at the time of the testing, potentially indicating some aspect of biological action. This is being further explored, including repeat testing and consideration of additional testing such as DNA testing of samples following demolition and sample extraction.

5.5.9 Field Spectroradiometry and Hyperspectral Imaging

Using field and laboratory spectroradiomters (ranging in the 280 to 2500nm spectra) in addition to a Raman spectroscopy device using an active light source (a monochromatic laser), further measurements of chemical composition can be remotely undertaken. Additional spectral analyses was carried out using a Specim IQ camera, recording in the 400 to 1000nm range.

Although full data processing has not yet been concluded, to date there have been no significant or noteworthy findings from the data obtained via these methods.

5.5.10 GPR Chloride Mapping

Using GPR data, Bridgology are able to develop a 'heat map' of chlorides and corrosion risk in a surface. In this case, the technology has used the Proseq GP8000 GPR scan, undertaken in scans 100mm apart and along two perpendicular directions (i.e. forming a grid of data). As shown in Figure 9 below, the technique has found some indicators of elevated risk of corrosion, particularly focused around the re-entrant corner of the half joints. This is of particular interest, and is not unexpected due to the known cracking along this location and historical deterioration of the structure.

FIGURE 9

Chloride and Concrete Cover 'Heat Maps' developed through GPR Surveys

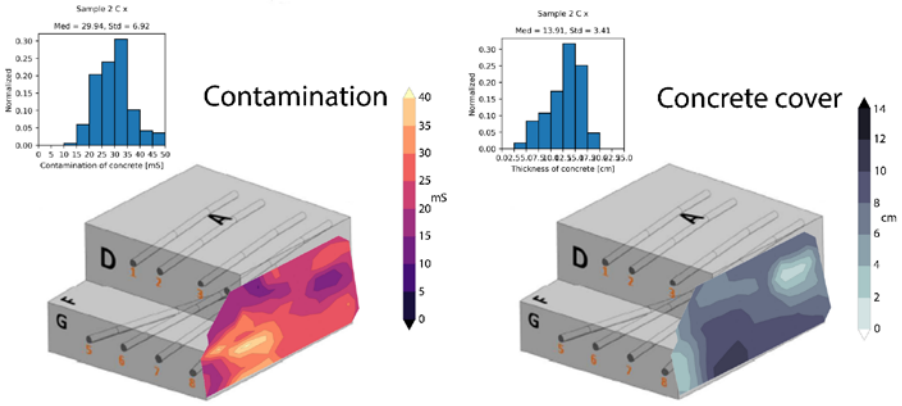

5.5.11 Magnetic Flux Leakage (MFL)

German-based company IFDB were engaged to deploy MFL testing, which involves remotely magnetizing the tendon from the sample surface and then measuring the magnetic flux density along the tendon path using magnetic sensors (see Figure 10).

FIGURE 10

Magnetisation and measurement of flux on Sample 3

Due to the specifics around the magnetization and interference/reflection from cut ends, the MFL technology is most suited to large, planar surfaces or long lengths of beams. As such, there were limited areas of applicability for MFL within the A14 samples. However, it was successfully used on Sample 3, both on the top surface and the exposed web. The team were successfully able to obtain signals from 5 of the 7 ducts within Sample 3, however there was no clear evidence from this technology of wire breaks within the strands.

5.5.12 Muon Tomography

The final technique tested uses an emerging technology called Muon Tomography. Muons are subatomic particles – similar to electrons - that are formed when cosmic radiation hits the earth's atmosphere. Muons are harmless to life, and have very high levels of penetration, which make them ideal for inspecting through dense structures such as a bridge elements. There are a number of methods for tracking the passage of the muons, however the method deployed by specialists GScan for the Moonshot project use high-technology materials such as Plastic Scintillating Fibers and Silicon Photo-multipliers, allowing the path of individual muons to be measured. By measuring over a long period of time (several weeks), the deviations of the muons due to changes in medium (e.g. where they pass from concrete into a metallic duct) can be detected, allowing an image or model of the area in front of the scanning plates. The technology promises to provide not just an image/model showing the various key elements (e.g. duct, tendons, reinforcement), but also the chemical composition of the materials, potentially showing deterioration and the presence of rust. The key limitation for this technology at present is the infrequent nature of the passage of muons; In order to build up a picture that shows defects at the scale required (i.e. millimeter precision), the scanning devices need several weeks left in-situ, with the area under observation therefore limited to the size of the scanning plates. In addition, a continuous power supply – although not large – is currently required for the system, which may add logistical complexity for in-situ bridges.

For the purposes of the Moonshot trials, two number sensors were used, one above and one below the concrete flange of Sample 3, and left for a total length of five weeks (Figure 11). The arrangement was locally moved after 2 weeks, with the intention of the second position enabling a 3D image. At the time of publication, the images and data obtained are still under development, with further trials under discussion.

FIGURE 11

Installation of GScan Muon Tomography scanners

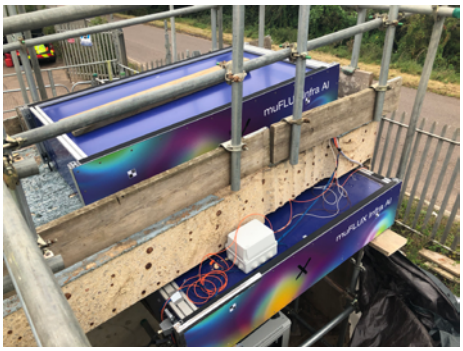

5.6 HYDRODEMOLITION

This aspect of the project has now moved into the final phase of work, being the controlled demolition of the samples and extraction of key elements such at the tendon and ducts, samples of concrete in areas of interest and key reinforcement bars for further testing (e.g. reinforcement critical to the half joint strength).

The PT ducts are the key elements of interest, which have been cut into 1m to 2m sections, and will be transported to a more controlled environment for opening and inspection. At this time, the ducts will first be inspected, photographed and measured, before being carefully cut and peeled from the grout and tendon. Again, the grout and any exposed tendon will be inspected and documented, with samples of the grout taken for compositional testing. The locations of any identified voids in the grout will be identified for comparison with the NDT findings. Finally, the grout will be mechanically and chemically removed, exposing the individual strands for inspection and testing, again for comparison with specific NDT findings.

The majority of the ducts have not yet been opened and inspected, however some exploratory work has already been undertaken, particularly with the ducts extracted from Sample 1 (Figure 12). An immediate observation was that the majority of the ducts have suffered deterioration to some extent, and in some cases the ducts were almost entirely non-existent along large lengths of the exposed ducts. Furthermore, the mortar was found to be missing or of very poor quality. Where the ducts were intact with grout present, a small number were cut and opened to expose the tendons and grout. In these cases, the grout was found to be of uniformly low strength, extremely soft and friable, and purely the removal of the duct was enough to cause the mortar to disintegrate and peel away from both strands and duct. This will be key area for further study, including the chemical composition of the grout and its remaining strength.

FIGURE 12

Duct extraction
and inspection

6. Programme and Next Steps

6.1 PROGRAMME AND BROADER MOONSHOT OBJECTIVES

This phase of the Structures Moonshot is scheduled to run until the end of 2024 or early 2025, by which point the planned R&D being undertaken by Sentec and Omnia will have reached the intended conclusions and the NDT on the A14 samples will have been assessed and documented. As noted in this document, National Highways' current aspiration is that this work is continued to consider other 'high priority' areas and structure types; this will likely be informed by the success and direction of these initial phases and the value delivered.

A key objective of the project is around knowledge sharing and dissemination. In addition to publication of key findings, part of the project scope is to host an industry conference at the end of the project, inviting the wider industry to attend and explore the findings and their implications, including asset owners, consultants, contractors, NDT providers and technology developers.

6.2 DATA COLLECTION, BIM APPROACH AND HARNESS OF ARTIFICIAL INTELLIGENCE

Throughout the NDT trials of the A14 sections, data has been captured in such a way that it can be considered holistically. The aim is to be able to draw conclusions and identify relationships between the findings of different techniques and approaches, tied to the as-found condition of the samples. This is founded on a clear and simple referencing system for the NDT specialists to adhere to, and will be augmented by transposing these data into a single federated 3D model, providing a 'Digital Twin' of the samples. Using typical BIM products such as Autodesk Revit, Navisworks and Bentley BIMTrack, the samples have been recreated as 3D models, upon which the NDT defects can be layered, along with the physical findings. Over and above this, the project team have been carrying out Lidar scans of the samples throughout the hydrodemolition process, providing 3D meshes of the exposed tendons in-situ, which can also be layered into the digital twin and explored in parallel to the NDT findings.

In addition to the exploration of the data by the project team, the goal is to be able to harness new approaches to data review such as Machine Learning and Artificial Intelligence, with the digital twin described above will be a key building block for this work. As noted, industry engagement is a key tenet of the project, and it is intended that further 'Open Invites' may be launched to expose the gathered data to industry AI and ML specialists, allowing the data to be much more broadly explored and different approaches tested.

7. Summary and Conclusions

Although still in progress, the project has already yielded significant insights and progress. The low TRL technologies explored by Omnia and Sentec are each pushing boundaries of what is achievable, particularly in the field of guided waves. In this aspect of the project, progression of the technologies will now start moving from what is theoretically possible to the practicalities of deployment in a real situation, and the relative value derived from its application.

Again, with respect to the NDT trials of the A14, although the data collation and assessment is still underway, a number of interesting observations and avenues have already been identified, and a broad suite of NDT techniques deployed. The industry engagement has also been very strong, with the NDT providers engaged being both collaborative and inquisitive, which has allowed the collation of information to be much broader than initially anticipated, which will in turn yield greater insights as the project turns to the data assessment.

Acknowledgements

The Authors would like to thank all of the parties involved in this project to date. These include the client and project sponsors National Highways (and the funding by National Highways' designated funds for Innovation and Modernisation Fund), the AtkinsRéalis and Jacobs joint venture project team, Main works contractor VSL, R&D partners Sentec (supported by Lucy Electric) and Omnia (supported by Vallen Systeme and ARCES) and NDT specialists Mistras, Bridgology, CTS, Allied Associates, Screening Eagle, the Royal Agricultural University (supported by the University of Bristol and Pro-Lite Technology), Hausbots, Hilti, GScan and IFDB.

References

AECOM. 2021 – Huntingdon Railway Viaduct Research Feasibility (Rev 003). *Highways England.*

Atkins. 2020. Post-Tensioned Non-Destructive Testing and Monitoring Techniques. *Highways England*.

Atkins. 2023. Task 164. Management of High Priority Structures – RIS3 Funding Estimate (Rev 2). *National Highways.*

BBC News Article. 2020. https://www.bbc.co.uk/news/uk-england-nottinghamshire-51467740.

Fisk, P., & Armitage, B. 2019. Nondestructive testing for voided and soft grout in internal post-tensioning ducts. *PTI Journal* 15(1), 31-35.

WSP. 2017. Task 622: Review of standards for post tensioned brigdes (v 8.0). *Highways England.*

Louise Morris
Associate
Infrastructure
Epsom, UK

Dr Inan Ekici
Head of Acoustics, Noise and Vibration
Infrastructure
Cambridge, UK

Henrik Malker
Associate
Infrastructure
London, UK

Philip Hainsworth
Associate
Infrastructure
Birmingham, UK

Tejin Jose
Associate Group Engineer - Acoustics
Engineering Net Zero and Sustainability Services, Global Technology Centre
Bangalore, India

Water and Environment

03: Nuisance and Health Impacts of Railway Noise

Abstract

Over the coming years, rail traffic is expected to experience significant growth as a means of achieving decarbonisation targets in the transportation sector. However, there are concerns this growth will increase the public health burden caused by railway noise. Exposure to environmental noise is associated with a range of health effects, including annoyance, sleep disturbance, and cardiovascular health outcomes. Recent research has challenged the view that railway noise is more acceptable than other transportation noise sources, with evidence indicating that an increasing number of individuals are being annoyed by railway noise. Despite the implementation of various noise mitigation measures and innovative solutions, complaints about railway noise remain high. Against this backdrop, this paper examines the health effects and nuisance caused by railway noise in the context of European railways, exploring the primary sources and characteristics of railway noise, the factors that drive individuals to complain, and the resulting health outcomes.

KEYWORDS

Noise; Railway; Health impacts; Complaints; Nuisance

1. Introduction

There is a clear requirement for increased rail transportation across Europe to meet environmental pollution goals, with a significant growth expected in both passenger and freight rail traffic over the coming years. Future development of the rail sector will need to proactively consider the impacts of noise on public health and socio-economic welfare and implement adequate levels of protection against noise.

Noise from railways is a combination of a number of individual sources, including some with distinctive acoustic characteristics. The source characteristics and noise emissions of freight trains varies from that of passenger trains. Due to the expected doubling of freight train traffic by 2050 (European Commission, 2020), it is recognised that reducing noise emissions from freight trains in particular is key to substantially reducing the undesirable impact of railway noise as their noise levels are associated with higher levels of annoyance than those from passenger trains (Lercher and Botteldooren, 2006).

There is a perception within the European railway sector that the rate of noise complaints from communities living along parts of the railways remain high, despite evidence that noise levels are decreasing as a result of a range of innovations and mitigation measures being employed across Europe. Understanding the main sources and characteristics of railway noise, and the relationship between noise exposure and health/ complaint outcomes is key to identifying appropriate cost-effective noise mitigation measures that can help reduce the number of people disturbed by railway noise.

This paper presents the outcomes of research commissioned by the International Union of Railways (UIC) in 2022 to obtain a representative picture of the nuisance effect of rail pass-by noise from conventional and high-speed services and its impact on human health in European railways. In particular, this paper provides an overview of health impacts from noise, the human response to noise and how this influences, complaint generation, methods to reduce noise impacts, and the current experiences reported by European infrastructure managers and operators. The study was supported by a detailed literature review and a critical assessment of the quality of research to determine the state of the current evidence base and identify remaining knowledge gaps to prioritise for future research.

A key part of the study has been to acquire a representative picture of the nuisance effect of railway noise for European railways. This has been undertaken by issuing a questionnaire to infrastructure managers and operators about noise complaints on their network, including how they are investigated, managed and resolved. The questionnaire responses were critically reviewed alongside the key outcomes from the literature review to identify knowledge gaps, discrepancies and topics to focus on for future phases of this project.

The combined outcomes from the literature review and questionnaire will support more effective policy and efficiently direct resources to improve noise and vibration management.

Although the term 'nuisance' can have a specific meaning in law, in this paper it is referenced in a general sense as a particular noise exposure resulting in a community or an individual response, in the form of either a health impact or a complaint. These responses may vary for different railway noise sources and the perceptions of noise may differ between population groups and countries.

2. Impact of Noise from Railways

2.1 SOURCES OF RAILWAY NOISE

Overall railway noise is dominated by **power/ traction/ auxiliary** noise at lower speeds (typically below 50 km/h), **rolling noise** at most operating speeds, and **aerodynamic** noise at higher speeds (such as 250 km/h). Individually noise from each of these components display a linear relationship with logarithmic train speeds (UIC, 2021a). Acting as a whole, there is an interaction between the different components, particularly at the cross-over speeds, to influence the overall noise from railways.

Freight trains produce higher maximum noise levels in dB L_{Amax} than passenger trains and their noise emissions are often more variable due to their composition. In regular operational scenarios, where freight trains operate or where the speed of passenger trains is above 100 km/h, the maximum noise levels at 25m from the track are expected to exceed 80dB L_{Amax}. Taking into account more specific railway features (such as flanging, squeal from tight curves, impact noise from joints, train horns and wheel flats), the levels could be significantly higher, more variable and tonal at certain locations.

2.2 COMPLAINTS

The World Health Organisation's (WHO) Constitution defines health as '*a state of complete physical, mental and social wellbeing and not merely the absence of disease or infirmity*' (WHO, 1946). It is recognised that being undisturbed by noise in all activities, including sleep, is an asset worthy of protection (WHO, 2018).

Noise annoyance is defined as '*...as a feeling of displeasure, nuisance, disturbance or irritation caused by a specific sound...*' in the context of long-term noise (WHO, 2018). What constitutes a noise annoyance may vary for different railway noise sources and perceptions of noise may differ between population groups and countries. In this context, consideration of non-acoustic confounding factors is relevant.

There is an expanding evidence base on a variety of cardiovascular, metabolic and other critical outcomes and risk indicators associated with noise (Guski, 2016; Foraster et al, 2017; Eze et al, 2017; 2020), including those reported by the SiRENE study (Rudzik et al, 2018; Brink et al, 2019; Swiss Tropical and Public Health Institute, 2021). More recently, the increased risk of dementia and Alzheimer's disease associated with transportation noise from road traffic and railways has been investigated (Cantuaria et al, 2021). Currently, the self-reported effects of noise on **sleep** and **annoyance** are two of the key indicators for evaluating health outcomes along railways (WHO, 2018). These health outcomes are significant due to their relevance to public health, policy and stakeholder engagement.

The railway sector is faced with noise complaints from the communities living along the railways, which is an active expression of dissatisfaction with the noise environment. There is a reasonable expectation on the railway sector to investigate and address complaints. A complaint may not always be directly linked to noise exposure but is typically a function of the '**arousal**' effect of noise - a conscious recognition of a change in acoustic environment from an unusual noise stimulus.

Research on community complaints to noise shows there are complex cognitive and psychological factors underlying a decision to complain (Guski, 1977; Luz et al, 1983; Shigenori, 2020). A conceptual framework has been proposed by Luz et al (1983), reproduced in Figure 1.

FIGURE 1

Conceptual framework for noise complaints (after Luz et al. 1983)

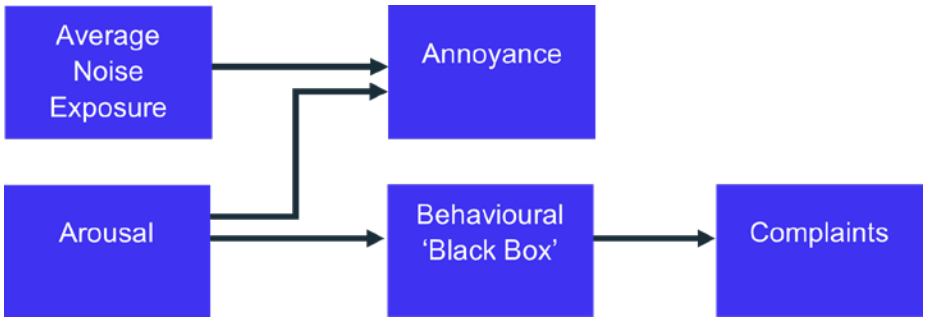

According to this framework, 'annoyance' is a function of both 'average noise exposure' and 'arousal' however 'complaints' are a function of 'arousal' only. The authors propose the following detailed model to describe the process governing complaints:

1. The human brain has a 'neural template' of what one expects to hear.
2. When the brain is first exposed to a new stimulus, it responds with a series of reflexes designed to gather more information.
3. If the stimulus is typical (has no good or bad meaning) and is repeated, the effects will be unconsciously integrated with past noise exposure.
4. If an unusual noise has occurred, this results in a conscious recognition as a change and could be considered as an 'arousal'. This intrusion into conscious thought can be an annoyance and, depending on the meaning of the noise, the person will take steps to make sure it stops or is not repeated. To eliminate the noise, the individual chooses the behaviour that has been most reinforced in the past. If this behaviour alleviates or is perceived to alleviate the noise issue, it becomes more probable in the future. If noise remains an annoyance, the chosen action becomes less likely in the future.

Therefore, the act of 'complaining' could be considered as a form of reaction and a coping mechanism to noise annoyance. Complaint behaviour is influenced by several factors, not just the noise level, and does not provide an accurate measure of community annoyance (Maziul et al, 2005). For example, there may be residents living in relatively high noise areas who do not complain, or residents living in areas with relatively low noise levels who do complain. There may be groups of people who declare to be highly annoyed (e.g. as part of community perception studies) but do not lodge complaints (Maziul et al, 2005).

The following general observations can be made on the nature of community complaints to noise, based on past research.

- A change in the stimulus is required for the brain to become aroused, leading to potential complaints.
- Often it is observed that complaints are generated by unusual rather than typical steady state events or conditions. e.g. intermittent sounds which may not contribute to the statistical analysis of sound distribution over a day. In this context, intermittent events which are higher intensity or distinct in character are more likely to cause arousals.
- People are more likely to respond defensively to an addition of sound than to a deletion of sound (Luz et al, 1983).
- The most frequently mentioned effects of an acoustic nuisance are disturbances of rest at night. These are typically caused by activities which generate sound during the night and early hours of the morning.
- There is a weak correlation between long-term noise exposure and complaints.
- There are qualitative differences in the nature of complaints between different kinds of noise sources. Freight trains are rated more annoying than passenger trains at the same vibration level (Lercher and Botteldooren, 2006).

Separate from discussions on long-term health impacts, the increased probability of awakenings from events affects quality of life and could point to a link between intermittent noise events at night and the likelihood of 'arousals' leading to complaints. Such atypical events may include the passage of freight trains, curve squeal and train horns.

2.3 OBSERVATIONS ON GLOBAL ANNOYANCE CURVES

WHO indicates that attitudes to railway noise, as measured by the percentage of population annoyed and sleep disturbed, have become more adverse over the years. However, there is also recent research which suggests annoyance reactions to road traffic noise and aircraft noise (Gjestland, 2020a; 2020b) have been stable over the years, and that the observed differences in WHO curves may be a function of the limited size of data and the methodology used in earlier statistical analyses of data. A review by Brown and van Kamp (2017) indicated that, in the case of road traffic, step changes in noise (such as those due to interventions at source or transmission path) could result in an 'excess response' in annoyance, over and above those estimated using the exposure-response functions which represent steady-state conditions. The review does not identify research on the effects of step-change or gradual change in railway noise on community annoyance or sleep disturbance.

Various recent studies point to a general trend in the community to rate railway noise less favourably compared with two decades ago (Miedema and Oudshoorn, 2001; WHO, 2018; Brink et al, 2019; Lechner et al, 2021). However, the strength of the responses appears to differ widely between studies. A review undertaken by Guski et al. (2017) indicates that due to the limited number of studies which were available for inclusion in the WHO analysis, some of the studies representing particular **local characteristics**, as well as **methodological differences** when analysing meta-data from social surveys, may have contributed to an increased percentage of highly annoyed people.

The general findings of this review are:

- **Individual sensitivity** – There is strong evidence that noise exposure explains only a small part of the variation in self-reported individual reactions. Individual sensitivity can be affected by non-acoustic factors (e.g. personal attitudes, age, education, other health indicators) and should be taken into account when assessing specific issues.
- **Community** – There may be local factors affecting community perception in different ways (e.g. common history, culture, politics, socio-economic indicators, availability and accessibility of information on noise impacts).
- **Local physical factors** – Specific sound propagation conditions including topography and meteorology can affect noise levels and community perception (e.g. noise propagation in a valley).
- **Confounding factors** – Noise in conjunction with vibration or other issues (e.g. air quality or wider environmental issues), historic attitudes to the source and the operator may affect community perceptions.

Global exposure response curves may be desirable from the perspectives of policy and community **health** protection. However, they do not represent an optimal tool for **managing local issues** encountered along the railways and designing **mitigation**. The above review has shown that local acoustic and non-acoustic factors should be taken into account in the identification of issues and measures along the railways to address these issues. Further research is needed to better understand the influence of local acoustic and non-acoustic factors on dose-response curves. Individual sensitivity, community perception, local physical characteristics as well as other confounding factors are relevant.

2.4 NOISE INDICATORS

The use of long-term noise indicators such as L_{den} (day-evening-night weighted sound pressure level) or L_{night} (equivalent continuous sound pressure level between 23:00 and 07:00) may limit the ability to observe associations between exposure to noise at night and some health outcomes such as **awakening reactions** (WHO, 2018), which has been identified as a supplementary health indicator. Although there is no robust reported link between 'objective' (physiological) short-term sleep effects and long-term annoyance/ sleep disturbance outcomes, the increased probability of awakenings from events affects quality of life. There is also a link between intermittent noise events at night and the likelihood of 'arousals' leading to complaints. Further investigations in this area would be desirable to assess potential relationship between long-term subjective sleep, short-term objective sleep and complaints at night.

Research indicates that the judgement of acceptability depends on the maximum noise levels (L_{Amax}) as well as factors such as the type of source, number and the distribution, predictability and regularity of noise events. The parameters that could have significance as physiological sleep metrics for night-time noise protection include; number of noise events, maximum noise levels, event rise time in decibel/second, length of noise-free period and characteristics of noise. The probability for awakenings has been shown to increase with the number of noise events per night and the longer a noise-free interval lasted (Elmenhorst, 2019).

Of the various noise indicators considered as a supplement to long-term indicators, it is noted that $\mathbf{L_{Amax}}$ is the most commonly used indicator in practice. It is used in the evaluation of short-term sleep effects, it is representative of 'arousal' responses which may lead to complaints and it appropriately reflects the intermittent nature of railway operation and the large variability in emissions found in practice. Use of L_{Amax} may be supplemented with additional descriptors to account for the characteristics of railway noise, such as intermittency (Brink et al, 2019), noise level and number of events (Elmenhorst et al, 2019; Association of Noise Consultants, 2019), and spectral composition of the noise (Elmenhorst et al, 2019).

2.5 METHODS TO REDUCE IMPACTS FROM NOISE

The three main approaches to noise mitigation are noise control at the source (e.g. infrastructure measures and quieter rolling stock), along the propagation path (e.g. noise barriers); and at the receiver (e.g. sound insulation treatments).

Lineside noise barriers or façade insulation are often used to reduce railway noise (UIC, 2021a). However, the PHENOMENA study shows that rail/track improvements are the most commonly specified noise abatement measure as part of the EU Members Noise Action Plans (European Commission, 2021). This shows the changing emphasis over the years towards mitigating the source of the problem. Retrofitting freight wagon brakes can be an effective means of reducing noise, but if a freight train partially comprises wagons with noisier brakes, this prevents the overall benefits to be fully realised. Similar focus will be needed to address specific issues which may need attention as part of ongoing maintenance, such as wheel flats. This requires concerted effort to maintain the existing state of acoustic environment, rather than reduce noise exposure, as would be understood from a traditional 'noise mitigation' measure.

In practice, there are limitations to noise reductions achievable by mitigation methods. Although they reduce overall noise exposure, they may not adequately deal with the 'arousal' aspects of atypical high-noise events leading to short-term sleep disturbance and complaints. Experience on mitigation of noise across other industries indicates 'hard' and 'soft' methods should be considered together to control perception of sound along railways, particularly with complaints. The United Nations Environment Programme (2022) highlights the importance of desirable soundscapes. As a concept, this could encapsulate the creation of relatively quiet areas, encouraging natural sounds and reinforcing sounds we value in our cities. In the context of railways, it could represent an innovative approach to dealing with the characteristics of railway noise which may lead to annoyance/ sleep disturbance and complaints. For example, the FAMOS study aims to assign benefits to non-acoustic factors responsible for community annoyance response (Force Technology et al, 2021). These benefits would be expressed in terms of equivalent subjective decibel changes. In circumstances where actual reduction of noise levels may no longer be feasible, this approach could be used to reduce the adverse community impact of road traffic noise by addressing the non-acoustic moderators.

With potential worsening attitudes of railway noise, working closely with the communities is key to the sustainability of the rail sector. The railway sector is very diverse in terms of its roles and responsibilities across geographic boundaries and type of assets. From a community perspective, whether a noise issue is related to the performance of a track or a train may not be very relevant beyond the nuisance caused. The overall perception is that this is a 'railway' related issue. A local train operating company, a trans-national freight operating company and a track asset owner may all need to work together to tackle issues. This necessitates a proactive sharing of information, knowledge and experience across different sectors to identify the issues and take appropriate action. This in turn requires having in place simple, transparent and effective processes to capture emerging concerns, take required action, evaluate effectiveness of actions and provide a feedback loop on lessons learnt as part of continual improvement.

These considerations highlight the importance of active stakeholder communication with individuals, communities, action groups, local authorities and other interested parties. The feasibility and cost-effectiveness of mitigation measures along existing railways is a key consideration in identifying suitable measures and should form part of these discussions when engaging stakeholders. The reasons for the appropriate action taken need to be clear to enable public scrutiny.

3. Situation of European Railways

3.1 METHODOLOGY

To address current information gaps on complaints along European railways, an online questionnaire was issued to railway infrastructure managers and operators to better understand the causes of railway noise complaints linked to the infrastructure management, operation, and maintenance of railways across Europe (UIC, 2021b).

The questionnaire focussed on noise complaints from train pass-bys and covered the following topics: regulatory framework, general complaints management, noise indicators, mitigation measures and complaints history at hotspots on the participant's network. The questionnaire was open for responses from 24 November 2021 to 22 March 2022 and was accessed through an email newsletter issued by the UIC to their membership and other invited participants. Reminder emails were issued to encourage participation.

The data gathered from the questionnaire has been used to provide context for complaints encountered in Europe. The questionnaire was used to identify the most frequently reported noise issues by the lineside population.

It is acknowledged that a limitation of the questionnaire outcomes is that complaint statistics are based on operator/infrastructure manager interpretations of received complaints rather than a direct analysis of complaint records.

3.2 RESULTS

3.2.1 Response Rate

The online questionnaire was completed by 18 stakeholders from across European and international railways. Respondents included a mix of operators and infrastructure managers, and the countries represented accounted for a total of 64% of the total length of railways in Europe, amounting to over 150,000 km.

In the sections that follow, values shown in brackets indicate the number of supporting responses to a specific question are shown against the overall number of responses, for example (10/15) would show there were 10 answers supporting a finding out of 15 answers given.

3.2.2 Regulatory Framework

The responses illustrate that the emissions of noise from the railways are well regulated across the rail sector, either in the form of legal limits or other Regulatory Controls. Where there are legal limits on noise emissions, there are typically different limits for new and existing railways (11/15). An example of how these are differentiated is having more stringent noise limits for new lines compared to existing lines (typically by 5 to 10dB) or having limits for new lines additionally based on the change in existing ambient noise. Additionally, the majority (11/15) of respondents do not differentiate between passenger trains, high speed trains and freight trains in relation to operational noise limits. Respondents that do differentiate between passenger trains and freight trains tend to include some of the larger European railway networks (representing about 25% of total length of railways in Europe).

Differentiating between new and existing railway infrastructure acknowledges that a change in noise is perceived more annoying than an existing noise and demonstrates a pragmatic approach by recognising that the opportunities for controlling noise emissions are far wider when designing new infrastructure. However, the 'global response curves' do not make the distinction between new and existing networks or passenger and freight rail services. Furthermore, the treatment of passenger and freight traffic as a combined noise source in the majority of cases could prevent effective actions from being identified as freight trains are associated with higher levels of annoyance.

3.2.3 Complaint Volumes and Management

Generally, the number of noise complaints received can be correlated to the size of the rail operator/network. Half (9/18) of the respondents indicated that they received more than 1,000 noise complaints over the past five years, of which two received more than 5,000 complaints. There are no published data in the railway sector to act as a benchmark for these complaint statistics, however, these complaint statistics seem favourable compared to similar numbers, for example, from major airports.

The responses show that noise complaints are generally monitored well and recorded in a way to enable future analysis, with many operators and infrastructure managers utilizing dedicated complaint handling teams and storing complaint data on central databases. Generally, a sufficient level of information is collected to enable meaningful analysis of complaints, although there is some variation across the networks on the nature of data captured, which affects the depth of analysis possible.

Fewer than half of the survey respondents (8/18) indicated that they have a legal requirement to act on noise complaints. The majority of respondents (11/18) stated that noise monitoring is never or rarely used to investigate complaints. The most frequently used noise indicators to investigate complaints are $L_{Aeq,T}$ (equivalent continuous sound pressure level), L_{night}, L_{den} and L_{Amax}. The limitations of indicators such as $L_{Aeq,T}$, L_{night}, L_{den} were highlighted above, particularly in assessing awakening reactions and arousals from atypical sound sources.

When a complaint (or group of complaints) is investigated and the noise levels are found to be compliant with national standards/laws/requirements, the majority (12/18) of survey respondents would not take further action on the complaint. A complaint could have the potential to escalate if the resident perceives that the authority is not positively engaging to help. Investigating complaints is therefore partly shaped by external stakeholder pressure and a desire to minimise reputational risk to the railway sector. Noise limits represent an aspiration to minimise long-term noise exposure (e.g. L_{den}, L_{night}). However, there are no exposure-response relationships for noise complaints. In this sense, a factual report linked to noise limits, without the consideration of complainant sentiment, may not resolve the complaint fully.

The industry response may go some way in explaining the observation that complaints along parts of the network remain high even though the overall noise levels have been reduced over the years. As complaint statistics are somewhat disconnected from noise emissions, they are not always linked to a certain noise level being exceeded. Having noise limit values may be desirable for transparency and effective use of public funds for prioritising mitigation measures. However, on their own, without consideration of the subjective 'arousal' effect of noise, the approach may have some limitations. This is an opportunity for the industry to manage complaints via sharing and implementation of a framework of best practice.

3.2.4 Causes of Complaints

The most common concern by complainants is disturbance to sleep or rest during the night-time period, which supports outcomes reported by other studies. Other common concerns are health consequences and depreciation of real estate. There are also concerns regarding the perception of not being listened to and/or improvements being unlikely (i.e. the attitude of the railway industry to resolving complaints) despite effective stakeholder communication being an integral part of tackling complaints.

The most common railway features causing complaints were ranked as follows:

1. Freight trains.
2. New, upgraded or altered infrastructure.
3. Maintenance operations, such as rail grinding.
4. Frequency of services.

Other features stated as being common causes of complaints included points (i.e. turnouts and crossovers), tight curves and train horns, as shown in Figure 2.

FIGURE 2

Railway features and how common they are in causing complaints

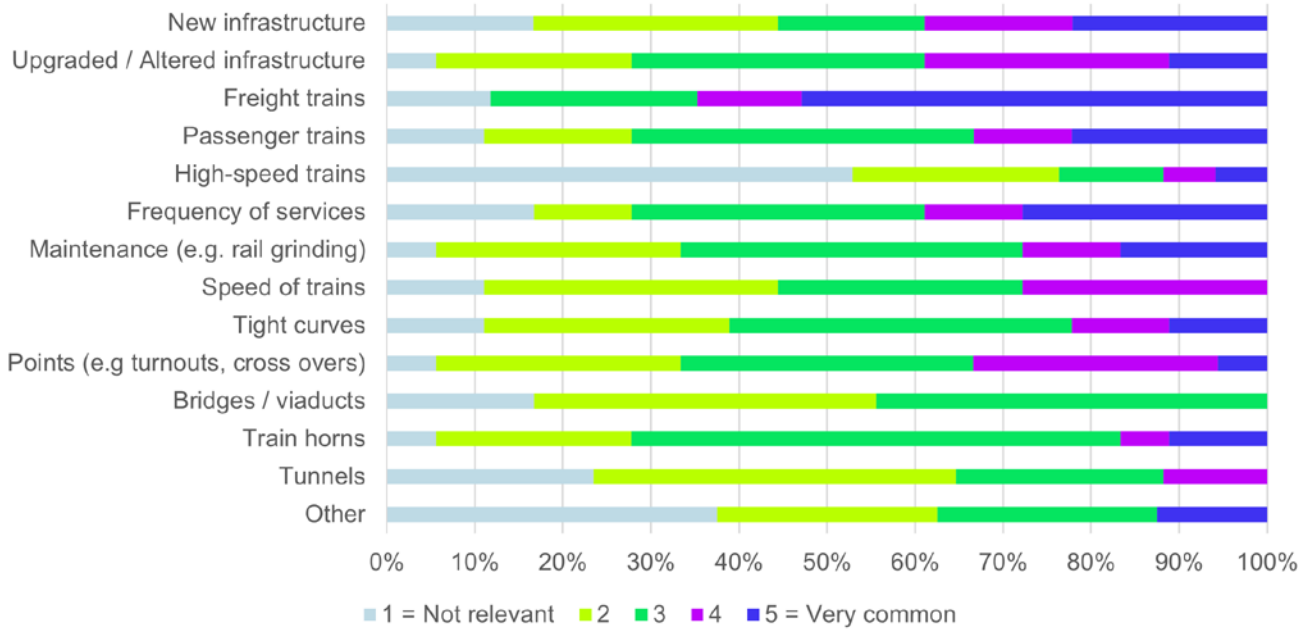

The case studies provided by respondents support the above observations above that complaints are focussed on "atypical noise" (i.e. rail grinding, curve noise), change in noise, areas of extreme sensitivity or where noise limits are exceeded but are difficult to mitigate. One respondent noted that despite legal indoor noise limit being met, complaints persist and are predominantly due to singular events such as individual pass-by events, wheel squeals and train horns at night. These observations support research findings that atypical sounds resulting in arousal reactions are more likely to result in complaints, particularly at night and associated with sleep and rest periods.

Only one respondent stated high-speed trains were a very common feature causing complaints and that national regulations are being revised to tackle this issue. Further work would be needed in this area to better understand the public perception of the impact of high-speed railways.

Socioeconomic political factors were noted as contributing factors affecting the likelihood of complaints, as well as perceived lack of action despite availability of effective and easy to implement mitigation measures. This again highlights the significance of non-acoustic factors and effective stakeholder communication.

When asked if there was a change in the pattern or number of complaints during the past five years, the responses showed no correlation with respondent network size and the mixed responses indicated there is no consistent pattern of increases in complaints. Of the 6 respondents (44%) who reported a change, 3 reported a persistent increase in complaints. Where an increase had been noted in complaints, despite no increases to the railway noise levels, the perceived causes for the changes summarised from free-form survey responses are as follows;

- Home confinement due to the COVID-19 pandemic and being exposed to railway noise during extended periods while working from home. This is a major point highlighted by many.
- Residents living near the tracks having a reduced tolerance and acceptance of noise.
- WHO publications and an increase in the number of published articles on this subject.
- Global aspirations for a better quality of life.
- Campaigns by rail operators resulting in the public being more informed about the options available to express concerns.
- More legislation that protects citizens.

This supports the observation that an increased awareness of adverse impacts of noise on health could be a factor in the apparent hardening of attitudes noted in recent annoyance/sleep disturbance studies.

3.2.5 Mitigation Measures

The majority of the respondents highlighted that the key factors driving the implementation of noise mitigation are value for money (13/18) closely followed by compliance with legal limits (12/18). Rail grinding and the retrofitting of freight wagons with composite brake blocks are two of the more commonly implemented and effective measures to reduce noise. This aligns with the PHENOMENA study which concluded that the best railway noise scenario in terms of their reduction in health burden and benefit-to-cost ratio was smoother and quieter vehicles and tracks. Although retrofitting freight wagons reduces complaints, the questionnaire responses indicated that that typical perceptions of this measure from lineside residents are not positive as the change is progressive. It is a general opinion among the respondents that, unless the noise emission is removed completely, complaints typically persist from the affected areas despite the overall noise levels being reduced or the frequency of the events occurring reduced. This aligns with research findings that people are more likely to respond defensively to an addition of sound than to a deletion of sound (Luz et al, 1983).

However, the most commonly sought-after mitigation measure by complainants was stated to be noise barriers with a close second being noise insulation treatment such as high-performance acoustic glazing. This also correlates with the order of complainant satisfaction of specific noise mitigation measures. It should be noted that the measures are not necessarily the most acoustically effective but are the ones which complainants perceive to be the most effective.

Reductions in train speeds were also highly sought after by complainants. This is not considered a practical mitigation measure by operators and infrastructure managers as it would reduce the efficiency and competitiveness of railways over other modes of transport.

Noise mitigation is most effectively used in combination with strong stakeholder engagement to minimise complaints. Frequently it may not be possible to mitigate the underlying cause of the noise complaint. However better provision of information, communication and consideration of community sensitivities could help address the frequency and severity of complaints.

4. Conclusion

The review presented in this paper provides a valuable contribution to the growing body of evidence on the impacts of railway noise on public health and well-being. Recent studies suggest that exposure-response relationships no longer favour railway noise over other transportation sources and the number of people annoyed by railway noise may have increased. There has been a perception within the railway sector that the rate of complaints from communities living along parts of the railways remain high, despite evidence that noise levels are decreasing as a result of a range of innovations and mitigation measures being employed across Europe. This is supported by the questionnaire responses, where a third of the respondents reported an increase in complaints despite no change in railway noise. Therefore, using the noise complaint rates as a metric might be misleading in addressing the issue of nuisance and health impacts from railway noise. The outcomes emphasise the necessity for robust and practical noise indicators, complementing existing metrics to better represent the characteristics of railway noise, including interdisciplinary efforts to understand public perception.

The questionnaire responses identified freight trains operating during night-time as the most common cause for complaints. The case studies provided by survey respondents revealed that the most common situations causing complaints are regarding a change in noise, presence of "atypical noise", areas of extreme sensitivity or where noise limits are exceeded. This is in line with research findings that noise complaints are a result of the 'arousal' effect of exposure to atypical high-noise events, when there is a conscious recognition of a change. However, these effects are not adequately measured using long term noise indicators such as L_{den} or L_{night}. The review highlights the importance of supplementary short-term noise indicators, such as L_{Amax}, to more accurately reflect the arousal response of individuals to atypical high-noise events, which may lead to short-term sleep disturbance.

To effectively mitigate railway noise, conventional measures must be combined with innovative approaches that more specifically address annoyance and complaints caused by railways, such as soundscape-based approaches. Infrastructure managers and operators need to work collaboratively to achieve cost-effective noise mitigation measures.

Further research is required to better understand the different exposure-response relationship for freight and passenger trains, and how these are influenced by local acoustic and non-acoustic factors. Investigations into annoyance from high-speed rail and perceptions of atypical noise, such as curve squeal, impulsive noise from joints and train horns, could lead to improvements in railway noise assessment, management and mitigation. Such research will be critical in developing evidence-based policies that reduce the adverse impacts of railway noise on public health and well-being.

Acknowledgements

This paper was originally published as: International Union of Railways (UIC) (2022). Nuisance and Health Impacts of Railway Noise (NOVITÀ project). Paris: UIC. Available online at: https://uic.org/IMG/pdf/nuisance_and_health_impacts_of_railway_noise.pdf.

References

Association of Noise Consultants, Institute of Acoustics and Chartered Institute of Environmental Health. (2017). ProPG: Planning & Noise, Professional Practice Guidance on Planning & Noise, New Residential Development, Appendix A. Dealing with Noise Events. [Online]. Available at: https://www.ioa.org.uk/publications/propg.

Brink, M., Schäffer, B., Vienneau, D., Foraster, M., Pieren, R., Eze, I.C., Cajochen, C., Probst-Hensch, N., Röösli, M., and Wunderli, J-M. (2019). A survey on exposure-response relationships for road, rail, and aircraft noise annoyance: Differences between continuous and intermittent noise. *Environment International*, Volume 125, p. 277–290.

Brown, A. L. and van Kamp, I. (2017). WHO Environmental Noise Guidelines for the European Region: A Systematic Review of Transport Noise Interventions and Their Impacts on Health. *International Journal of Environmental Research and Public Health*, 14(873), pp. 1-49.

Cantuaria, M.L., Waldroff, F.B., Wermuth, L., Pederson, E.R., Poulson, A.H., Thacher, J.D., Raaschou-Nielson, O., Ketzel, M., Khan, J., Valencia, V.H., Schmidt, J.H., and Sørensen, M. (2021). Residential exposure to transportation noise in Denmark and incidence of dementia: national cohort study. BMJ, 374(8305), p1954.

Elmenhorst, E., Griefahn, B., Rolny, V. & Basner, M., 2019. Comparing the Effects of Road, Railway, and Aircraft Noise on Sleep: Exposure–Response Relationships from Pooled Data of Three Laboratory Studies. *International Journal of Environmental Research and Public Health*, 16(1073).

European Commission (2020). Sustainble and Smart Mobility Strategy – putting European transport on track for the future. COM(2020) 789 final. Brussels: EC.

European Commission (2021). Assessment of Potential Health Benefits of Noise Abatement Measures in the EU. Phenomena project. Contract number 07.0203/2019/ETU/815591/ENV.A.3., Brussels: EC.

Eze, I.C., Foraster, M., Schaffner, E., Vienneau, D., Héritier, H., Rudzik, F., Thiesse, L., Pieren, R., Imboden, M., von Eckardstein, A., Schindler, C., Brink, M., Cajochen, C., Wunderli, J-M., Röösli, M., and Probst-Hensch, N. (2017). Long-term exposure to transportation noise and air pollution in relation to incident diabetes in the SAPALDIA study. *International Journal of Epidemiology*, 46(4), pp. 1115-1125.

Eze, I.C., Foraster, M., Schaffner, E., Vienneau, D., Pieren, R., Imboden, M., Wunderli, J-M., Cajochen, C., Brink, M., Röösli, M., and Probst-Hensch, N. (2020). Incidence of depression in relation to transportation noise exposure and noise annoyance in the SAPALDIA study. *Environment International*, Volume 144, p. 106014.

Foraster, M., Eze, I.C., Schaffner, E., Vienneau, D., Héritier, H., Endes, S., Rudzik, F., Thiesse, L., Pieren, R., Schindler, C., Schmidt-Trucksass, A., Brink, M., Cajochen, C., Wunderli, J-M., Röösli, M., and Probst-Hensch, N. (2017). Exposure to Road, Railway, and Aircraft Noise and Arterial Stiffness in the SAPALDIA Study: Annual Average Noise Levels and Temporal Noise Characteristics. Environmental Health Perspectives, 125(9), p. 097004.

Force Technology, Lärmkontor and Sintef, 2021. FAMOS. [Online] Available at: **http://famos-study.eu/** [Accessed 25 03 2022].

Gjestland, T. (2020a). Annoyance from road traffic noise has NOT changed. The annoyance reactions have been stable across the past five decades. In: *13th ICBEN Congress on Noise as a Public Health Problem*, Stockholm, 15-18 June 2020.

Gjestland, T. (2020b). New recommendations from WHO to limit annoyance from aircraft noise is not supported by existing evidence. In: *13th ICBEN Congress on Noise as a Public Health Problem*, Stockholm, 15-18 June 2020.

Guski, R. (1977). An Analysis of Spontaneous Noise Complaints. *Environmental Research*, Volume 13, pp. 229-236.

Guski, R. (2016). NORAH Overview. In: *Inter-Noise 2016*, Hamburg, 2016.

Guski, R., Schreckenberg, D. and Schuemer, R. (2017). WHO Environmental Noise Guidelines for the European Region: A Systematic Review on Environmental Noise and Annoyance. *International Journal of Environmental Research and Public Health*, Volume 14, p. 1539.

International Union of Railways (2021a). Railway Noise in Europe – State of the Art report. Paris: UIC. ISBN 978-2-7461-2990-0.

International Union of Railways (2021b). Railway Noise Complaints - UIC Noise and Vibration Sector Survey. [Online] Available at: https://uic.org/events/railway-noise-complaints [Accessed 15 06 2022].

Lechner, C., Schnaiter, D. and Bose-O'Reilly, S. (2021). Application of the noise annoyance equivalents model for aircraft, rail and road traffic noise to self-reported sleep disturbance. *Acta Acustica*, 5(12).

Lercher, P. and Botteldooren, D. (2006). General and/or local assessment of the impact of transportation noise in environmental health impact studies? In: *Proceedings of Euronoise 2006, CD-ROM edition*, Tampere, Finland, 30 May - 1 June 2006.

Luz, G.A., Raspet, R. and Schomer, P.D. (1983). An analysis of community complaints to noise. *Journal of the Acoustical Society of America*, 73(4).

Maziul, M., Job, R.F.S., and Vogt, J. (2005). Complaint data as an index of annoyance – theoretical and methodological issues. *Noise Health*, 7(28), pp. 17-27.

Miedema, H.M. and Oudshoorn, C.G. (2001). Annoyance from transportation noise: relationships with exposure metrics DNL and DENL and their confidence intervals. *Environmental Health Perspectives*, 109(4), pp. 409-16.

Rudzik, F., Thiesse, L., Pieren, R., Wunderli, J-M., Brink, M., Foraster, M., Héritier, H., Eze, I.C., Garbazza, C., Vienneau, D., Probst-Hensch, N., Röösli, M., and Cajochen, C. (2018). Sleep spindle characteristics and arousability from nighttime transportation noise exposure in healthy young and older individuals. *SLEEPJ*, 41(7), pp. 1-14.

Shigenori, Y., Makoto, M. and Takashi, Y. (2020). Causal analysis of complaint behaviours due to environmental noises. In: *INTER-NOISE and NOISE-CON Congress and Conference Proceedings, InterNoise20*, Seoul, Korea, 2020.

Swiss Tropical and Public Health Institute, Centre for Chronobiology, Empa and Nsphere. (2021). What is the SiRENE study? [Online] Available at: http://www.sirene-studie.ch/ [Accessed 25 03 2022].

United Nations Environment Programme. (2022). Noise, Blazes and Mismatches. Emerging Issues of Environmental Concern, Frontiers 2022. Nairobi: UNEP.

World Health Organization (1946). Constitution of the World Health Organization. [Online] Available at: https://www.who.int/about/governance/constitution [Accessed 27 03 2022].

World Health Organization (2018). Environmental Noise Guidelines for the European Region. Copenhagen: WHO Regional Office for Europe. Available at https://www.euro.who.int/en/publications/abstracts/environmental-noise-guidelines-fo

Ken Hunu, EngD, PE, DWRE, PMP, CFM
Sr Technical Manager
Technical Professional Organization, Water
Raleigh, NC, USA

Rebecca Purvis, PhD, PE
Sr. Engineer
Technical Professional Organization, Water
Raleigh, NC, USA

Amit Sachan, PE, CFM
Sr. Project Director
Infrastructure Solutions, USA
Raleigh, NC, USA

Water and Environment

04: Hydrologic and Hydraulic Design of the West Lumberton Flood Gate, Lumberton, NC

Abstract

The western part of the City of Lumberton is protected from flooding from the Lumber River by a levee system that consists of three segments: the levee that was designed and constructed by the Natural Resources Conservation Service (NRCS) (formerly the Soil Conservation Service), a portion of I-95 highway embankment, and a portion of Alamac Road. An opening exists within the I-95 highway embankment portion of the levee system to allow a rail corridor and a road to traverse under the highway. During extreme storms, the Lumber River overflows its banks and floods the western part of the city through this opening. Flow also overtops low segments of the I-95 portion of the levee protection system. Floodwaters from recent extreme weather events, like Hurricane Matthew (2016) and Hurricane Florence (2018), flooded the city through the opening in the I-95 embankment, causing major damages to residences and businesses. The City of Lumberton plans to improve its flood resiliency by installing a flood gate closure structure along the opening within the I-95 highway embankment to prevent future flooding. The hydrologic and hydraulic design of the gate was completed by AtkinsRéalis and included the development of a detailed hydrologic model, a detailed hydraulic model, and wave runup calculations to estimate freeboard. The recommended range of top of flood gate elevations is 129.6 to 134.2 feet; NAVD88 provides protection up to the 1,000-year flood.

KEYWORDS
Flood gate design; Hydrologic and hydraulic modeling; Resiliency; Wave height and runoff; Freeboard

1. Introduction

The City of Lumberton, NC is susceptible to flooding from the Lumber River. An existing levee system provides flood prevention to the City of Lumberton. The levee system consists of three segments: the levee that was designed and constructed by the Natural Resources Conservation Service (NRCS), a portion of I-95 highway embankment, and a portion of Alamac Road (Figure 1). An opening exists within the I-95 highway embankment to allow a CSX rail corridor and VFW Road to traverse under the highway. During extreme storms, the Lumber River overflows its banks and through the opening in I-95, flooding portions of the City of Lumberton. Floodwaters from recent extreme weather events, like Hurricane Matthew (2016) and Hurricane Florence (2018), flooded the city through the I-95 embankment opening, causing major damages to residences and businesses. During Hurricane Matthew, no attempts were made to close the opening, resulting in significant flows through the opening into the protected area. In preparation for Hurricane Florence, sandbags and temporary barriers were placed across the opening. While these measures eventually failed and washed out, they did provide initial protection. For this reason, the City of Lumberton wants to install a permanent protection method in the form of flood gates across the I-95 opening; this would require closing gates over the existing CSX railroad corridor and local road to prevent floodwaters from entering the southern part of City. The purpose of this project is to design and install the flood gate at this most vulnerable location to improve the flood resilience of the City of Lumberton.

To establish the height of the flood gate closure structure, a detailed hydrologic and hydraulic (H&H) study of the Lumber River is required. The H&H study includes a hydrologic analysis of the Lumber River from the headwaters located near Eagle Springs, North Carolina (NC) to the confluence of the Lumber River and Jacob Swamp located about 4 miles downstream of Lumberton. A hydraulic model was developed along the Lumber River and of its tributaries near the city of Lumberton to establish flood elevations for use in the flood gate closure design.

FIGURE 1

Lumberton site location map

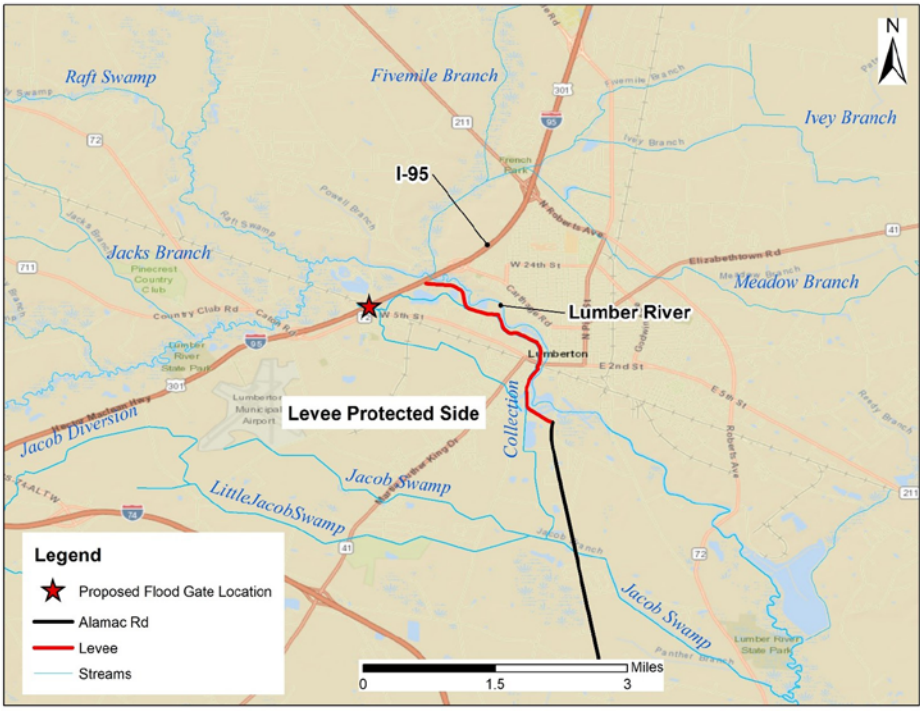

The Lumber River basin is in southeastern North Carolina, approximately 30 miles (mi) south of Fayetteville, NC, and has a total drainage area of 748 mi^2 at the confluence of the Lumber River and Jacob Swamp. The Lumber River basin at the gauge location is entirely within the state of North Carolina and encompasses portions of six different counties: Robeson, Hoke, Scotland, Moore, Richmond, and Montgomery.

The state of North Carolina is divided into eight climate regions (NOAA, 2020). The Lumber River basin is in two of the regions: Southern Piedmont for the northern quarter and Southern Coastal Plains for much of the basin. The mean annual precipitations for the NOAA-defined NC climate regions of Southern Piedmont and Southern Coastal Plain are 46.59 in and 49.23 in, respectively, which are well above the national average of 29.94 in (NOAA, 2020).

Significant rainfall fell across the entire state of North Carolina in September 2004 as a result of Hurricane Frances. Rainfall gauges near the Lumber River basin reported total rainfall depths from the storm from 4.31 to 11.87 in (NCSCO,2015). The USGS gauge on Lumber River at Lumberton (USGS 02134170) reported a peak streamflow of 7,420 cubic feet per second (cfs) in the early hours of September 11, 2004 (USGS, 2020).

The flood of October 2016 was the result of Hurricane Matthew. The total recorded precipitation depth in Lumberton, NC from this storm was 12.53 inches. Recorded peak flow at the USGS gauges in Lumberton (02134170) and Boardman, NC (02134500) were 14,600 cfs and 38,200 cfs, respectively (USGS, 2020). The recorded peak of 38,200 cfs at the USGS gauge in Boardman, NC is the highest ever recorded flow to date and it resulted in a peak stage of 14.43 ft (USGS, 2016). The levee did not overtop or fail during Hurricane Matthew. Flooding in the area was caused by overtopping of I-95, flow through the I-95 opening at VFW Road/CSX Railroad underpass, and inadequate capacity of the internal drainage system (Figure 2).

FIGURE 2

Flooding along I-95 and inside the Lumberton Levee from Hurricane Matthew; area to right of road is the levee protected side of Lumberton (Source: City of Lumberton)

The flood of September 2018 was the result of Hurricane Florence. Total rainfall values reported by NOAA at stations 2.3 mi northeast of Lumberton and 2.6 east-southeast of Lumberton are 22.8 inches and 21.4 inches, respectively. Hurricane Florence resulted in the highest ever recorded peak flow at the USGS gauge in Lumberton (02134170 Lumber River at Lumberton) of 17,100 cfs with a peak stage of 22.21 ft. Hurricane Florence caused major flooding within the City of Lumberton as floodwaters passed through the opening under I-95 at the VFW Road and CSX railroad intersection into the city (Figure 3). USGS estimates about 12 percent of the total recorded peak flow passed through the opening under I-95.

FIGURE 3

Flooding under I-95 at VFW Road and CSX railroad in Lumberton, NC from Hurricane Florence (Source: City of Lumberton)

2. Data Collection

The majority of the Lumber Basin consists of B and C soils, with some D soils and minimal A soils (USDA, 2020). The northern portion of the watershed is primarily evergreen forest, while the southern half is cultivated crops and the developed area of Lumberton, NC (USDA, 2020).

Terrain tiles were QL2 Light Detection and Ranging (LiDAR) obtained from the North Carolina Floodplain Mapping Program (NCFMP). The elevation within the Lumber River basin ranges from 102 to 734 ft NAVD 88. Bathymetric data for Lumber River, Jacob Swamp, and Little Jacob Swamp were obtained from the Preliminary Lumber River one-dimensional (1D) Hydrologic Engineering Center's River Analysis System (HEC-RAS) model obtained from NCFMP as part of this project. Cross section data was collected in the field for Fivemile Branch, Meadow Branch, Gum Branch, Cotton Mill Branch, and the Collection Canal. Field survey was conducted to validate structure dimensions from effective models/inspection reports and collect dimensions for structures without pre-existing data. Field survey was also conducted to gather cross section information for reaches within the levee protected area that did not have an effective model with bathymetry.

There are 11 precipitation gauges within or nearby the drainage basin, 8 of which had precipitation data for selected calibration and verification storms. For each event, Thiessen polygons were created based on the rainfall gauges with available data to estimate the rainfall contribution from each gauge for each sub-basin. The storm hyetograph applied to a sub-basin is the weighted average from all contributing rainfall gauges.

There is a USGS stream gauge approximately 1.7 mi downstream of the Lumberton flood gate location, USGS 02134170 Lumber River at Lumberton, NC (Figure 4). Additionally, there is a gauge upstream on Lumber River in Maxton, NC (USGS 02133624) and a gauge downstream of our modeled basin on Lumber River in Boardman, NC (USGS 02134500). Eleven high water mark (HWM) locations and depths were obtained from a field visit with City of Lumberton waterworks department personnel. Additionally, HWM for Hurricanes Matthew and Florence were obtained from the USGS Flood Event Viewer application (United States Geological Survey, 2019).

FIGURE 4

USGS gauge (02134170 Lumber River at Lumberton, NC) within the Lumber River basin

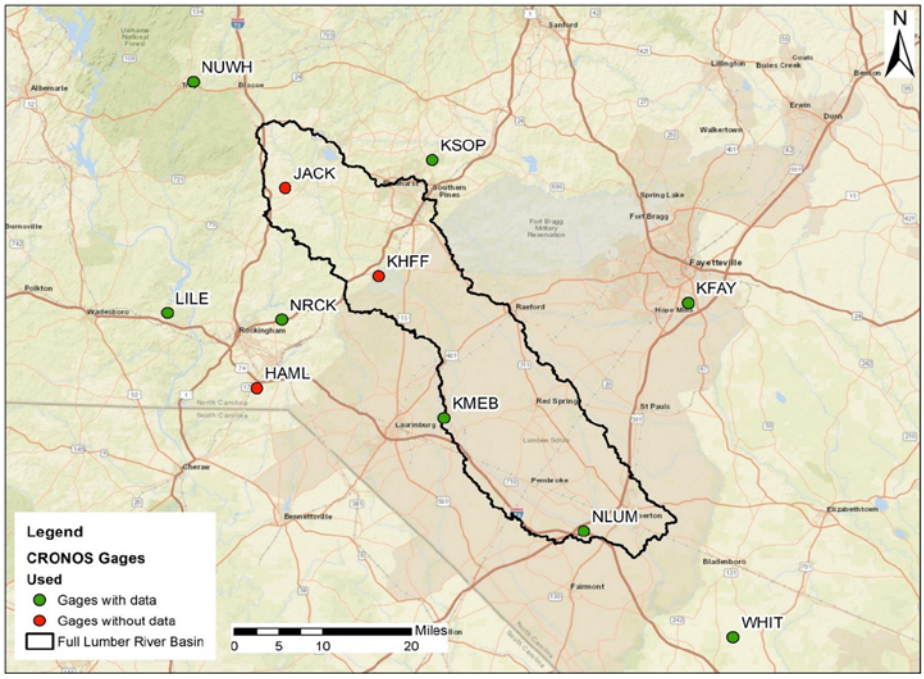

An inventory of hydraulic structures was obtained from the North Carolina Flood Risk Information System website (NCFMP, 2019) and NCDOT Bridges Map (NCDOT, 2019). Levee data was obtained from AECOM Project No. 60548447, Lumberton Flood Mitigation Report Levee Plans.

3. Design Flood Selection

3.1 REVIEW OF FEMA LEVEE ACCREDITATION GUIDELINES

FEMA provides guidelines and requirements that must be met for levee systems to be accredited (FEMA, 1986). The FEMA requirements, as specified in 44 Code of Federal Regulations (CFR) 65.10 (FEMA, 2008), related to levee height are as follows:

- Levees mush have a minimum freeboard of 3 ft above the 100-year flood elevation (base flood elevation), with
- an additional 1 ft of freeboard at locations within 100 ft of structures (such as bridges) or wherever the flow is restricted, and
- an additional 0.5 ft of freeboard at the upstream end of a levee.

The minimum elevation of the flood gate will therefore have to be above the 100-year water surface elevation plus 4.5 ft in order to meet FEMA accreditation requirements. The levee is currently not FEMA accredited.

3.2 FLOOD FREQUENCY ANALYSIS

It is the desire of the City of Lumberton to have a flood gate that can, at a minimum, prevent flooding from events like that of Hurricanes Matthew and Florence, which are the highest recorded flooding events in Lumberton. Flood frequency analysis was performed to estimate the recurrence intervals of historic floods (Hurricane Matthew and Hurricane Florence) near the site. For reference, the recorded peak flow rate from Hurricane Matthew at the Lumberton and Boardman gauges were 14,600 cfs and 38,200 cfs, respectively, and the recorded peak flows for Hurricane Florence at the Lumberton and Boardman gauges were 17,100 cfs and 35,400 cfs, respectively.

Flow measurements at the Lumberton gauge during Hurricane Matthew did not account for flow that was diverted through the I-95 opening at the VFW Road and the CSX railroad track. The actual peak flow at Lumberton from Hurricane Matthew is therefore larger than the reported peak flow of 14,600 cfs. USGS records indicate that diverted flow through the I-95 opening during Hurricane Florence was about 2,000 cfs, approximately 12% of the total flow (USGS Correspondence). Based on the recorded water surface elevations at the USGS gauge in Lumberton (119.7 ft for Hurricane Florence versus 119.4 ft for Hurricane Matthew) for the two events, a similar amount of flow can be assumed to have been diverted through the I-95 opening during Hurricane Matthew. This implies that the actual peak flow at Lumberton from Hurricane Matthew is about 16,600 cfs. This estimate is consistent with the simulated peak flow from the Hydrologic Engineering Center's Hydrologic Modeling System (HEC-HMS) model. Additional analysis was performed with the adjusted peak flow for Hurricane Matthew to assess the sensitivity of the estimated return periods to the change in the peak flowrate for that event.

PeakFQ (version 7.3) (USGS, 2019a) was utilized for the analysis. The flood frequency analysis was conducted for the gauge at Lumberton (Gauge 1, USGS 02134170). This gauge had a record from 2001-2018 and the downstream gauge (Gauge 2, USGS 02134500) had a record from 1901-2018.

Two different methods were used in estimating the return periods in order to assess the impact gauge record length and method for gauge adjustment based on nearby gauge(s) with longer records:

- Method 1 uses Gauge 1 observed data only.
- Method 2 extends the record at Gauge 1 based on Gauge 2 using the MOVE method.

3.2.1 Method 1

The results of the analysis based only on the Gauge 1 records with the reported and adjusted peak flow rates of 14,600 cfs, and 16,600 cfs for Hurricane Matthew are shown in Table 1. Based on this data, the return periods for Hurricane Matthew and Florence are between 30 to 50 years. The upper (95%) and lower (5%) confidence limits of the peak flow estimates are also reported to show the potential range of peak flows that could occur for each return period.

TABLE 1

Calculated discharge per return period at the Lumberton gauge (USGS 02134170)

Return Period (years)	With Reported Matthew Peak Flow Rate			With Adjusted Matthew Peak Flow Rate		
	Peak Flow (cfs)	Peak Flow 5% Lower Bound	Peak Flow 95% Upper Bound	Peak Flow (cfs)	Peak Flow 5% Lower Bound	Peak Flow 95% Upper Bound
1.25	1,654	1,122	2,269	1,645	1,109	2,267
2	3,130	2,283	4,375	3,145	2,282	4,427
5	6,139	4,389	9,687	6,254	4,440	9,979
10	8,856	6,103	15,830	9,099	6,218	16,510
25	13,240	8,603	28,460	13,740	8,836	30,140
50	17,270	10,680	43,080	18,050	11,030	46,170
100	22,020	12,920	64,080	23,170	13,410	69,470
200	27,600	15,330	94,040	29,230	15,990	130,100
500	36,460	18,760	153,600	38,940	19,700	171,000

3.2.2 Method 2

The maintenance of variance estimator (MOVE) method described in Bulletin #17C (USGS, 2019 b) was used to extend Gauge 1 records. This method extends a shorter record series using a supplemental series while maintaining the variance of the extended series. The procedure of the MOVE adds observations (ne) to the original records (y). The values of the new observations have the information to transfer the mean and variance of the original records. The statistical analysis following this procedure resulted in a total of 38 records (n1+ne), compared to 18 in the original records (n1). A linear regression model was developed to estimate an additional 20 observations (ne). The 38 records were used as inputs for PeakFQ analysis. Table 2 below show the frequency analysis results.

TABLE 2

Calculated discharge per return period based on the extended Lumberton gauge records (USGS 02134170)

Return Period (years)	Peak Flow (cfs)	Peak Flow 5% Lower Bound	Peak Flow 95% Upper Bound
1.25	2,080	1,736	2,442
2	3,305	2,821	3,898
5	5,419	4,547	6,734
10	7,109	5,826	9,393
25	9,588	7,561	14,000
50	11,700	8,923	18,580
100	14,040	10,330	24,370
200	16,640	11,800	31,680
500	20,530	13,820	44,300

The estimated return periods for Hurricane Matthew and Florence are approximately 120 and 235 years, respectively. When using the updated peak flow value of 16,600 cfs for Hurricane Matthew in the analysis, the return period for hurricane Matthew and Florence are approximately 170 and 190 years, respectively. Table 3 below show the results of the analysis using the adjusted flow for Hurricane Matthew.

TABLE 3

Calculated discharge per return period based on the extended Lumberton gauge records (USGS 02134170) and altered Hurricane Matthew

Return Period (years)	Peak Flow (cfs)	Peak Flow 5% Lower Bound	Peak Flow 95% Upper Bound
1.25	2,080	1,742	2,436
2	3,325	2,844	3,916
5	5,500	4,626	6,837
10	7,255	5,964	9,609
25	9,852	7,795	14,460
50	12,080	9,242	19,320
100	14,560	10,750	25,500
200	17,340	12,320	33,340
500	21,520	14,500	46,990

3.2.3 Gauge Weighted Regression Estimates

Regional regression flow rate for each return period was calculated using USGS-developed regional regression equations for North Carolina (USGS, 2009). StreamStats was used to determine the basin percentage in each hydrologic region (1-5). A total of 45 percent of Lumber River basin is in Region 3 and 55 percent is in Region 4 (USGS, 2016). Based on the PeakFQ estimated gauge peak flow at the Lumberton gauge (USGS 02134170), regression estimated peak flow, and variance of prediction for each value, the gauge weighted peak flow was estimated for the 2 – 500-year return periods (Table 4). The resulting return periods for Hurricanes Matthew and Florence remain the same as using only the gauge estimates.

TABLE 4

Regional regression weighted peak flow rate estimates for Methods 2 approaches

Return Period (years)	Regression Peak Flow Rate (cfs)	Weighted Peak Flow Rate (cfs)	
		Method 2 – unaltered Matthew	Method 2 – altered Matthew
2	4,006	3,410	3,429
5	6,740	5,546	5,616
10	8,797	7,320	7,449
25	11,440	9,903	10,125
50	13,620	12,090	12,400
100	15,799	14,463	14,864
200	18,043	17,029	17,539
500	20,993	20,678	21,347

3.3 RECOMMENDED DESIGN FLOOD FREQUENCY

The results of the analysis indicate that there is a high amount of uncertainty in regard to the return periods for floods produced by Hurricanes Matthew and Florence at Lumberton, NC. This is due to the limited gauge records at that location. Updating the limited gauge data at the USGS gauge at Lumberton based on the longer record at the USGS gauge in Boardman provides more realistic estimates of the return periods. Based on this approach, the return periods for the flood produced by both Hurricanes Matthew and Florence are about 170 and 190 years, respectively.

The minimum top of gate elevation must be the higher of the peak water surface elevation from Hurricane Florence at the gate location or the 100-year elevation at the gate plus 4.5 ft of freeboard. The return period of such a flood will be about 200-years or greater.

4. Hydrologic Model Development

4.1 GENERAL METHODOLOGY

The Hydrologic Engineering Center Hydrologic Modeling System (HEC-HMS) version 4.2.1 software was used to model the Lumber River basin and develop outflow hydrographs for each sub-basin. Sub-basins were based on StreamStats delineation (USGS, 2016) and verified using the QL2 LiDAR. There are 12 sub-basins for tributaries to the Lumber River and an additional 2 sub-basins within the HEC-HMS model to account for the drainage area right along the channel, which was not accounted for in the other basins. The sub-basins are called: Back Swamp, Bear Swamp, Fivemile downstream, Fivemile upstream, Lumberton Canals, Ivey Branch, Jacks Branch, Jacob Branch, Jacob Swamp, Lumber downstream, Lumber upstream, Meadow Branch, Raft Swamp, and White Oak (Figure 5).

FIGURE 5

HEC-HMS sub-basins, reaches, and junctions

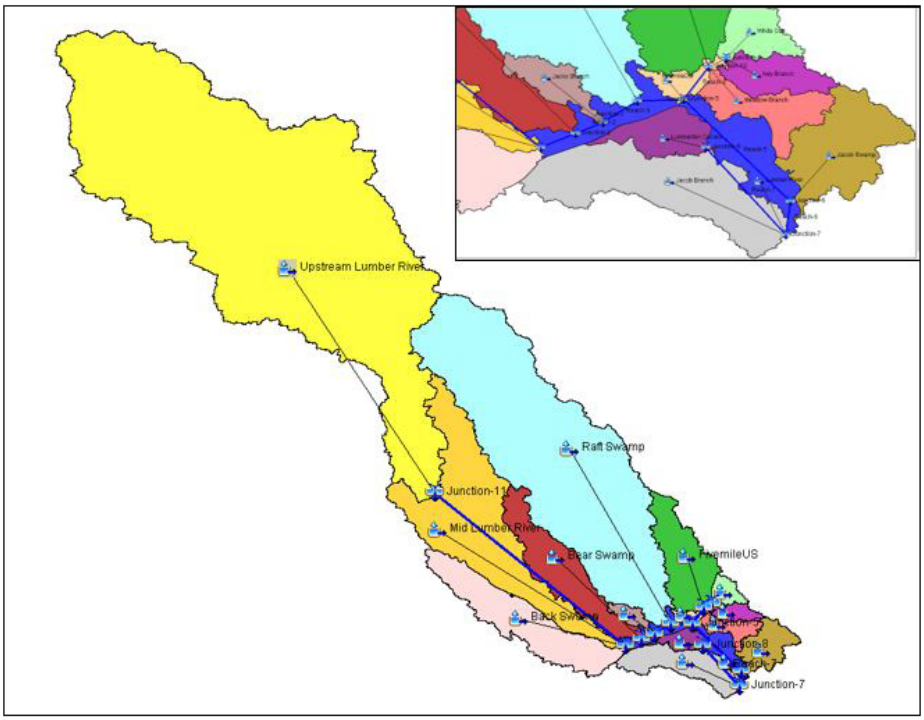

Predictive ability of the modeling method based on experience was also a factor. Based on these factors, the Snyder Unit Hydrograph method was selected and used to characterize the rainfall-runoff relationship of the sub-basins within the watershed. The Snyder Unit Hydrograph method allows for parameters to be compared across events and sub-basins so that the method can be transformed to ungagged sub-basins. The loss method was set to 'Initial and Constant.' The constant loss, lag time, and peaking coefficient are variables based on basin characteristics and thus were calibrated. Initial losses were calculated based on each sub-basin curve number and were adjusted during calibration based on known antecedent soil conditions for each calibration and verification storm.

Rainfall and streamflow data were added as time series data. A precipitation gauge was added for each basin for each simulated event. The number of precipitation gauges added per event was based on the number of rainfall gauges with available data and the associated weighted rainfall developed. The precipitation gauges included values covering the full time period of the control specification with a one-hour interval. Discharge gauges were added for each event at the calibration points within the model (USGS Gauge 02133624 at Maxton and USGS Gauge 02134170 at Lumberton). The discharge gauges contained the discharge data for each storm as recorded at those gauge locations. Discharge was added at a 15-minute interval.

Initial parameter estimates were estimated using Geographic Information System (GIS) data and applicable parameter ranges. Model parameters were refined through calibration and validated by comparing model results to historic flow measurements. Cross-section data was obtained from the effective 1-D cross-sections or LiDAR data for each reach to incorporate flow routing.

4.2 MODEL CALIBRATION TO HISTORIC EVENTS

Four events were selected based on peak discharge: September 2004, October 2015, October 2016 (Hurricane Matthew), and September 2018 (Hurricane Florence). The 2004, 2015, and 2018 events were used for calibration and the 2016 event used for validation of the model.

The points of comparing simulated and observed peak flow rate, volume, and time of peak are at a junction along Lumber River where the USGS gauge in Lumberton is located and at the location of the USGS gauge in Maxton. During calibration trials the peak simulated flow rate, hydrograph shape, and time of peak flowrate were compared to what was observed at the USGS gauges from the respective storm event. Calibration of the model to the observed values at the USGS gauge in Lumberton was prioritized over the observed values at the USGS gauge in Maxton due to the proximities of the 2 gauge locations to the location of the proposed gate.

The calibration parameters were changed for each of the sub-basins, relative to basin characteristics, until the peak flow rate, volume, and time to peak were as close to that of the observed as the model could achieve. Results for each calibration are shown in Tables 5, 6, and 7. The calibrated parameters were able to accurately model the peak flow rate and time of peak for all the storms. Except for the October 2015 storm, the calibrated parameters were also able to accurately model the hydrograph shapes and volumes for the storms. The October 2015 storm is the smallest of the three storms, with a return period of less than 2 years. Since the design storms are more like the other two storms in terms of magnitude, additional iterations of the calibration parameters to get a better match for the volume for that storm was not necessary.

The calibrated parameters for each of the three calibration storms were averaged to obtain the calibrated parameters for the sub-basins. The calibrated and verified model was then used to simulate design flood hydrographs that were routed in a hydraulic model.

TABLE 5

Peak flow comparison between observed and simulated calibrated events

Storm	Peak Flow rate (cfs)		
	Observed	Simulated	% Difference
	At Lumberton Gauge (USGS 02134170)		
Sept 2004	7,420	7,097	-4%
Oct 2015	2,390	2,421	1%
Sept 2018	17,100	17,257	1%

TABLE 6

Time of peak comparison between observed and simulated calibrated events

Storm	Time Date and Time		
	Observed	Simulated	Difference (hrs)
	At Lumberton Gauge (USGS 02134170)		
Sept 2004	9/11/2004 0:30	9/11/2004 12:00	10
Oct 2015	10/9/2015 15:45	10/9/2015 12:00	-3.75
Sept 2018	9/17/2018 11:00	9/17/2018 11:00	0

TABLE 7

Volume comparison between observed (USGS 02134170 at Lumberton) and simulated calibrated events

Storm	Volume (ac-ft)		
	Observed	Simulated	% Difference
	At Lumberton Gauge (USGS 02134170)		
Sept 2004	152,897	149,569	-2%
Oct 2015	38,912	27,568	-29%
Sept 2018	230,179	229,185	-0.4%

4.3 MODEL VALIDATION TO HISTORIC EVENTS

Following calibration, the average parameters were applied to a verification event. Hurricane Matthew, which occurred in October 2016, was selected as the verification event. Verification using the average parameters overpredicted the peak flow rate but matched the time of peak (Tables 8, 9, 10). Graphical inspection of the observed and simulated hydrographs also indicates a good match of the rising and falling limbs. As discussed previously, the recorded peak flow at the USGS gauge of 14,600 cfs during Hurricane Matthew did not account for the diverted flow through the I-95 opening. Thus, this verification, while higher, is an accurate representation of the peak flows in the area.

TABLE 8

Peak flow comparison between observed and simulated for a verification event

Storm	Peak Flow rate (cfs)		
	Observed	Simulated	% Difference
	At Lumberton Gauge (USGS 02134170)		
Oct 2016	14,600	16,550	13%

TABLE 9

Time of peak flow comparison between observed and simulated for a verification event

Storm	Time Date and Time		
	Observed	Simulated	Difference (hrs)
	At Lumberton Gauge (USGS 02134170)		
Oct 2016	10/10/2016 7:00	10/10/2016 10:00	3

TABLE 10

Volume comparison between observed and simulated for a verification event

Storm	Volume (acre-ft)		
	Observed	Simulated	% Difference
	At Lumberton Gauge (USGS 02134170)		
Oct 2016	223,956	197,598	-12%

4.4 DESIGN FLOOD SIMULATIONS

Using the calibrated and verified parameters, floods from a 100-year to 1,000-year return period were simulated in HEC-HMS. A 48-hour rainfall event was selected as the design flood duration with an SCS Type II rainfall distribution (NRCS, 2019) and the assumption that the peak rainfall occurred within the first 24-hour period of the event. The developed rainfall distribution was added to the HMS model as a cumulative precipitation gauge for each event. Simulated peak flow rates were lower than both those from FEMA and the gauge statistics (Table 11). The FEMA peak flow estimates are based on regression equations which are regionally based and not specific to the Lumber River Basin. The simulated results are from a calibrated and verified model for the basin and hence provide a more reliable estimate of both the peak flow and streamflow hydrograph for the basin.

TABLE 11

Peak flow comparison between simulated HEC-HMS, FEMA reports, and gauge statistics for a 48-hour event

Recurrence Interval (years)	Simulated Peak Flow (cfs)	FEMA Peak Flow (cfs)	Gauge Statistics Flow (cfs)	% Difference FEMA	% Difference Gauge
100	13,140	14,900	14,000	-13%	-11%
500	22,110	20,200	20,530	9%	3%
1,000	26,990	-	-	-	-

5. Hydraulic Model Development

A detailed two-dimensional (2-D) model of the City of Lumberton, Lumber River, and its tributaries in the vicinity of the city was developed to help determine design flood elevations for the proposed gate (Figure 6). The model was developed using version 5.0.7 of the USACE HEC-RAS model (USACE, 2019). The locations of the boundary conditions were placed far enough from the location of the proposed gate so that boundary condition impacts would be null. The location and geometry of the flood gate within the model is based on the initial designed layout of the flood gate.

Base model Manning's n coefficients were based on "normal" applicable values per land use class (Chow, 1959; Calenda et al., 2005). A GIS shapefile of Lumber River and Fivemile Branch was used to override the land use of Lumber River and Fivemile Branch. The channel segment was assigned a base Manning's n coefficient of 0.045. The initial roughness coefficients were modified during the model calibration phase.

A mesh resolution of 250 ft was applied to the 2-D flow area. Refinement regions were used to represent areas of higher urbanization, Lumber River, and the flood gate location. A resolution of 100 ft was applied for urban areas and Lumber River, while a resolution of 50 ft was used for the flood gate location. The mesh utilized refinement regions, 2-D connections, and breaklines to accurately capture focal points and variations within the terrain.

The Lumberton levee was included as a 2-D connection with top of levee elevations taken from AECOM Project No. 60548447, Lumberton Flood Mitigation Report. Provided surveyed top of levee elevations were within a few inches of the top of levee elevations in the terrain. For levee segments that were not surveyed, LiDAR elevations were utilized. Levee grid size was enforced as 20 x 20 ft to define the top width.

Hydraulic structures within the modeled domain were modeled as either culverts or as 2-D connections with notches. The normal 2-D equation was selected as the overflow computation method as it is computationally more stable compared to the weir equation option. Gravity drains were not modeled. For bridges along Lumber River, the total open area of each modeled culvert was derived from the effective Lumber River model or field survey.

FIGURE 6

2-D model extent and boundary condition locations

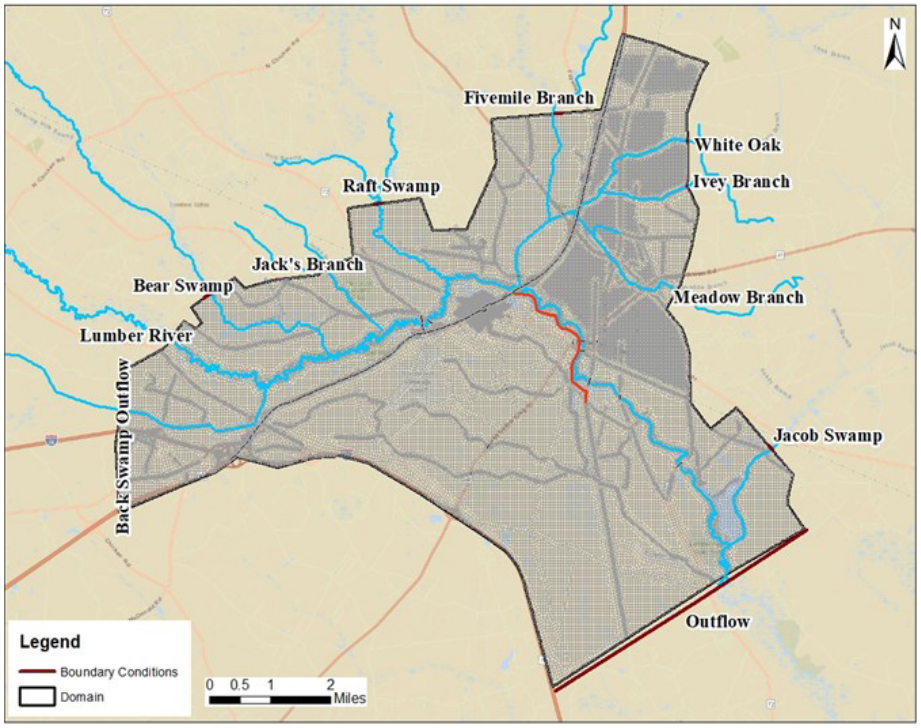

The 2-D HEC-RAS model was calibrated and verified by comparing the simulated peak stages and flows to observed peak stages and flows, and high-water marks. Two flooding events were identified and selected for use in calibration and verification (Table 12). Hurricane Florence in September 2018 was used for calibration and Hurricane Matthew from October 2016 was used for verification. Matching HWMs in the vicinity of the proposed gate was prioritized over matching water surface elevations at the USGS gauge location during the calibration process.

TABLE 12

Observed versus simulated results at the USGS Gauge in Lumberton

Gauge vs. Simulated Results

Storm	Peak Flowrate (cfs)			Peak Stage (ft, NAVD88)		
	Observed	Simulated	% Difference	Observed	Simulated	Difference (ft)
Calibration						
Sept 2018 (Hurricane Florence)	17,100	16,361	-4.3	119.7	120.9	1.2

The difference between the simulated peak water surface elevation and the USGS high-water marks ranges from -1.6 ft to 1.1 ft. Near the gate, the model results ate within 0.2 ft of the USGS HWM elevations. The simulated peak water surface elevation is about 1.1 ft higher than the observed elevation at the location of the surveyed high-water mark near the proposed gate location. The analysis shows that for USGS high-water marks around the gate location, the model tends to underpredict values. Whereas for field collected high-water marks around the gate location, the model overpredicts values. This trend may reflect inherent errors associated with the collection of the high-water mark data. Achieving calibration results that fall in-between the two data sets was the desired goal.

During the calibration process, the Manning's n values were generally increased to achieve a better match between simulated and observed water levels. Changes to the Manning's n values for all land use classes are within the published Manning's n value ranges (Chow, 1959; Calenda et al., 2005). The calibrated Manning's n coefficient was used to simulate Hurricane Matthew for verification. The results are shown in Table 13.

TABLE 13

Lumber River verification historical storms data versus simulated results

Gauge vs. Simulated Results

Storm	Peak Flowrate (cfs)			Peak Stage (ft, NAVD88)		
	Observed	Simulated	% Difference	Observed	Simulated	Difference (ft)
Verification						
Oct 2016 (Hurricane Matthew)	16600	15,055	-9.3	119.4	120.8	1.4

5.1 DESIGN FLOOD SIMULATIONS AND RESULTS

5.1.1 Design Flood Simulations

The 100-year, 500-year, and 1,000-year peak stages at the proposed gate location were simulated using the calibrated HEC-RAS model. The 100-year, 500-year, and 1,000-year hydrographs developed were used as the inflow boundary conditions for the simulations. The duration of all the design storms was 48 hours.

Geometry files were created with and without the proposed gate. There are low segments of I-95 that overtop during extreme events (storms equal to or greater than the 100-year flood). NCDOT is planning on widening and raising the top elevation of the segment of I-95 that form part of the City of Lumberton flood protection system. A separate geometry file was created with the low segments raised so they are not overtopped. All three geometry files use the calibrated and verified Manning's n-coefficients.

Ten different runs were performed using the three different geometry files. The ten plans are:

1. **100yr without gate** – Unsteady flow: 100YR, Geometry: Lumber River without Gate-Calibrated
2. **100yr with gate** – Unsteady flow: 100YR, Geometry: Lumber River with Gate-Calibrated
3. **100yr with gate and raised I-95** – Unsteady flow: 100YR, Geometry: Lumber River with Gate and Raised I-95
4. **500yr without gate** – Unsteady flow: 500YR, Geometry: Lumber River without Gate- Calibrated
5. **500yr with gate** – Unsteady flow: 500YR, Geometry: Lumber River with Gate - Calibrated
6. **500yr with gate and raised I-95** – Unsteady flow: 500YR, Geometry: Lumber River with Gate and Raised I-95
7. **1,000yr without gate** – Unsteady flow: 1,000YR, Geometry: Lumber River without Gate - Calibrated
8. **1,000yr with gate** – Unsteady flow: 1,000YR, Geometry: Lumber River with Gate - Calibrated
9. **1,000yr with gate and raised I-95** – Unsteady flow: 1,000YR, Geometry: Lumber River with Gate and Raised I-95
10. **Florence Design** – Unsteady flow: Hurricane Florence, Geometry: Lumber River with Gate and Raised I-95

Plans using the geometry "Lumber River without Gate - Calibrated" represent existing conditions, without the gate in place or with I-95 raised. Plans with the geometry "Lumber River with Gate - Calibrated" represent proposed conditions with the flood gate in place but without any changes to the top of road elevation of I-95. Plans with the geometry "Lumber River with Gate and Raised I-95" are represent proposed conditions with the flood gate in place and with the top elevations of I-95 raised to prevent overtopping. Simulations with and without the gate provide insights into possible impacts from the installation of the flood gate and raising the top elevations of I-95. Hurricane Florence was also simulated with the gate in place and with I-95 raised to determine the resulting peak water surface elevation at the proposed gate location for the flood of record.

5.1.2 Hydraulic Results

The maximum water surface elevations from the 10 simulations are summarized in Table 14. The maximum water surface elevations were extracted from a profile line along the upstream end of the proposed gate location in RasMapper.

TABLE 14

Maximum Water Surface Elevation (WSE) from simulations at location of flood gate

Storm Event	Maximum WSE (feet, NAVD88)		
	Without Gate	With Gate	With Gate and Raised I-95
100 YR	123.9	124.2	124.2
500 YR	125.1	125.2	127.6
1,000 YR	125.3	125.4	128.1
Hurricane Florence	124.7	-	125.9

Under the 100-year flood conditions, Lumber River overtops its banks and flows through the I-95 opening at the VFW Road (proposed gate location). The peak water surface elevation upstream of the gate is 123.9 ft, NAVD88. No segments of the levee system are overtopped. Installing the floodgate results in an increase in the peak water surface elevation of 0.3 ft upstream of the gate. Raising I-95 does not result in additional increases in water surface elevations.

Under the 500-year flood conditions, Lumber River overtops its banks and flows through the I-95 opening at the VFW Road (proposed gate location). About 1,800 cfs of flow goes through the I-95 opening. In addition to flow through the I-95 opening, flow overtops the low segments of I-95 east and west of the proposed gate location. Installing the floodgate results in an increase in the peak water surface elevation of 0.1 ft upstream of the gate. The overtopping flowrate at the low segments of I-95 increases from about 3,500 cfs to 4,100 cfs on the west side and from about 5,000 cfs to 6,100 cfs on the east side. No overtopping occurs with the gate in place and I-95 raised. Peak water surface elevation upstream of the gate under this scenario is 127.6 ft, NAAVD88. This elevation is 2.5 ft higher than the scenario without gate.

Under the 1,000-year flood conditions, Lumber River overtops its banks and flows through the I-95 opening at the VFW Road (proposed gate location). About 2,000 cfs of flow goes through the I-95 opening. In addition to flow through the I-95 opening, flow overtops the low segments of I-95 east and west of the proposed gate location. Installing the floodgate will result in an increase in the peak water surface elevation of 0.1 ft upstream of the gate. The overtopping flowrate at the low segments of I-95 increases from about 4,700 cfs to 5,400 cfs on the west side and from about 7,000 cfs to 8,100 cfs on the east side. No overtopping occurs with the gate in place and I-95 raised. Peak water surface elevation upstream of the gate under this scenario is 128.1 ft, NAAVD88.

Note that there is some flooding within the protected area under the 500-year and 1,000-year scenarios with the gate in place and with I-95 raised. This flooding is a result of Lumber River backing up along Jacob Swamp through the opening in Alamac Road.

Peak water surface elevations upstream of the gate for the flood of record (Hurricane Florence) under existing conditions is 124.7 ft, NAVD88. Installing the gate and raising I-95 to prevent overtopping increases the peak water surface elevation to 125.9 ft, NAVD88.

6. Freeboard Estimation

The proposed flood gate will impound water leading to a temporary pond-like situation at the northern side of the gate. This situation is expected to last for about 5 days during the design flood. During this temporary pond-like situation, wind setup caused by the horizontal stress exerted on the water surface by the winds and runup associated with wind generated waves may develop. The height of the flood gate should include freeboard allowance that considers these wind effects on the surface of water.

This section outlines the procedure used to calculate the wind setup and wave run-up based on simplified wave models.

6.1 ESTIMATE AVERAGE WIND SPEED OVER AN APPROPRIATE FETCH

6.1.1 Fetch

Fetch is defined as the unobstructed distance along which wind blows over the surface of water to create wind generated waves. The inundation extents computed from H&H modeling for the 500-year storm with gate and I 95 raised was superimposed on satellite imagery to determine the longest unobstructed distance (measured along a straight line) that is exposed to wind effects when water pools behind the Lumberton Flood Gate during the flood. The longest fetch was estimated to be around 2 mi to the northwest of the flood gate (Figure 7).

FIGURE 7

Fetch line (red) superimposed on 500-year depth raster and satellite imagery

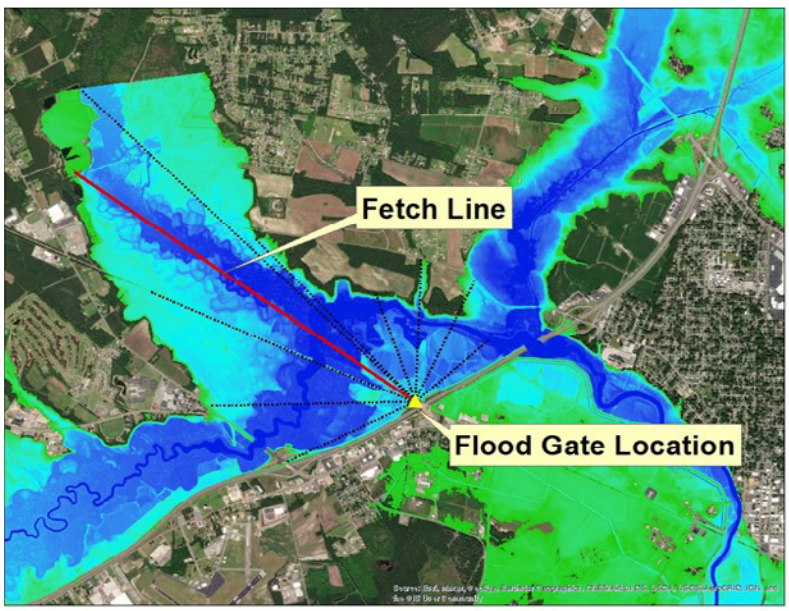

6.1.2 Wind Speed

Annual extreme fastest mile wind speed measured at 30 ft for 138 stations around United States was used to draw maps for the 2-year, 50-year and 100-year mean recurrence intervals (Thorn, 1968). The 2-year return period wind speed from that dataset was used as the input to compute the design wind speed. The estimated 2-year fastest mile wind speed over the state of North Carolina is 50 mi per hour.

The following assumptions (USACE, 1989) are made about the wind speed used as input for wave growth models:

- Wind fields are well organized and can be adequately described using an average wind speed and direction over the entire fetch.
- Wind speed should be corrected to the 33-ft (10 m) level.
- Wind speed should be representative of the average wind speed measured over the fetch.
- When the fetch length is 10 mi (16 km) or less, the wind has not fully adjusted to the frictional characteristics of the waves.
- When the fetch length is greater than 10 mi (16 km), thermal stability effects must be included in the wind speed transformation.

To satisfy these assumptions, the following adjustments are made to the wind speed.

6.1.2.1 Height and Overland Wind Adjustments

Since the wind speed was measured at 30 ft, a height adjustment was applied to get the equivalent wind speed at a height of 33 ft using the 1/7 power law (USACE, 1989).

The fastest mile data is based on measurements at land-based stations. Under comparable meteorological conditions, wind velocities over water are higher than over land surfaces because of smoother and more uniform surface conditions. Factors to adjust land-based wind speed measurements to account for these effects are presented on page 15-2 of USACE, 1997. For a wind fetch of 2, the ratio of winds over water to the winds over land (FWL) was estimated to be 1.21.

6.1.2.2 Computing Adjusted Wind Speeds based on Averaging Time

There are two approaches (fetch-limited and duration-limited) for determining the characteristics of wind generated waves. Fetch-limited conditions assume that the wind blows with a constant speed and direction over a certain fetch for sufficient time for the waves to travel the entire fetch length (Ozeren et al., 2009). Within this time, steady state conditions are achieved within the fetch. If the wind duration is less than the required time for the waves to travel the fetch, then the wave conditions will be time dependent, and such wave conditions are described as duration-limited.

In the present work, since the wind-generated waves are limited by the extent of the ponded areas adjacent to the flood gate, the assumption of fetch limited conditions is appropriate. Therefore, a minimum duration (t) must be selected to meet the assumptions of the fetch limited conditions discussed above. An averaging interval (larger than the minimum duration, t) over which wind speeds are relatively constant should also be selected and the corresponding averaged wind speed has to be computed.

The equations for computing wind speeds over different averaging intervals is based on Figure 5-26 in USACE, 1989.

First, the duration corresponding to a fastest mile wind speed of 50 mph was determined from the relationship t = 3600/U (from Figure 5-35 in USACE, 1989), where Ut is the fastest mile wind speed. Thus, t = 72 s.

The 72 s fastest mile winds to which overland adjustment has been applied is converted to 1-hour averaged wind speed, resulting in a speed of 50.13 mph.

6.2 ESTIMATE WAVE HEIGHT AND WAVE PERIOD

Deepwater wave characteristics based on the fetch and adjusted wind speeds computed are determined using hindcasting charts for deep water waves (Figure 5-34, USACE, 1989). The computed wave heights, periods and minimum duration are shown in Table 15.

TABLE 15

Deep water wave characteristics

Adjusted Wind Speed (mph)	Fetch (miles)	Duration (min)	Deep water Wave Height (ft)	Deep water Wave Period (s)
50.13	2	45	3	3

The minimum duration computed from the chart is around 45 minutes, therefore the assumption of fetch limited conditions is valid if we assume a duration of 1 hour. Therefore, the design deep water wave height and period is selected to be equal to 3 ft and 3 seconds (s), respectively.

Next, we compute the deep water wavelength using the dispersion relationship to verify the assumption of deep-water conditions. The calculated deep water wavelength was 46.12 ft.

For deep water wave growth to be unimpeded by the bottom, the ratio of water depth to wavelength must be equal to or greater than 0.5 (USACE, 1989). Design flood depth at the gate is about 8 ft so the ratio of the water depth to wavelength is 0.17 which is significantly less than half the wavelength. Therefore, the assumption of deep-water wave growth is not applicable. The wave height and period should therefore be based on shallow water curves. The hindcasting charts for computing shallow water wave characteristics at a depth of five feet is shown in Figure 5-36 USACE, 1989. For a wind speed of 50.13 mph and fetch of 2 mi, the shallow water wave height and wave period are **2.5 ft** and **2.75 s**, respectively.

6.3 ESTIMATE WIND SETUP AND WAVE RUNUP

Set-up (S_e) is the piling up of water at the leeward end, and a lowering of water level at the windward end in a reservoir caused by wind. Wind set-up can be estimated for the reservoir (USACE, 1989), resulting in a set-up of 0.3 ft.

Wave runup is defined as the height above still water level to which a wave will rise on a structure or beach. The upper limit for relative runup on smooth vertical, is presented in the U.S Army Corps of Engineers miscellaneous paper CERC-90-4 (USACE, 1990). Based on this scenario the wave runup was calculated at 6.25 ft.

References

1. Federal Emergency Management Agency, 2008. Meeting the Criteria for Accrediting Levee Systems on NFIP Flood Maps. Federal Emergency Management Agency (FEMA), 2008, Meeting the Criteria for Accrediting Levee Systems on NFIP Flood Maps, www.fema.gov/media-library-data/20130726-1600-20490-4180/lv_accredit_checklist_nov08.pdf.

2. Federal Emergency Management Agency, 2006. Mapping of areas protected by levee systems. Code of Federal Regulations Title 44 Section 65.10. Federal Emergency Management Agency, Aug. 25, 1986.

3. National Oceanic and Atmospheric Administration, 2020. Climate at a Glance-Statewide Time Series. National Oceanic and Atmospheric Administration National Centers for Environmental Information. Available at: ncdc.noaa.gov/cag/statewide/time-series.

4. North Carolina Department of Transportation, 2019. North Carolina Department of Transportation Bridges Map, ncdot.maps.arcgis.com/home/webmap/viewer.html?webmap=db3b56c3228743b3811e36761393d661. Date accessed: 9 Dec. 2019.

5. Ozeren, Yavuz & Wren, D., 2009. Technical Note: Predicting Wind-Driven Waves in Small Reservoirs. Transactions of the American Society of Agricultural and Biological Engineers, Vol. 52(4), pages 1213 – 1221.

6. State Climate Office of North Carolina, 2015. NC Extremes: Damaging hurricanes from slopes to shores. NC State University. Available at: http://climate.ncsu.edu/climateblog?id=157.

7. Thorn, H.C.S, 1968. New Distributions of Extreme Winds in the United States. Journal of the Structural Division, 1968, Vol. 94, Issue 7, Pg. 1787-1802.

8. United States Army Corps of Engineers, 1989. "Water Levels and Wave Heights for Coastal Engineering Design," US Army Corps of Engineers EM 1110-2-1414, July 5, 1989.

9. United States Army Corps of Engineers, 1990. "Maximum Periodic Wave Runup on smooth slopes", US Army Corps of Engineers Miscellaneous Paper CERC-90-4.

10. United States Army Corps of Engineers, 1997. "Hydrologic Engineering Requirements 1. for Reservoirs," US Army Corps of Engineers EM 1110-2-1420.

11. United States Department of Agriculture Natural Resources Conservation Service. Geospatial Data Gateway [internet database] available at: https://datagateway.nrcs.usda.gov/. Accessed October 30, 2019.

12. United States Geological Survey, 2009. Magnitude and Frequency of Rural floods in the Southeastern United States, through 2006: Volume 2, North Carolina. U.S department of Interior, U.S Geological Survey.

13. United States Geological Survey, 2016. The StreamStats program. Available at: http://streamstats.usgs.gov. Accessed on: November 1, 2019.

14. United States Geological Survey, 2019 b. U.S. Guidelines for Determining Flood Frequency. Bulletin 17C.Techniques and Methods 4-B5 version 1.1., Department of Interior, U.S. Geological Survey, May 2019.

15. United States Geological Survey, 2020. USGS Current Conditions for North Carolina. Available at: https://waterdata.usgs.gov/nc/nwis/uv?. Accessed on January 4, 2020.


LAMPSON

Mikaela Matkowski
Mechanical Engineer II Energy Nuclear
Eagle River, AK, USA

William. J. Young
Washington River Protection Solutions
Richland, WA, USA

Nuclear Engineering

05: Safe Transportation of LAW Melter in Support of Hanford Cleanup

Abstract

The U.S. Department of Energy (DOE) Office of River Protection (ORP) oversees the direct feed low- activity waste (DFLAW) program, which will enable operation of the Vitrification Facility to immobilize Low Activity Waste (LAW). To support continued operation, new LAW Melters must be fabricated, assembled, stored, and transported. Within an assembled LAW Melter, there are refractory components that are precisely placed to accommodate thermal expansion during heat-up; during transportation, these components could shift. A transportation test and route survey was performed to verify the transportability of the LAW Melters. A simulated ~600,000 lbs. Melter Mockup was designed and constructed to be prototypic of a LAW Melter. Six accelerometers were placed on the Melter Mockup to gather acceleration data that conservatively bounds what the refractory would experience during an actual LAW Melter transport. The lowest acceleration that could cause refractory to tip or slide was conservatively calculated assuming a constant force.

Extensive data was collected for numerous maneuvers. Initial evaluation compared the data to the predetermined acceleration limits to determine when significant accelerations occurred. All of these high accelerations were momentary spikes, not constant forces. Filtered data showed that significant accelerations were recorded during only a handful of trials. Significant accelerations were correlated with controllable parameters to define operational limits in future LAW Melter movement procedures.

KEYWORDS
Nuclear waste; Low-activity waste; Transportation; Logistics; Safety

1. Introduction

The U.S. DOE ORP oversees the DFLAW program, which will enable operation of the Vitrification Facility to immobilize LAW. At the LAW Facility, waste will be processed and transformed into an immobilized form safe for storage via the vitrification process. The waste will be mixed with silica and glass-forming materials, fed into LAW Melters (Figure 1), and heated to 2100 degrees Fahrenheit. Commissioning is underway and operation of the two joule-heated ceramic LAW Melters may begin as early as the end of 2024. To support continued operation of the LAW Vitrification Facility, new Melters must be fabricated, assembled, and stored in preparation for replacement of the installed Melters which have a design life of 5 years.

The LAW Melter is to be assembled in the AtkinsRéalis Engineering Laboratory (AEL) facility in Richland, WA, where it will be stored until replacement at the LAW Facility is requested. Inside of the LAW Melter are layers of refractory blocks. These blocks are assembled with gaps between them to accommodate thermal expansion. Since some of them are not mechanically secured, they are at risk of movement during LAW Melter transportation. The blocks most vulnerable to movement are the top row of refractory called "H-block" or "H Soldier block" (Figure 2) [1]. These blocks may move in the direction of travel or horizontally perpendicular to the direction of travel. The Melter must be proven able to be transported without shifting or damage to these blocks so it can be installed to replace a spent in-service LAW Melter. WRPS contracted AtkinsRéalis to plan, perform, and document the results of a representative LAW Melter movement demonstration.

FIGURE 1

Melter CAD model

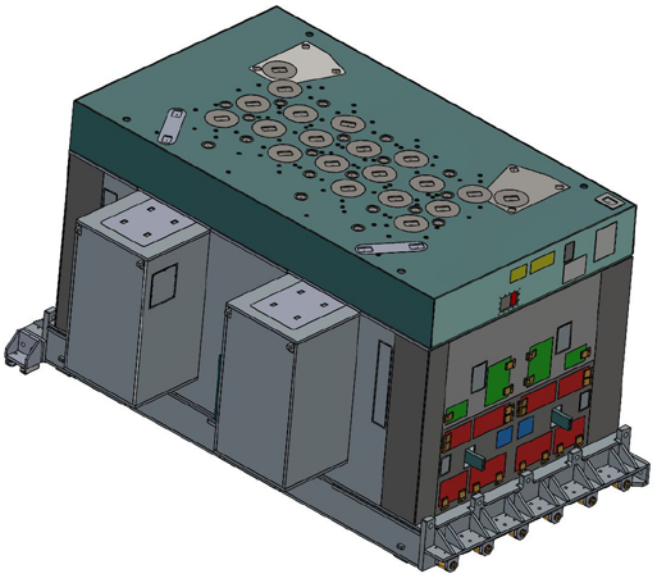

FIGURE 2

Refractory block

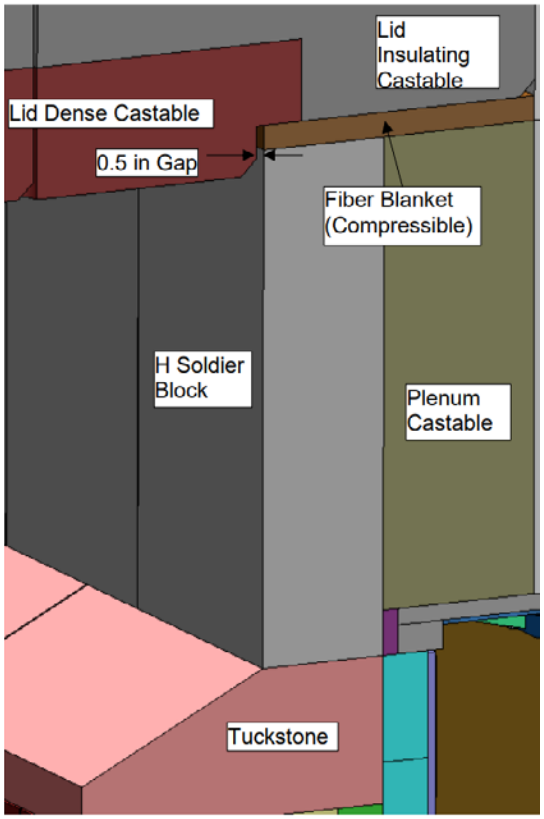

2. Discussion

2.1 TEST DEVELOPMENT

The Melter Mockup Assembly (MMA) was designed to be representative of a LAW Melter based on weight, center of gravity, and accelerometer post configuration. The accelerometers' positioning and configuration were designed to gather data that would be bounding of accelerations an H-block would experience during Melter movement. The final configuration for the MMA is shown in Figure 3.

Data from each sensor had unique significance:

- The sensor on the base (VE-0005) collected accelerations which represented base excitation.
- The rigid bracket (VE-0004) data was similar to base excitation with some modification due to interfaces and included global rotations, such as when the MMA turned a corner.
- The sensor on the freestanding block (VE-0003) was representative of a freestanding H-block inside a Melter, ignoring the compressed blanket which would rest atop (this was conservative).
- The sensor on the strapped block (VE-0004) was intended to demonstrate the effect of a downward force and be prototypic of an H-block with a compressed blanket resting on top.
- The post sensors (VE-0001 and VE-0002) showed amplification at the configurations' natural frequencies and were vulnerable to local events. These post sensors were deemed not entirely representative of H-block accelerations. They were intended to simulate mounting sensors on the outside surface of the Melter.

FIGURE 3

Melter mockup assembly

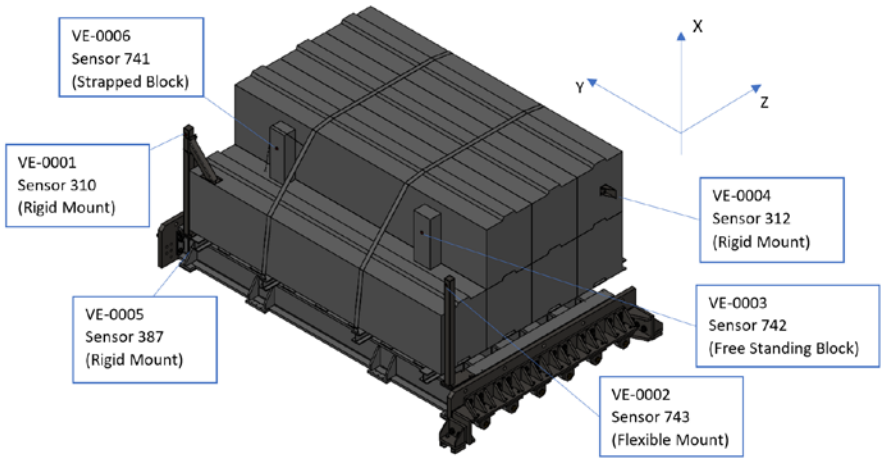

A series of demonstration activities were designed based on two potential routes from the assembly facility to the Waste Treatment Plant (WTP). These routes require a winching system to pull the load out of the assembly facility along rails (Figure 4), a lifting system to lift/lower the Melter (Figure 5), and a transporter to drive the Melter to WTP (Figure 6).

FIGURE 4

Winching MMA

FIGURE 5

Lifting MMA

FIGURE 6

Transporting MMA

Demonstration activities included maneuvers for each system, such as winching the MMA into position outside of the facility, lifting and lowering the MMA onto a transporter, and driving along a route that included various turns and slopes.

2.2 DATA ANALYSIS

The acceleration-time data was analyzed to determine periods of significant accelerations and the test logs were referenced for mention of an outlier or specific event. For occurrences of significant accelerations, fast Fourier transform was performed on the original time history data. The results indicated that most measured accelerations existed at high frequencies. For example, base excitation data (VE-0005) indicates accelerations above 100 Hz as shown in Figure 7.

FIGURE 7

Discrete Fourier transform for VE-0005

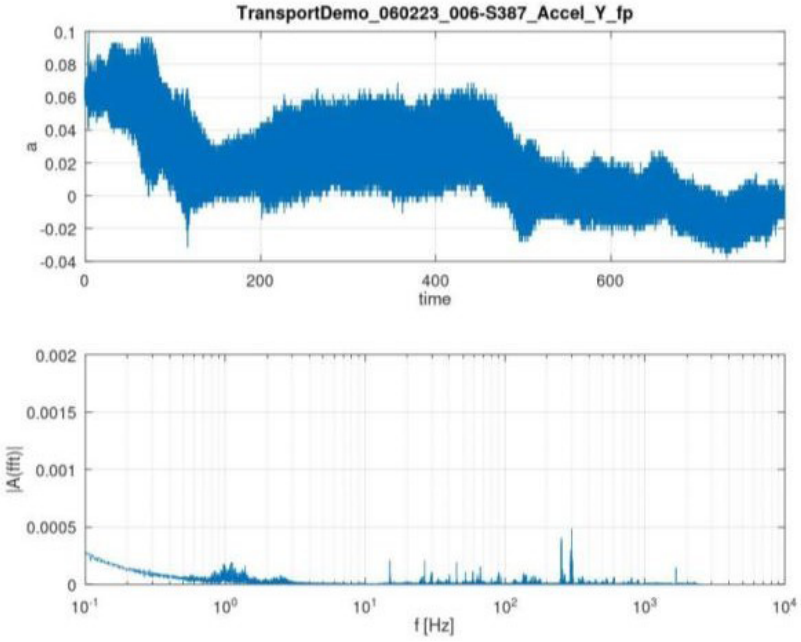

An example of the measured accelerations in the direction of travel (z-direction) are shown in Figure 8, where the accelerations are shown in the associated frequency bands of 0-10 Hz and 10-1000 Hz. The higher frequency band contained greater magnitude accelerations than those within the lower frequency band (considering peaks, 0.1 g compared to 0.03 g).

FIGURE 8

Accelerations at frequency bands (0-10 Hz and 10-100 Hz)

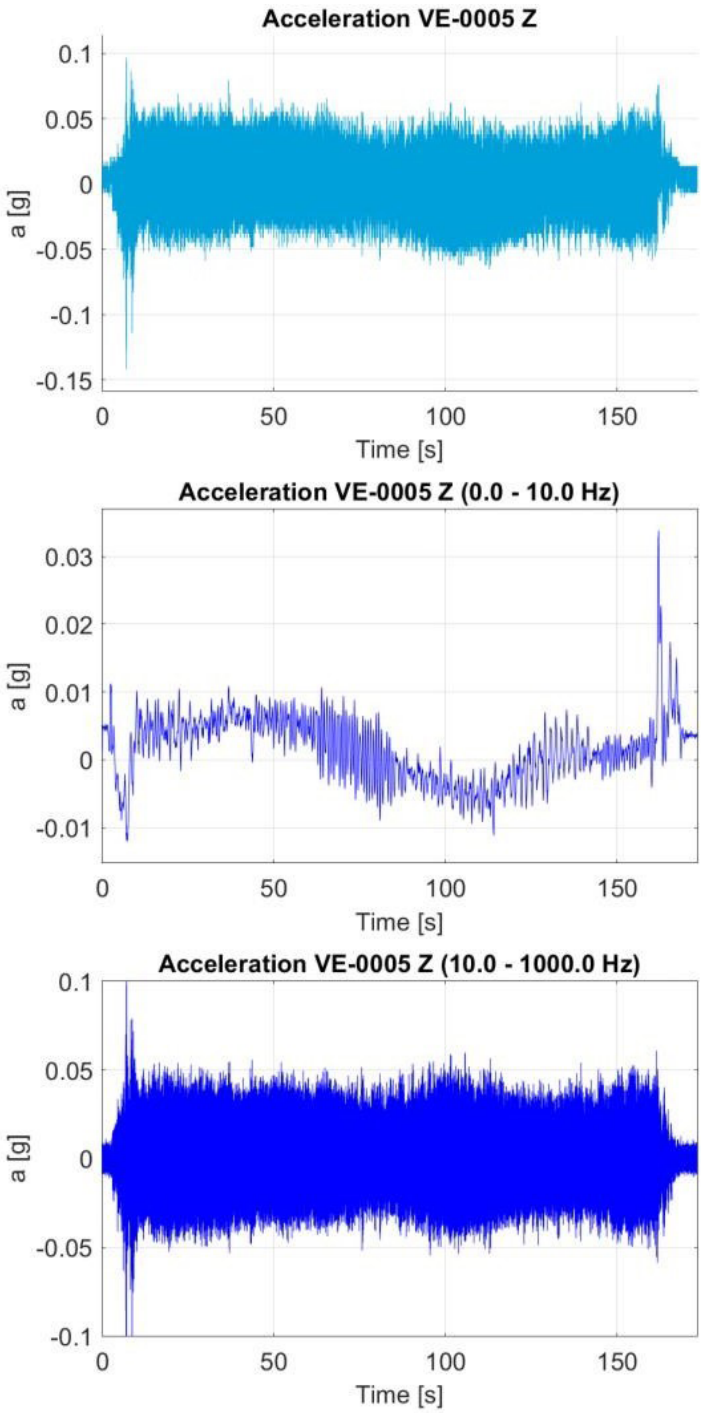

Transmissibility of an H-block was computed and the block was shown to attenuate accelerations above 80 Hz (Figure 9). This attenuation of the block could be seen by comparing the data from rigid sensors (such as VE-0004 and VE-0005) to data from the block sensors. A filter was designed to mimic the attenuation seen in the block transmissibility and this filter was applied over the acceleration data.

FIGURE 9

Transmissibility Function, single degree of freedom with natural frequency of 55 Hz, 5% critical damping [2]

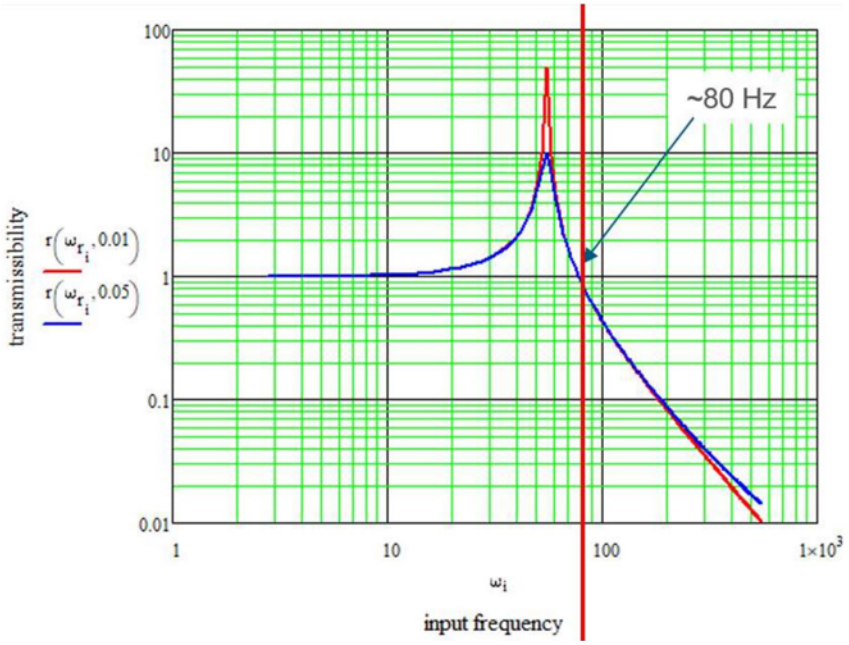

After filtering, demonstration activity data was re-evaluated to determine which activities resulted in significant accelerations. The activities with resulting significant accelerations were reviewed in-depth to determine the associated conditions and whether the cause of significant acceleration could be controlled. Each significant acceleration correlated with a controllable test condition. For example, using flat deck parallel to the roadway while traveling uphill, instead of an angled deck to compensate for the slope. Recommendations were made to prevent these test conditions from arising during future movement.

Filtered horizontal accelerations were found to not be significant enough to move an H-block.

Next, conservatively using unfiltered acceleration data, the possible accumulative movement was investigated.

Sliding analyses was conducted by a vibrations Subject Matter Expert to determine the potential for sliding based on raw acceleration for each trial [2]. These analyses assessed whether sliding could happen per trial based on the simultaneous vertical and horizontal accelerations recorded by sensors VE- 0003 through VE-0006. These sliding analyses were conservative for the following reasons:

- Uplift and the corresponding decrease in friction is accounted for. The analysis ignores the downward force of the blanket which would counteract uplift.
- The raw accelerations used in the sliding analyses included high frequency accelerations though these frequencies would be attenuated by an H-block in practice.

All occurrences of potential sliding were associated with raw accelerations at the rigid bracket or base sensors (VE-0004 and VE-0005). Unlike the bracket and base sensors, the freestanding block and strapped test block sensors (VE-0003 and VE-0006) naturally attenuated high frequency accelerations and their measured accelerations did not indicate potential for sliding. This difference in sliding analysis results showed how the rigid bracket and base sensor acceleration data included more high frequency effects, which made their data more conservative.

The potential sliding distances were minor, with the largest being less than two micrometers. These potential sliding distances were used in determination of accumulative movement. The accumulative movement is based on a list of maneuvers necessary to transport a melter from AEL to WTP along the primary route [3]. The prototypic demonstration activity and associated max potential sliding was noted next to each movement. The maximum potential sliding differences were summed for each occurrence of each movement extrapolated to the full primary route.

The calculation for accumulative potential sliding relied on the following assumptions:

- All potential sliding movements were assumed to be in the same direction, but this would not always be the case. For example, when starting and stopping, potential sliding movements would be in opposing directions. This assumption was conservative.
- Fifteen miscellaneous stop/starts were added to the accumulative movement. This was conservative.
- The potential sliding distance for a start/stop occurrence was based on the transport demonstration activity with highest theoretical sliding, which is the Uphill on 7% slope maneuver. This was conservative.
- Many activities inherently included a start/stop. The inclusion of start/stops within trial data was conservative.
- Deck angle was assumed for certain terrain cross slopes. Based on the pitch test results, rolling the transporter deck was assumed to not result in significant accelerations. There was not acceleration data for rolling the transporter deck.
- When the route survey noted an unidentified number of inclines and declines 4% or less on Route 4S, there was assumed to be 5 occurrences before and after the Wye Barricade.

Based on accelerations observed during demonstration testing, the highest theoretical movement expected by route completion was 0.013mm, less than 1% of the gap between blocks. This distance is less than the average width of a strand of human hair; it's essentially zero.

3. Conclusions

This work assessed the risk of H-block refractory movement. For insight into accumulative movement, the maximum potential sliding that could result from measured test accelerations was calculated for each maneuver. Max sliding amounts were summed along the primary route from AEL to WTP. During the full route, the total potential sliding was 0.013mm (less than 1% of the gap between blocks), which is effectively zero. In conclusion, based on empirical evidence and data analysis, the accelerations measured during the performance of the demonstration tests would not have caused detriment to refractory. These tests are considered bounding of movement of an assembled Melter along the pre-determined routes but may not be bounding of different systems (transporter, winch, or lifting system).

Acknowledgements

This paper was previously presented at the Waste Management Symposia, WM2024 Conference, March 14, 2024, Phoenix, Arizona, USA.

This work was supported by the U.S. Department of Energy Office of River Protection and Washington River Protection Solutions. Demonstration testing was completed in collaboration with Lampson International. Special thanks to Berislav Kralj, Tim Migala, Jared Rieck and Joshua Bonderman for their contributions to analysis and demonstration testing. Additionally, to David Bergmann, Richard Christensen, Philip Jensen, Richard McIntire and Rocky Crisp for their review and insight. Thanks to William Young and Lawrence Curtis for their support throughout the development of this work.

References

[1] C. Gorschboth, RPT-LAWMAST-EG-0006, *LAW Melter, Storage, & Transportation - Accelerometer Location Basis Report,* AtkinsRéalis, 2021.

[2] B. Kralj, *RPT-21-00828-EG-0001 LAWMAST Vibrations Measurements Analysis,* AtkinsRéalis, 2023.

[3] VS-2100853-105-01, *Lampson - LAW Melter Route Survey LIL-RS-1425-01,* Lampson, 2022.


ATKINS
NEW ST STN
A 38

Venkata Bhargava Sai Bhimavarapu
Senior Managing Consultant
Global Technology Centre (GTC)
Bangalore, India

Pawan Kumar Adike
Associate Technical Director
Global Technology Centre (GTC)
Bangalore, India

Rajesh Jayapalan
Technical Director
Global Technology Centre (GTC)
Bangalore, India

Transportation

06: Principles of Absolute Model Applied Incrementally (AMAI) in Travel Demand Forecasting

Abstract

Large-scale models developed for several regions are intended to predict the traffic flows that are likely to result from assumed exogenous developments and transport policies affecting people and businesses in the relevant area. The modelling process involves a series of mathematical models which attempt to simulate human behaviour while travelling. The accuracy of the model over a wide range of policy measures is crucial to determine the quality of the information that can be extracted as input to the planning and policy analysis process.

There are two fundamental model forms that are widely used across the modelling field namely synthetic (or 'absolute') models and incremental (also called 'pivot-point') models that predict changes relative to a base-year situation. Both model forms have their merits and demerits.

A new approach has evolved over the last decade which aims to solve the challenges in both incremental and absolute model approaches. This new form, termed as Absolute Model Applied Incrementally (AMAI), uses absolute model estimates to apply changes to a base matrix. This paper discusses the pivoting theory, the available variable demand modelling guidance focusing on the United Kingdom's Transport Appraisal Guidance (TAG) followed by a presentation of our experience in using the AMAI model form and concludes with suggestions for future practice.

KEYWORDS
Modelling; Incremental Models; Pivot-point; Absolute Models

1. Introduction

Large-scale model systems have been developed for several cities, regions, and countries to support the development of transport policy. These large-scale models are intended to predict the traffic flows that are likely to result from assumed exogenous developments and transport policies affecting people and businesses in the relevant area. The modelling process involves a series of mathematical models which attempt to simulate human behaviour while travelling. The models are formulated in a sequence of steps that answer a series of questions about the traveller's choices. Four Stage Modelling process is a primary tool for forecasting travel demand and the performance of a transportation system. The accuracy of the model over a wide range of policy measures and exogenous developments is crucial to determining the quality of the information that can be extracted as input to the planning and policy analysis process.

Traditionally, the model alone has been used to produce purely 'synthetic' (sometimes called 'absolute') forecasts, meaning forecasts built using secondary data such as population, jobs etc. excluding the current state. However, another frequent approach to modelling, which can substantially enhance the accuracy of the model, is to formulate the model as predicting changes relative to a base-year situation. Often, base-year traffic flows can be observed rather accurately and the restriction of the model to predicting differences reduces the scope for errors in the modelling – whether they be caused by errors in the model itself or the inputs to the model – to influence the outputs. Such approaches are called 'pivot point' methods, the name given to them by Manheim (1979) [1] or 'incremental' models [Appendix]. The approaches have proved beneficial in practical planning situations and are part of the recommended variable demand model procedures.

While the error-reducing principle of the pivot point is clear, the implementation of the principle in practical model systems can be done in several ways and the choice between these can have substantial influence on the model forecasts. Modellers need to consider:

- whether the change predicted by the model should be expressed as an absolute difference or a proportional ratio, or whether a mixed approach is necessary.
- how to deal with growth in 'green field' developments, when the future is likely to be very different from the present situation when applying these approaches.
- at what level in the model should the pivoting apply, i.e., at the level of mode choice, destination choice, overall travel frequency or combinations of these.
- whether the pivoting is best undertaken as an operation conducted on an explicit 'base matrix' or the model is constructed so that it automatically reproduces the base year situation with base year inputs.

This paper discusses the alternative approaches to each of these issues, the available variable demand modelling guidance and attempts to establish the basis on which alternative approaches might have been established; in particular, whether pivoting is treated as a correction to a model which is in principle correctly specified but incorporates some error, perhaps from faulty data, or as a partial replacement for a model that handles at best, part of the situation. These views of the pivoting lead to different procedures.

In this paper 'pivoting' is used as a broad term, describing the use of a model to predict changes relative to a fixed or more reliable base point. One may distinguish two broadly separate procedures for pivoting:

- the use of two identifiable synthetic model results, applicable to base and forecast cases, which are then used, either as a ratio or as a difference, to adjust the base point – we call these factors pivoting and difference pivoting.
- the specification of a model which can only predict changes relative to a base, – we use the common name of incremental modelling.

It should be clear that either of these pivoting methods will reproduce the base when the forecast case has inputs equal to the base inputs. Moreover, there is little difference in practice between an absolute forecast in which large numbers of correction terms have been included, factor pivoting and incremental modelling. Details are explained in section 2.1.

The following section of the paper discusses the theory of pivoting and its approaches to solve modelling problems. We then discuss the existing variable demand modelling guidance in the United Kingdom, chosen because UK practice is reasonably well-developed and gives a good basis for illustrating the issues, followed by a presentation of our own experience. The final section presents conclusions for future practice.

2. Pivot Theory

Following Manheim (1979), the process of taking a fixed base point and making forecasts relative to that is called pivoting. In most large-scale model systems, forecasts are developed of changes in a series of traveller decisions (frequency, destination, mode and departure time choice, for example) which are expressed in the form of forecast matrices which are then assigned to highway and/or public transport networks. The objective of the pivoting approach in this context is therefore to predict changes in the base matrix.

The reasoning behind the choice of a pivoting approach is chiefly that it reduces error. When the base matrix can be estimated with greater accuracy than can be achieved by a model, it makes sense to use the base matrix to predict 'most' of the trips, using the model to predict the changes relative to that, obtaining a smaller error from the model because a smaller number of trips is being predicted.

In this section of the paper, three theoretical issues are discussed. First, the equivalence of several factoring approaches is established. Then a comparison is made between factoring and additive approaches, and this is followed by a discussion of the issues arising in multi-stage modelling. Finally, a review is given of the competing advantages of the different approaches.

2.1 EQUIVALENCE OF FACTORING APPROACHES

To define the notation, suppose there is a synthetic (logit) model predicting the probability of choosing each of several alternatives.

$$S_{b_i} = {e^{G_i}}/{\sum_j e^{G_j}} \qquad (1)$$

where G_i gives the utility of each alternative.

The incremental approach (Bates, Ashley, and Hyman (1987) [2] quotes a 1980 paper by Kumar) predicts T_i choices for alternative i.

$$T_i = {B_i * e^{\Delta G_i}}/{\sum_j B_j * e^{\Delta G_j}} \qquad (2)$$

where B_i is the observed (base) probability of choosing each alternative and ΔG gives the change in utility.

The synthetic model can be used to make synthetic predictions S:

$$S_{f_i} = {e^{(G_i+\Delta G_i)}}/{\sum_j e^{(G_j+\Delta G_j)}} \qquad (3)$$

So, we can calculate:

$${S_{f_i}}/{S_{b_i}} = \left\{\frac{e^{(G_i+\Delta G_i)}}{e^{G_i}}\right\} * \left\{\frac{\sum_j e^{G_j}}{\sum_j e^{(G_j+\Delta G_j)}}\right\} \qquad (4)$$

$${S_{f_i}}/{S_{b_i}} = e^{\Delta G_i} * constant \qquad (5)$$

Since the term in the second { } is a global constant, the incremental calculation can then be expressed as:

$$T_i = B_i * {S_{f_i}}/{S_{b_i}} \Big/ \sum_j B_j * {S_{f_j}}/{S_{b_j}} \qquad (6)$$

The incremental calculation is therefore the same as factoring the observed choices B by the ratio of the synthetic forecasts, providing the total number of choices is normalised to remain constant.

In the incremental or factoring approaches, it is not possible to make decisions in situations where one or other of the inputs is zero, for example in the case of 'greenfield' developments. However, the factoring approach can be adapted to use mixtures of synthetic and factored (and even difference) approaches.

2.2 ADDITIVE APPROACH

In the previous section, the basic equivalence of incremental and factoring methods was noted. However, a substantially different approach is the use of synthetic matrices to adjust base matrices by adding the difference between synthetic forecast and base demand, i.e., in the notation of the previous section:

$$T_i = B_i + S_{f_i} - S_{b_i} \qquad (7)$$

Zero inputs do not cause a specific problem with this approach. However, a problem that may be encountered is that a negative result may be obtained, at which point the output value zero would normally be substituted.

However, if all the results remain positive without correction the calculation will maintain the number of forecast trips as expected, i.e.,

$$\Sigma_j T_j = \Sigma_j S_j \qquad (8)$$

The primary disadvantage of the additive approach is that it relates poorly to the specification of most of the models that are used. Specifically, the models predict the proportions of trips making each choice and there is no way to correct the models so that a given difference in the number of trips will be predicted. The models are fundamentally models of choice and the appropriate correction for such models is by factoring, not by adding a correction.

In another important example, the numbers of trips predicted by our models are proportional to the 'sizes' of the generating and attracting zones. An error in measuring these sizes cannot easily be corrected in a way that would yield a fixed number of additional car trips in the morning peak.

For this reason, the use of differences must be considered as an unusual approach, for application only in special circumstances.

In the case of 'greenfield' developments, where the base observed and base synthetic are both zero or near zero, an additive approach is more or less equivalent to using the synthetic forecast. In fact, there is little choice in this context - the synthetic forecast is the only information available.

2.3 PIVOTING IN MULTI-STAGE MODELS

Many model systems are composed of multiple stages, with several travel choice decisions treated in sequence: travel frequency, destination, mode, departure time, etc., each stage further splitting the demand forecast by the previous stage. In these cases, pivoting can be considered at each stage in sequence or as a final step.

When the model is formulated incrementally, pivoting is effectively conducted for each step in a sequence. However, when pivoting is performed by factoring with synthetic model output, the choice of a normalisation (detailed in section 3.2) of the total trips at each stage becomes a real issue. This is because there is no guarantee that the sum of factored trips is equal to the forecast total, as has already been noted in section 2.1.

An important special case is when the base matrix is defined with a different level of geographical aggregation than some components of the model. For example, the base may be defined with an aggregated zoning system or with fewer purpose categories than the model to enhance the reliability of the base data. Alternatively, the matrix may be defined over public transport stations, which occurs particularly often when ticket sales information is an important data source. These approaches can be useful to maintain proper respect for the base matrix data.

2.4 CONSIDERATIONS IN THE CHOICE OF APPROACH

Between pivoting approaches, the additive approach should be used only in special circumstances. Some of these circumstances are described in our practical experience set out in section 3.2.

Between the factoring approaches, it should be noted that the factoring procedure with explicit base, synthetic base and synthetic forecast matrices is clear, simple to program (because the same program can be used for the two synthetic matrices) and the base matrix is prominent as a component of the modelling process.

On the other hand, incremental approaches give automatic normalisation at each stage, but if normalisation is carried out at each stage in multi-stage models there is effectively no difference between any of these methods in terms of the results obtained.

In practice, a decisive consideration may be the need to adapt the pivoting method to accommodate zeros and other difficult cases.

3. UK Guidance and AtkinsRéalis India Experience

3.1 UK GUIDANCE

This section of the paper reviews current practice in using pivot-point and related procedures in the United Kingdom, chosen because UK practice is reasonably well-developed and gives a good basis for illustrating the issues.

In the UK, the Department for Transport provides guidance for Variable Demand Modelling (TAG M2.1 [3]), which has been designed as a reference document for use during the model design stage, with sections outlining the issues to be considered at each stage of model development. TAG M2.1 discusses the decision as to whether to apply the 'synthetic' model predictions directly or to employ an 'incremental' approach where changes are predicted relative to an observed base.

The guidance states that 'the preferred approach is to use an incremental rather than a synthetic model, unless there are strong reasons for not doing so' but also notes that a purely incremental approach may not be sensible where there are large changes in land use between the base and forecast years, which will significantly change the distributions of origins and destinations.

To deal with the problem of empty cells in the observed base matrices, the guidance suggests that a weighted average of observed and synthetic matrices is used in the base. This approach gives greater weight to cells where there are more observed trips than expected from the synthetic model.

Therefore, the UK's Transport Appraisal Guidance suggests three forms of models:

- Absolute models, that use a direct estimate of the number of trips in each category.
- Pivot-point or Incremental models, that use cost changes to estimate the changes in the number of trips from a base matrix.
- Absolute Models Applied Incrementally (AMAI), that use absolute model estimates to apply changes to a base matrix.

3.2 ATKINSRÉALIS EXPERIENCE

3.2.1 Introduction

In this section, we describe some of our own experiences in several large-scale modelling studies. In these studies, we have consistently applied pivoting using the factoring of synthetic matrices, for the reasons given in section 2.4.

Pivoting is carried out at the matrix cell level. That is, for a specific origin, destination, mode, time of day and purpose, adjustments are made relative to the corresponding cell in a base matrix. As has been noted, issues may arise that affect marginal totals in the matrices and corrections may be necessary for those. However, for the sake of clarity in this section of the paper, this issue is neglected here. The specific procedures proposed in this section can also be adapted for row or matrix pivoting.

The procedures set out below are based on AtkinsRéalis India's experience with several models used in their transport demand forecasting systems. These models have procedures to adjust the calculation when the growth in a specific cell is considered to be 'extreme'. Extreme growth situations can often be identified with 'greenfield' developments. Our preferred approach involves automatic selection of the 'extreme' cases and is therefore reflected in the procedures set out below.

3.2.2 AMAI Pivoting Procedures

For the reasons explained above, the preferred approach to pivoting is to apply the ratio of model outputs for base and forecast situations as a growth factor to the base matrix, i.e., in a given cell the predicted number of trips F is given by:

$$F = B \times \frac{S_f}{S_b} \qquad (9)$$

where:

S_f is the modelled matrix, i.e., 'synthetic' trips for a future year from the VDM;

S_b gives the equivalent synthetic trip matrix for the base year from the VDM;

B is the observed (base) matrix.

However, for two reasons, it is not always possible to apply this calculation as simply as stated.

First, any combination of the three components on the right-hand side of this equation may be zero (or very small) making the calculation impossible or meaningless. Eight possible such combinations of zero values arise, and these are dealt with separately in the recommendations below.

Second, particularly when there is a land-use change affecting a currently undeveloped zone, the change may be quite extreme and strict application of the formula above can lead to an 'explosion' in the number of trips. In such cases, it is better to pivot by applying the difference method, i.e. $(S_f - S_b)$, to the base matrix, rather than a factor as shown above. In the recommendations below, difference pivoting is applied to all cases when S_b is zero and to other cases when S_f/S_b exceeds a specified factor (including 'infinity' when S_b=0 and S_f is non-zero).

Therefore, the possible eight cases and their recommended treatments are discussed in Table 1.

TABLE 1

The 8no. cases used in the AMAI pivot process

Case	Base (B)	Synthetic Base (S_b)	Synthetic Forecast (S_f)	Forecast (F)		
1	0	0	0	0		
2	0	0	>0	S_f		
3	0	>0	0	0		
4	=0	>0	>0	0	Normal Growth	$B \sim S_b$
						$B << >> S_b$
				$S_f - S_b$	Extreme Growth	
5	>0	0	0	B		
6	>0	0	>0	$B+S_f$		
7	>0	>0	0	0		
8	>0	>0	>0	$B \times S_f/S_b$	Normal growth	$B \sim S_b$
						$B << >> S_b$
				$B + S_f - S_b$	Extreme growth	

To complete the specification of the calculation, it is necessary to define when a cell is considered to be zero (our experience has led us to use a test value of 10^{-3}) and when and how extreme growth (for Case 7) is to be applied. The switch point to absolute growth is dependent on the relation between B and S_b.

Recent AtkinsRéalis India experience in the application of pivoting theory to several projects demonstrated that careful consideration needs to be given to the choice of the switching factor, and the importance of testing the application of the pivoting procedure to ensure the plausibility of the model forecasts.

In general, the base matrices were based on the expansion of survey data or other sources such as mobile phone information and consequently were significantly sparser in coverage than the synthetic model matrices.

This meant that when both B and S_b are non-zero, B was larger on average than S_b because a significant volume of S_b occurs in cells where B is exactly zero. The impact of this characteristic was that the trigger point for extreme growth was not being reached even in cases where $S_f >> S_b$, because both values were smaller than B. Modification to the switch point calculation to use the formula above solved this problem and following this change plausible model forecasts were obtained.

3.2.3 Continuity in Pivoting

Continuity of the results is an important issue in the use of the procedures as set out in the previous section. Clearly, transitions between any of the eight cases as a result of small changes in either of the matrix cells should not lead to substantial changes in predicted values. Therefore, we have tested the procedures for continuity in many directions.

Firstly, continuity in S_f should be the most important by far, since discontinuities could produce counter-intuitive differences between forecasts made from the same base. Secondly, transitions in B and S_b are much less important as they do not occur in standard applications of incremental models but only when changes in base values are considered.

Detailed examination of the 8no. cases in Table 1 shows the following:

- No discontinuities arise for changes in S_f, either between the even and odd-numbered cases or between normal and extreme growth in Cases 4 and 8. This is a key feature of the system, as it means that small differences between policies will not lead to large differences in forecasts.
- When B changes, there are no discontinuities.
- When S_b changes, there is potential for discontinuities between some cases with $S_b = 0$ and small positive values of S_b. This of course relates to the presence of S_b in the denominator of the pivot formula.

It does not seem possible to eliminate the discontinuities relating to S_b. However, once the base synthetic forecasts are fixed, they would not normally be changed, and these discontinuities will not affect the comparison of policy.

3.2.4 Requirement for Normalisation

When pivoting is carried out solely at the cell (individual zone-pair) level, there are several reasons why the aggregate (at a sector level) result can differ from that which would arise if the matrix totals were simply scaled. This naturally occurs where non-scalar growth is used as in Cases 1-3 and 5-7 noted in Table 1.

Moreover, small mismatches between the Assignment Base (B) and Synthetic Base (S_b) can also multiply to give uneven growth. The matrix example below gives a simplified case with two zones to illustrate this. Whilst the synthetic and assignment base have identical row and column totals, the patterns of movement differ slightly, with proportionally fewer intra-zonals in the assignment matrix. If the intra-zonals then grow more rapidly in the synthetic, this produces disproportionate overall growth in the assignment matrix (F). In this case, an excess of 6 trips in total.

The issue can be corrected by scaling the whole matrix (F_n) so that the matrix total returns to the correct target value, in this case, 48.

$$B = \begin{matrix} 12 & 6 & \mathbf{18} \\ 6 & 12 & \mathbf{18} \\ \mathbf{18} & \mathbf{18} & \mathbf{36} \end{matrix}, \quad S_b = \begin{matrix} 10 & 8 & \mathbf{18} \\ 8 & 10 & \mathbf{18} \\ \mathbf{18} & \mathbf{18} & \mathbf{36} \end{matrix}, \quad S_f = \begin{matrix} 20 & 4 & \mathbf{24} \\ 4 & 20 & \mathbf{24} \\ \mathbf{24} & \mathbf{24} & \mathbf{48} \end{matrix}$$

$$\Rightarrow F = \begin{matrix} 24 & 3 & \mathbf{27} \\ 3 & 24 & \mathbf{27} \\ \mathbf{27} & \mathbf{27} & \mathbf{54} \end{matrix}$$

$$\Rightarrow F' = \begin{matrix} \square & \square & \mathbf{24} \\ \square & \square & \mathbf{24} \\ \mathbf{24} & \mathbf{24} & \mathbf{48} \end{matrix}$$

$$\Rightarrow F_n = \begin{matrix} 21.3 & 2.7 & \mathbf{24} \\ 2.7 & 21.3 & \mathbf{24} \\ \mathbf{24} & \mathbf{24} & \mathbf{48} \end{matrix}$$

Hence, normalisation of this kind needs to be applied after the pivoting process to correct both of these issues.

3.2.5 Observations from the Model

The method described above has been used in several transport models implemented in various countries and has proven to yield acceptable results. The illustration of the results of the method is however, not very straightforward. Therefore, in this section, we present the results of the most common cases from Table 1: Case 8, where all Origin-Destination (OD) matrices have positive values, and we show the damping of the effects when extreme growth arises.

It is important to note that we are mostly interested in the effect that a change in the synthetic future year matrix (S_f) would have on the pivoted outcome (F). For that reason, we can rewrite the normal growth part of Case 8 from:

$$F = B \times \frac{S_f}{S_b} \text{ as } F = \frac{S_f}{S_b/B} \qquad (10)$$

The normal growth situation shows the linear relationship between F and S_f, apart from the factor as given in the denominator of Equation 10, which can be seen as an indicator of the match between the synthetic base matrix S_b and the base year value (B). In general, the denominator of Equation 10 remains equal for a given cell between different model applications, it is interesting to analyse the effects of different switch points on the predicted outcome.

Figure 1 illustrates several different values for the various matrices involved and consequently several sets of predictions are derived, clustered by the match between the two base year matrices: S_b/B (using lines for each value of this ratio as given in the legend).

FIGURE 1

Comparison of Synthetic vs Pivoted Forecast

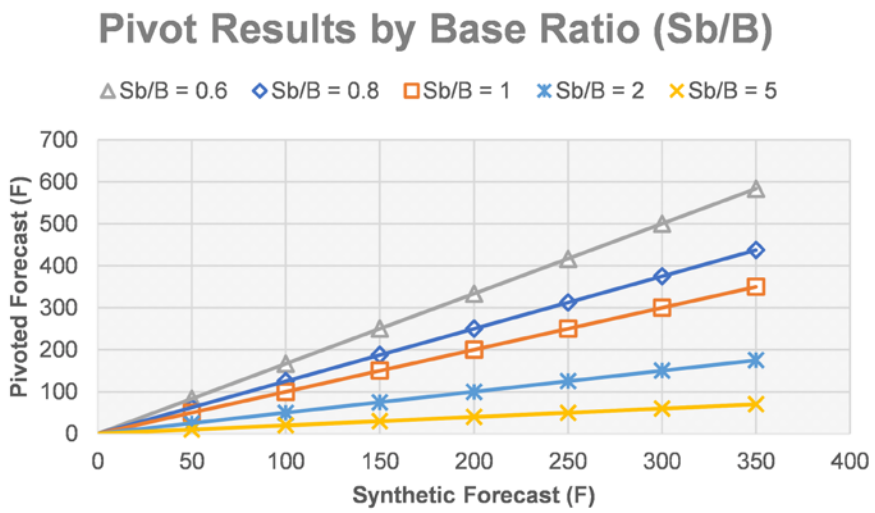

The results from Figure 1 demonstrate that the switch from relative to absolute pivoting is applied when the ratio S_b/B is smaller than 1.0 and that the switch point is applied earlier (with lower values for S_f) when the ratio S_b/B gets much smaller than 1.0. This reflects the requirement to damp the predicted outcomes and to use more absolute pivoting when cells of these two matrices are less comparable to one another.

Figure 2 presents the impact of zonal versus sector pivoting (as discussed above) to understand the need for normalisation. Several different values for the various matrices involved and consequently several sets of predictions are derived for a particular match of S_b/B=1 based on the above demonstration.

FIGURE 2

Comparison of Pivoted & Normalised Growth against Synthetic Growth

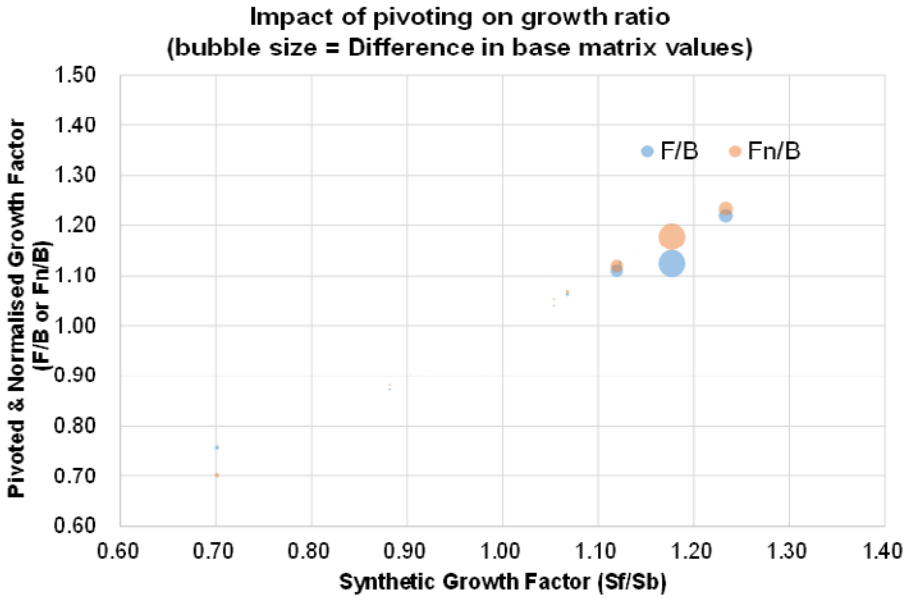

4. Conclusions

The use of pivoting is widespread in practical transport planning and has substantial advantages for reducing errors in forecasting. However, a purely incremental approach may not be sensible for large changes in land use between the base and forecast years. In the current practice both factoring and difference approaches to pivoting are used. The UK practice recommends the use of pivoting strongly but does not advocate one specific method. Other literature that we have found primarily focuses on the use of incremental modelling.

Incremental modelling and factor pivoting are closely equivalent, except when factor pivoting is used without 'normalising' to correct the total number of choices made. In general, forecasts should be normalised, because the function of each model is to predict proportions choosing each alternative, while the total number of choices to be made is usually the function of another model. The use of difference pivoting should be restricted to special cases.

In practical experience, a system of automatic selection of the appropriate pivot procedure for a range of cases can be set up. This paper explains the procedures used over several large-scale modelling studies. These procedures have many attractive properties, such as that they are largely continuous, i.e., small changes in the inputs are unlikely to lead to large changes in the outputs.

In summary, it is concluded that pivoting is a useful procedure which can improve the accuracy of model forecasts, but that care is required in practice.

Appendix - Incremental Model Formulation

The standard incremental multinomial logit model is given as:

$$p_p = \frac{p_p^0 \exp(\theta \Delta U_p)}{\sum_q p_q^0 \exp(\theta \Delta U_q)} \qquad (11)$$

where,

p_p is the forecast probability of choosing alternative p.

p_p^0 is the reference case probability of choosing alternative p (calculated from the input reference demand).

θ is the scaling parameter (always =1 for the bottom level of the hierarchy).

ΔU_p is the change in the utility of alternative p.

For the choice at the bottom level of the hierarchy the change in utility is given by

$$\Delta U^* = -\lambda * (C_p - C_p^0) \qquad (12)$$

where,

C_p^0 is the reference generalised cost and

C_p is the forecast generalised cost, skimmed from the latest assignment.

λ is the spread or dispersion parameter (defined by the user) - it should be positive.

For choices above the bottom level of the hierarchy the change in utility is the composite change over the alternatives in the level below:

$$\Delta U^* = ln \sum_p p_p^0 \exp(\Delta U_p) \qquad (13)$$

This model formulation can be used for mode choice, time period choice and singly constrained distribution.

Acknowledgements

This paper was originally presented at the 9th Conference on Transportation Systems Engineering and Management (CTSEM 2023), October 12-14, 2023, NIT Warangal, Hanamkonda, India.

References

[1] Manheim, M. L.: Fundamentals of Transportation System Analysis, The MIT Press, Cambridge, Mass (1979).

[2] J. Bates, D. Ashley, G. Hyman: The Nested Incremental Logit Model: Theory and Application to Modal Choice. In: 15th PTRC Summer Annual Meeting, University of Bath, England (1987).

[3] Transport Appraisal Guidance TAG M2.1, Department for Transport, UK.

[4] Andrew Daly, James Fox, Jan Gerrit Tuinenga: Pivot-point procedures in Practical Travel Demand Forecasting, European Congress of the Regional Science Association, Amsterdam (2005).

[5] Ortúzar J. de D., L. G. Willumsen: Modelling Transport, 3rd edn. John Wiley & Sons Ltd, Chichester, UK (2001).

[6] Andrew Daly, James Fox, Bhanu Patruni: Pivoting in Travel Demand Models, Association for European Transport and Contributors (2011).

Pankaj Mendiratta
Associate Design Manager
Global Technology Centre (GTC)
- Transportation, Signalling Systems
Gurgaon, India

John Lovick
Senior Signalling Design Manager
Transportation UK
Swindon, UK

Transportation

07: Overlay Axle Counter Automatic Half Barrier Crossing

Abstract

Railway track experiences all the climatic extremes the planet can throw at it. It is also subjected to heavy loads, vibration, pollution and electromagnetic interference. Detecting the position of a train on the track has historically been completed using track circuits – a simple electrical circuit that uses the rails themselves as part of the circuit. This is not the ideal environment for an exposed electrical circuit that is a safety-critical element of the signalling system.

That said, track circuits are generally highly reliable but, when they fail, this is usually due to environmental conditions interfering with the completion of the circuit.

As the system is fail safe, there is no safety risk, but such failures have a high service impact. At level crossings, this affects not only the railway but also the road users. Track circuits and directional treadles are less reliable on low use lines. This is one of the reasons that other train positioning systems such as axle counters are increasingly popular and are now the train detection system of choice for Network Rail.

Coltishall Lane & Belaugh Lane Level Crossings are the first Automatic Half Barrier Crossings (AHBCs) deployed in United Kingdom using an "Overlay Axle Counter" Solution.

The new Overlay Axle Counter AHBC solution offers increased economy in implementation and reliability in service over the existing practice of traditional AHBC using directional treadles and track circuits to determine the position of the train.

KEYWORDS
Overlay AHBC; Frauscher Axle Counter, Direction Treadle; Unconditional Reset; Reduced Complexity

1. Introduction

1.1 BACKGROUND

Coltishall Lane and Belaugh Lane were existing User Worked Crossings with Telephones (UWCT). The controlling signaller had no indication of the current state of the crossing.

Crossing users had to contact the signaller via the telephone provided at the crossing to obtain the authority to open the crossing gates and cross the railway and then close the gates afterwards.

Historically there was a high level of misuse at the crossings, where users have failed to use the telephones provided and crossed the railway without authority. This situation was expected to worsen as it was predicted that there will be increase in usage of the crossings.

FIGURE 1

Existing Coltishall Lane Level Crossing - UWCT

1.2 PURPOSE

Given the situation, AtkinsRéalis was approached by Network Rail to plan, organise and carry out improvement actions at these level crossings and renew the signalling technology. A critical element of this work was that the level crossing upgrades needed to be completed within the limited timeframe before the crossing use increased. The NR Anglia Route team completed an option selection report in which various options for changing the method of control for both level crossings was assessed. This report determined that the provision of Automatic Half Barrier Level Crossings (AHBCs) was the recommended option, as it was the only option that managed the risk posed at the crossings effectively. Both the UWCTs level crossings were to be upgraded to AHBCs to improve safety and satisfy the corrective action dates for the UWCT's.

2. Existing Signalling Systems

2.1 TRADITIONAL AHBC

Traditionally, AHBC are installed using a combination of track circuits and treadles for train detection/initiation of level crossing or a combination of axle counters for train detection/initiation of level crossing and directional treadles. This ensures that both the position and the direction of trains can be determined and improves the reliability of the train detection system for the level crossing.

FIGURE 2

Typical Treadle Arrangements at a Single Line Automatic Crossing

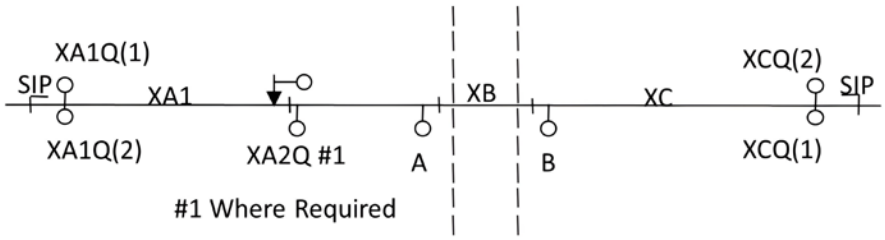

In Figure 2, XA1Q(1)/XA1Q(2) and XCQ(1)/XCQ(2) are directional treadles. XA1, XB, and xc are track circuits.

2.2 TRAIN DETECTION

A train detection system forms part of or provides the input to the signalling system to detect:

- that a train has reached, is passing or has passed a specific position (discrete systems),
- the presence or absence of vehicles within the limits of a track section (continuous systems), or
- the absence of vehicles within an envelope ahead of a train that progresses with the passage of the train (moving block systems).

Where required, a train detection system may additionally detect the direction in which a train is travelling. (In the case of axle counters, this is a requirement of this method of operation.)

Continuous train detection systems include all the various types of track circuits and confirm the presence or absence of a train along their entire length within the limits of the track circuit.

Discrete train detection systems include axle counters and wheel detectors (treadles or electromagnetic proximity devices) and rail circuits, which confirm the presence or absence of a train at discrete points along the track. These may be provided in addition to continuous systems.

In areas of track circuit block operation, which is based on dividing the railway into small track circuit sections to determine the position of all trains within the control area, it is possible to provide either continuous train detection (e.g., track circuits) or discrete entrance and exit monitoring (e.g., axle counters).

A key feature of the different types of train detection are the designed failure modes. Systems that fail in the occupied state can prove the absence of a train. For instance, the track circuit is a device designed to continuously prove the absence of a train from a given track section; it cannot absolutely prove the presence of a train since its designed failure mode provides the same indication as if a train is present.

Some train detection systems, such as axle counters, provide an undefined state in addition to occupied and clear indications. This can assist, under failure conditions, in ensuring that the safest state is achieved for all applications.

Existing AHB crossings in the area near Coltishall and Belaugh use directional treadles and track circuits specific to their own crossing to provide train detection and operation of the crossing. As previously stated, these are less reliable on low use lines.

2.3 INTEFACE OF TRADITIONAL AHBC WITH EXISTING INTERLOCKING

When renewing AHB level crossings and modifying the train detection system, it is typical that the train detection alterations would be incorporated into the existing signalling controls. However, this increases the volume of work required. In Wroxham Interlocking area, where Coltishall Lane and Belaugh Lane Level Crossing are present, it was not possible to convert the existing UWCTs to AHBCs using a traditional method (i.e., install new track circuits and directional treadles and interface the new AHBCs with the existing interlocking and use the track circuits for initiation of the Level Crossings) within the limited timeframe available. Interfacing with the existing interlocking would have increased the complexities of the project and it would have made the deadlines of the timeframe unachievable.

3. General

3.1 LEVEL CROSSINGS

For automatic level crossing operation (including manually controlled crossings equipped with auto-raise facilities), train detection is generally required to prove:

- the absence of an approaching train to allow the crossing to be open to road traffic, and
- the presence of the train on the exit side before the crossing can be normalised after operation.

Where additional integrity of the train detection function is required (e.g., for the operation of automatic level crossings (not locally monitored)), some form of diversity or duplication of train detection device may be required on the approach to the crossing.

Where operation is monitored locally by the driver observing an indicator, a lesser integrity of train detection may be sufficient to ensure safety.

3.1.1 Automatic Half Barrier Crossings - General Description

1. The crossing is worked automatically by the passage of trains.
2. Protecting signals shall be provided within ten minutes running time at permissible speed. This limit shall not apply in RETB or ERTMS areas where there is continuous voice communication between train and signal box, or arrangements are in place for each train to contact the signaller and obtain permission before proceeding over the crossing.
3. Where a protecting signal is not directly controlled or slotted by the signal box supervising the crossing, arrangements shall be in place to alert the signaller controlling the protecting signal to replace it to danger quickly in an emergency. For example: In an absolute block area, then sending the emergency alarm “6 bells” (communication code sent by signaller) is sufficient. In other areas, an emergency alarm or similar shall be provided.

4. AHB crossings have barriers pivoted at the nearside of the road and are of length up to the centre line of the road. The exit sides of the roads are kept clear to allow slow moving vehicles to clear the crossing.
5. Each road approach is protected by a minimum of two road traffic light signals (RTL's). One unit is sited on each side of the road approach.
6. Audible warnings are provided for pedestrians. There are a minimum of two units. They shall be normally sited at the diagonally opposite nearside corners of the crossing facing onto the crossing area. Larger crossings may use four audible warning devices with one at each corner.
7. A scaled level crossing ground plan defines and locates all equipment sited at the level crossing.
8. Telephones for users are provided. (The normal system used at AHB crossings is the P.E.Ts system.)
9. The maximum length of trains permitted to operate over the level crossing shall be documented in the design details.

3.1.2 AHBC - Train Detection System Controls

1. Train detection sections situated within the crossing control area, once occupied, shall initiate the crossing operation. The crossing operation shall be maintained (by means of a stick control) until:

    - The train has been proved to clear the crossing by sequential operation of the train detection sections, or
    - A suitable time has lapsed after the train detection section has cleared.

2. Failure of a train detection section shall result in the following consequences:

    - If a random train detection section occupation occurs which subsequently clears, the level crossing operating sequence shall be initiated. At a suitable time after train detection clearance (default of three minutes), the level crossing operating sequence shall be cancelled (unless other track sections within the crossing control area are also occupied).
    - If a random train detection section occupation occurs which does not subsequently clear, the level crossing operating sequence shall be initiated. After a suitable time (default of three minutes), the monitoring point shall receive an indication that the level crossing has failed. The level crossing operating sequence shall be maintained until the fault is cleared.
    - If an exit train detection section fails to clear after the passage of a train (which means a train movement has correctly initiated and subsequently cancelled the level crossing operating sequence), then after the exit track section has been occupied for a period (default three minutes or such period as moving trains may legitimately occupied the exit train detection section), the operating sequence shall re initiate and the monitoring point shall receive an indication that the level crossing has failed. The warning sequence shall be maintained until the fault is cleared. Where, however, trains may legitimately stand on an exit track circuit for a time (e.g., due to a station or signalling control), this feature is disabled and alternative protection arrangements are provided that prevent another train approaching until the fault is cleared.

3.2 AXLE COUNTERS

The axle counter system is a safety critical system responsible for providing reliable train detection information to the interlocking and signaller.

Axle counter systems utilise wheel detection points at each end of a section of track. The area of line between the wheel detection points forms an axle counter train detection section.

The wheel detection points count the number of wheels entering and the number of wheels exiting the axle counter train detection section. The section is deemed to be occupied once a wheel has been counted into the axle counter section and until all axles counted in have subsequently been counted out.

The function of counting the number of wheels into and out of the axle counter train detection section, and from that determining the occupancy status, is referred to as evaluation, and is carried out by the axle counter system. The axle counter system provides a permanent indication of axle counter section status (section occupied, clear or undefined).

Axle counter systems provide an alternative method of train detection to conventional track circuits.

A prime difference between a track circuit and an axle counter train detection section is that the occupancy status of an axle counter train detection section is fully determined by the wheel detection points at each end, unlike track circuits which continuously detect the presence (or absence) of a train throughout its length.

4. Proposed Overlay AHBC

4.1 TRAIN DETECTION - INITIATION OF LEVEL CROSSING

For Coltishall Lane and Belaugh Lane, Level Crossing Directional Treadles were not used for the initiation of the level crossing sequence.

The project developed a solution using Frauscher axle counter train detection points as an overlay train detection system for the initiation of the level crossing/detection of trains. This utilises an advanced feature of the axle counter system which determines the direction of train without the need of installing directional treadles. This contributes to minimizing the whole life maintenance cost as directional treadles are notoriously unreliable and maintenance-intensive.

Overlaying the level crossing in this scenario means the new level crossing is "overlaid" on the existing signalling system but has no interface to it. There are no control inputs from the new level crossing to the existing signalling. The existing train detection in this area remains but will not be used for the level crossing operation. Instead, Frauscher axle counters are being used for crossing operation.

4.2 ARCHITECTURE

Figure 3 shows the architecture used for Coltishall Lane and Belaugh Lane AHBC using overlay Frauscher axle counters. Each level crossing required the installation of a REB (Relocatable Equipment Building) to house the power supplies, VHLC level crossing object controller and the axle counter evaluation equipment. Separate FAdC evaluators were provided for each level crossing, which is a requirement from the Signalling Standards (NR/L2/SIG/30081).

BLA, BLB and BLC are axle counter sections for Belaugh Level Crossing, and CLA, CLB and CLC are axle counter sections for Coltishall Level Crossing. Figure 3 shows these axle counter detection points are interleaved at site, because the level crossings are in close proximity, but technically, they are not overlapping as different sections are provided for each independent FAdC evaluator.

Indication of the Level Crossing health status is sent to the control centre at Trowse via the Frauscher Axle Counter (FAdC) communications link through DDW modems. This integrates into the existing Frauscher transmission network to transmit the indications to the control centre.

FIGURE 3

Architecture

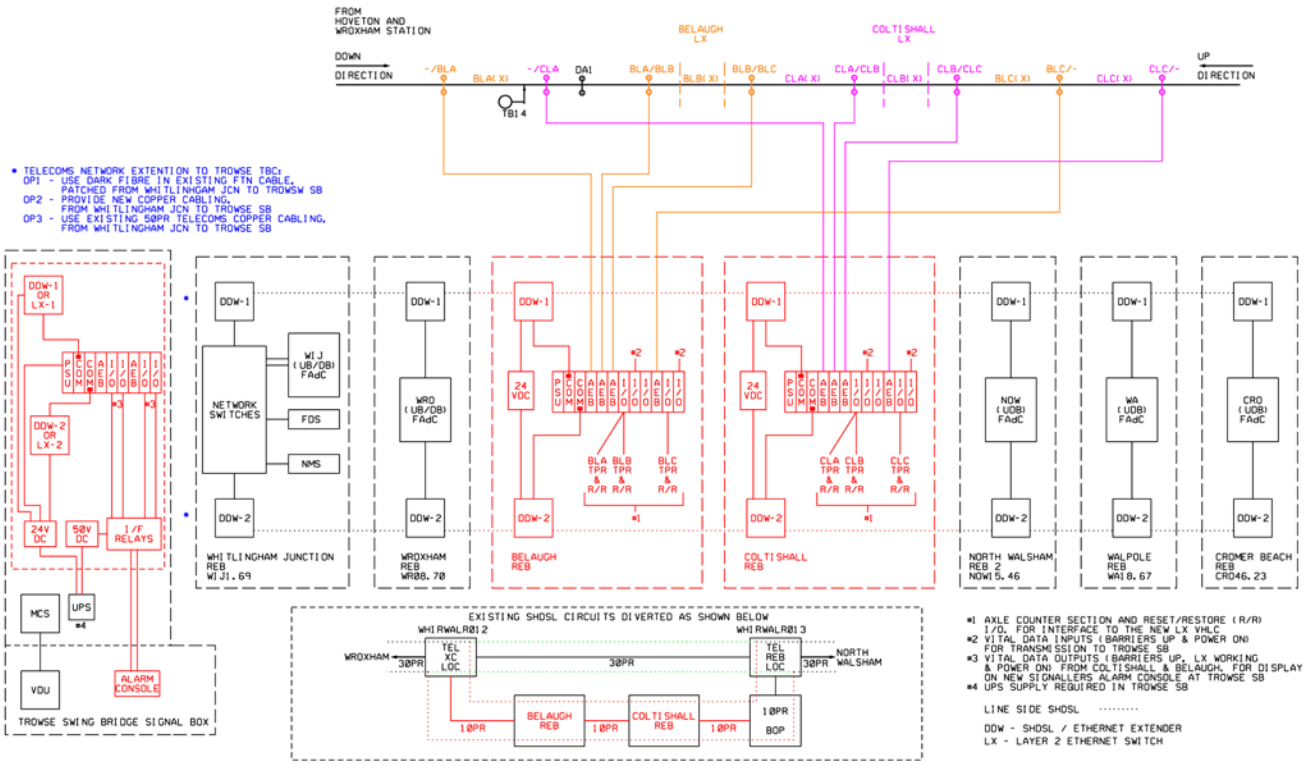

4.3 USE OF AXLE COUNTER AS DIRECTIONAL TREADLE

In this project, Frauscher axle counter head BLA(X) and CLA(X) are also used as directional treadles.

4.3.1 Requirement of Directional Treadle in the Project

Due to the proximity of the junction at Hoveton and Wroxham station to Coltishall Lane and Belaugh Lane Level Crossings, the likelihood that a train may arrive at the down direction strike is within the time provided for the exit section, CLA(X)/BLA(X), to time off, is considered.

In Figure 3, suppose a train leaves BLA(X)/CLA(X) section on the Up Line and there is a train at the station occupying BLA(X)/CLA(X) section moving in the Down direction within three minutes of a previous train departing. A three-minute default timer has been provided in the AHBC's controls to warn the signaller that the level crossing has failed in case the train detection section (axle counter section in this case) is occupied for a longer duration.

Therefore, a train arriving within three minutes and occupying the train detection section can generate the false level crossing failure alarm. To resolve this, we prove the direction of the train in the controls of the Level Crossing. The preferred solution of direction is to provide directional treadles or Frauscher wheel sensors (used in treadle mode) at the strike-in point. In our case, we used Frauscher axle counter detection points (same hardware as any normal axle counter head), and, using its unique software feature, configured the system to provide an output similar to the directional treadle, thus proving the train travelling in the down direction is a legitimate move and that the previous train has positively left the section and reset the timer. This avoided having to provide complex controls in the existing Wroxham interlocking.

In another scenario, a train can stop at signal TB14, occupying CLA(X)/BALX(X) axle counter section for an extended duration, which would cause the level crossing to fail. Again, proving the direction of the train helps in overcoming this situation, when level crossing is declared failed for a track section being occupied for excessive time.

4.4 RESET-RESTORE FUNCTION OF AXLE COUNTER

Axle counters differ from track circuits in that trains are not continuously detected, but instead wheels are counted into and out of an axle counter train detection section. This raises the possibility of counting errors and leads to the need for axle counters to be reset and restored into service following an incorrect count or disturbance. If the reset and restoration of axle counter train detection sections is carried out without ensuring the absence of trains in the section, it can pose a significant risk.

Facilities are provided to reset each axle counter section to a Clear state, from either a Disturbed or Occupied state.

The following types of resets are available with most modern microprocessor-based axle counter systems:

- Conditional (when the last wheel count is “out” in any direction, a conditional reset, which includes aspect restriction, is permitted);
- Preparatory (when the last wheel count is not “out” in any direction, preparatory reset requiring a train to traverse the section in any direction following a successful reset is permitted. This, however, delays the restoration by not reporting the status of the axle counter to the interlocking until after the passage of a train); and
- Unconditional (no conditions are applied).
- A fourth type of reset, co-operative, exists as a historical arrangement in a few locations but is non-preferred. Co-operative reset is not permitted for new work and where an extension to an existing system is proposed, a non-compliance should be sought.

4.4.1 Conditional Reset

4.4.1.1 Conditional Reset - General

Conditional reset is an "in service" reset that has less limitations than preparatory reset and is therefore more suited to complex, high-density and high-speed lines. However, the restoration function has to be controlled by the interlocking. For a conditional reset to be successful, the following conditions shall be true:

- The section shall be in a working state.
- The last count shall have been out of the section that is required to be reset (or the system should be in a disturbed state when it will reset irrespective of count status (i.e., the last count could have been into the section)).

4.4.1.2 Aspect Restriction Following Restoration (ARFR)

a) Provision of ARFR

Aspect restriction following restoration (ARFR) reinforces the need to stop and caution the first train after the signaller has reset the train detection section.

b) Application of ARFR

Where ARFR is provided then it shall be applied following successful reset of the section.

4.4.2 Preparatory Reset

Preparatory reset is an "in-service" reset that provides aspect restriction without any alteration to the interlocking being required. However, this is generally limited to areas of plain line or simple S&C (not using both routes regularly) with low train density due to the restriction it has on operations (including locking points in their last position until a train has passed). For a preparatory reset to be successful, the following conditions shall be true:

- The section shall be in a working or disturbed state.
- A train shall pass through the section and the count in and out shall evaluate to an effective zero (i.e., 10 axles in and 10 axles out 10–10 = 0);
- All detection points shall be working correctly whilst the train traverses the section.

Preparatory reset is the only reset that can provide both reset and restoration back into service within the axle counter system. The other types of resets require the process to be split between the axle counter system and the interlocking (or system other than the axle counter) to carry out the restoration back into service.

Preparatory reset can also be designed with an additional condition involving receipt of an acknowledgement from the reset operator following the passage of the first train. In this arrangement, this acknowledgment shall be received for the reset to be successful.

4.4.3 Unconditional Reset

Unconditional reset can only be applied to Network Rail axle counter applications where Engineers' Possession Reminder (EPR) is provided. For an unconditional reset to be successful, the following conditions shall be true:

- The section shall be in a working or disturbed state.

Unconditional reset can be used to reset a single section or a group of sections.

4.4.4 Type of Reset Used for Coltishall Lane and Belaugh Lane

From the section above, it is obvious that the Reset-Restore function is complex and requires an Aspect Restriction, following the restoration, to be applied. This involves signals and hence requires an interface to the existing interlocking. As explained in earlier sections, interfacing with the existing interlocking increases the complexity and the timescales of the works. Also, to reset the axle counters, an action from the signaller is required but, as per AHBC requirements, only the health of the crossing is indicated to the signaller and no signaller controls are typically provided for AHBs. Therefore, none of the typical methods of reset/restoration are suited to overlay AHBC application.

FIGURE 4

Signaller Indication Panel

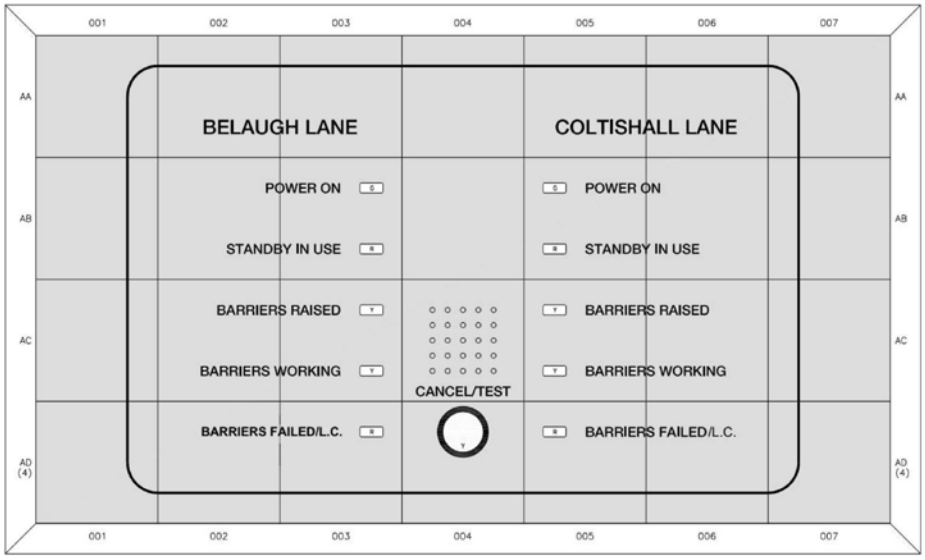

Figure 4 shows the Signaller Indication Panel for Belaugh Lane and Coltishall Lane Level Crossings.

As per Signalling Standards (NR/L2/SIG/30009/K210): "Free-standing axle counting equipment that is wholly contained within subsystems (such as overlay train detection provided for level crossings) or additional Axle-detecting devices, that are not provided for the interlocking of routes nor the clearance of signal aspects, but are used to indicate train position to signallers, should not be configured as axle counters." Therefore, Signalling Standards do not mandate the provision of a conditional reset or preparatory reset for restoration of disturbed axle counter.

In this project, if an axle counter fails, the signaller will receive a level crossing failure indication. The signaller will inform the technician of the failure. The technician will go to the site, identify the issue, repair the fault and then reset the failed axle counter; the method used for reset is “Unconditional Reset.” To ensure road and rail safety during unconditional reset, the level crossing control circuitry verifies that the technician has put the level crossing in local/manual mode before the unconditional reset of the axle counter section can be performed. The technician will then contact the signaller to ensure the crossing fail indication and alarm have been cleared.

FIGURE 5

Axle counter Reset Unit at Belaugh REB

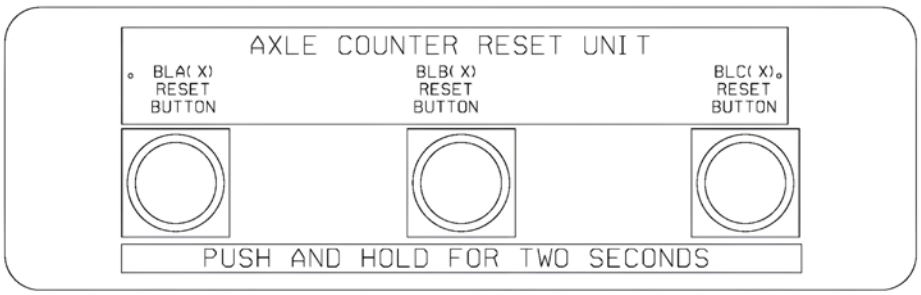

FIGURE 6

Axle counter Reset Unit at Coltishall REB

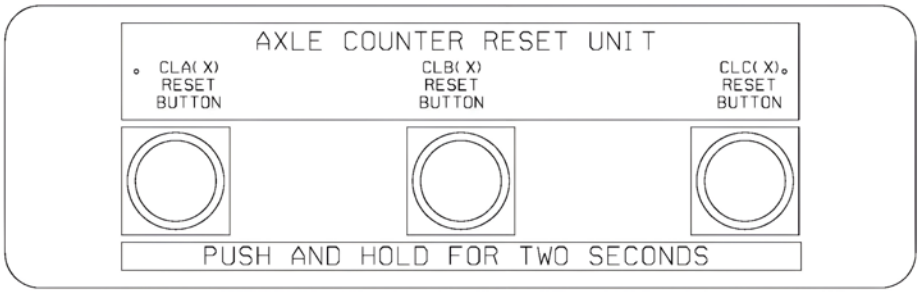

Figures 5 and 6 show the Axle Counter Reset Units provided at each Level Crossing REB to reset the individual axle counter sections.

4.4.5 Onsite Monitoring and Operational Feedback

Discussions with the Project team and operators at Trowes have provided feedback on the project in the six months post commissioning.

Technician call outs have been minimal, with only attendance for minor faults with the crossings. These have been categorised as the following:

- Failure due to misuse during engineering works – Disturbed axle counters.
- Axle counter failure – None known.
- Level crossing equipment failure – SPX barrier unit failure.

The operator and maintenance team have produced a standard operating notice to operate a failed crossing using the reset provided. This is reported as working well.

FIGURE 7

Coltishall Level Crossing with Overlay AHBC – The First Signalling Project to be Commissioned under brand name AtkinsRéalis

FIGURE 8

Belaugh Level Crossing with Overlay AHBC – The First Signalling Project to be Commissioned under brand name AtkinsRéalis

5. Conclusion

The Signalling system proposed here reduced the cost of the railway infrastructure upgrades by using the functionality provided in the Frauscher Axle Counter system in a more effective way. This resulted in installing less equipment at site (traditional directional treadle), minimizing whole life maintenance cost, and improved level crossing safety. The overlay axle counter solution delivered less complexity, easier integration to the existing signalling system, reduced level crossing closures, improved reliability performance and significantly reduced project implementation time and cost.

This solution can further be incorporated into other signalling architectures such as the Advanced Signalling Method (ASM). Integrated by AtkinsRéalis, ASM utilises ElectroLogIXS as the signalling interlocking, object controller and level crossing controller, making an overlay axle counter solution simple, effective and easily deployed at site.

Acknowledgements

The authors are grateful to the following for their contribution and support:

Neil Warburton (Transportation-UK), Mohan Sarvepalli (Transportation-GTC-India), Sethuraman Ramaswamy (Transportation-GTC-India), Rajeev Gupta (Transportation-GTC-India), Amit Kumar (Transportation-GTC-India).

References

Coltishall Lane & Belaugh Lane Level Crossing Upgrade Scheme Plan - 22-NE-0009. Internal AtkinsRéalis project document: unpublished.

Network Rail. NR/L2/SIG/11201, Mod X10 – Level Crossings: Automatic Half Barriers. In: Signalling Design Handbook, Sep 2011.

Network Rail. NR/L2/SIG/30081 Axle Counter System Design Principles and Generic Application Rules, Sep 2009.

Network Rail. NR/L2/SIG/30009, K210 Axle Counter System Application Principles. In: Signalling Principles Handbook, Dec 2021.

Network Rail. NR/SP/SIG/11752 Train Detection Handbook, Sep 2021.

Network Rail. NR/L2/SIG/11201, Mod X99 – Level Crossings: History of Level Crossings. In: Signalling Design Handbook, Sep 2011.

Belaugh Lane AHBC Interface Specification. Internal AtkinsRéalis project document: unpublished.

Coltishall Lane AHBC Interface Specification. Internal AtkinsRéalis project document: unpublished.

Arpley Bridge, Warrington, UK
Photo © Stephen Richards (cc-by-sa/2.0)

Sarbartha Banerjee
Engineer
Global Technology Centre
Bangalore, India

Abani Satapathy
Senior Design Manager
Global Technology Centre
Bagalore, India

Tiju Zachariah
Technical Director
Global Technology Centre
Bangalore, India

Harpreet Singh Sandhu
Principal Engineer
Transportation UK
Birmingham, UK

Jon Wang
Principal Engineer
Transportation UK
Birmingham, UK

Transportation

08: Assessment of River Mersey Steel Truss Bridge Using Non-Linear Finite Element Analysis

Abstract

United Kingdom's railway bridges, a majority of which are more than 150 years old, are owned, managed, and maintained by Network Rail (NR). For the safe and efficient administration of the rail network, it is essential to have up-to-date capability information for these ageing assets.

One example of its kind is River Mersey Bridge (SDJ2/38A). It was initially built in 1854 as a wrought iron tubular structure, before being later rebuilt with steel, except the central box girder, in the year 1908.

As per NR/GN/CIV/025, Level 1 assessment would not adequately depict the interaction between the main structural parts as expected for a structure of this age due to its known conservative nature. Therefore, it was beneficial to perform non-linear analysis as part of Level 2 assessment.

In order to properly simulate the structure and account for the potential failure modes of the structural components, this study took the complete structure into account. The paper also provides insight into the mathematical model developed to capture all the section losses obtained from the inspection for assessment report (IFA). The critical mode shape obtained from Eigenvalue buckling analysis was used as an input for initial imperfection to carry out the non-linear analysis (geometric and material). Discussions were carried out on the use of a model to calculate the Von Mises stresses in Ultimate Limit State (ULS) and Service Limit State (SLS), areas of material yield, and the tendency of local premature buckling.

KEYWORDS

Finite element analysis; Eigenvalue Analysis; Non-Linear Analysis; Geometric non-linearity; Material non-linearity; Long span bridge

1. Introduction

1.1 DESCRIPTION OF THE STRUCTURE

River Mersey Bridge (SDJ2/38A), also known as Arpley Bridge, is a single span under bridge which carries two non-electrified up main and down main tracks over river Mersey between Timperley Junction and Warrington bank quay station. The center-to-center distance between the bearings is 57.912 m. The structure has a limited line speed of 20 mph. Public walkways running along the length of the bridge on each side consist of a composite decking supported on the cross girders and intermediate members. The superstructure comprised of 2 nos external steel lattice truss girders, 1 no wrought iron center box girder with cast iron part of the top flange, 37 nos steel cross girders, (2x2 nos) longitudinal rail bearers, 2 nos parapet, deck plates, overhead lattice bracing, and 38 nos transverse RSJ's sit on top of the metallic rail bearers and found between every cross girder on both the upside and downside of the structure. The rails sit directly over the timber way beams supported by railway joists. Refer to Figures 1 and 2.

FIGURE 1

Cross-section of the bridge in the year 1853

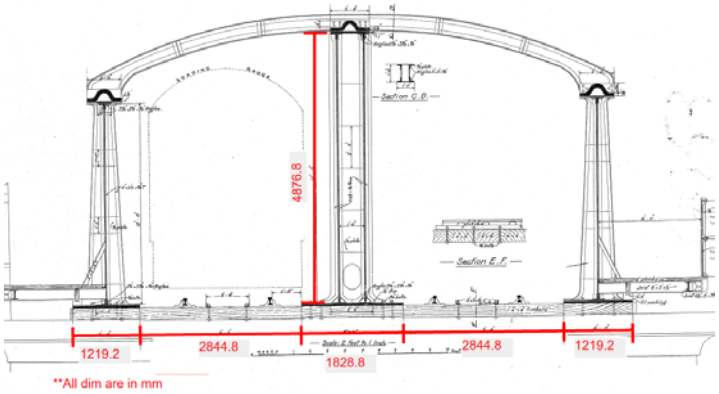

FIGURE 2

Cross-section of the bridge in the year 1908

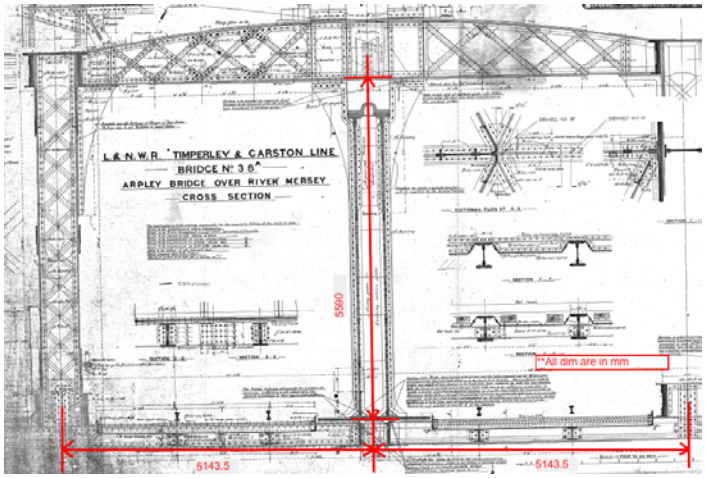

1.2 BACKGROUND

In 1908, the bridge was entirely reconstructed in steel except for the original wrought iron plated inner main girder, which was constructed in 1853 when the line opened.

A budget was proposed for 1972-1973 due to several severely damaged floor plates and rail bearers. There was a proposal to refloor the bridge in concrete, but the strength of the old wrought iron center main girder was in doubt. Hence, live load tests were conducted. The objective was to identify the live load distribution between the three main girders.

It was instantly clear from the test results that the central primary wrought iron girder was bearing a portion of the live load, and it was immediately advised not to add any extra dead weight. Later, all the original floor plates were taken away, and a flat steel plate was installed in their place. A glass reinforced plastic (GRP) walkway system was installed in 2007 to replace the old timber walkway deck. A new cross member, rail bearers, and deck were installed after the exposed steel girder and handrail were cleaned and repaired.

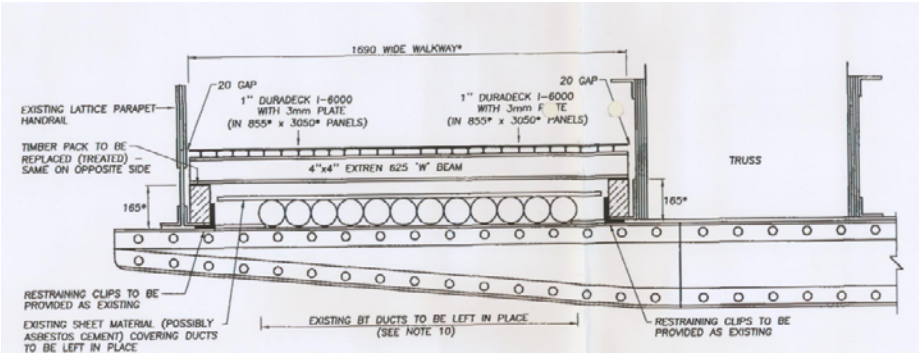

FIGURE 3

Cross-section of GRP walkway system

1.3 MONITORING

Aspen Burrow Crocker was appointed by Rail track NW to undertake the inspection and assessment of river Mersey bridge in the year 2003.

The live load carrying capacity of the bridge was found to be as follows:

- RA9 at the line speed of 40 mph.
- Sprinters (trains or locomotives capable of higher speeds) are accommodated at the line speed of 40 mph.
- 100-Tonnes fisons tanker (related to transporting nuclear materials) was not accommodated. The critical members were the bottom of the central girder which was overstressed by 3.8% under static loading and 7.8% under dynamic loading at 40 mph, and the bracing between on the external girder which was overstressed by 0.77% under static loading and 4.54% under dynamic loading at 40 mph.

Note: "RA rating" typically refers to the Load Rating Factor (RA) assigned to a bridge. The RA rating indicates the maximum safe load-carrying capacity of the bridge relative to the loads it's designed to support.

The main foundations had been qualitatively assessed as satisfactory.

ATKINS (now AtkinsRéalis) conducted an Inspection for Assessment (IFA) in December 2020 to scrutinize the bridge's current condition and gather additional data needed for the structural assessment and the calculation of the safe load capacity. As a result, reports of various section losses and corrosion were made.

FIGURE 4

[A] Bottom chord loss of section to gusset plate top flange.
[B] Loss of section to Gusset Plate
[C] Loss of section to bottom chord top flange 600 mm x 40 mm

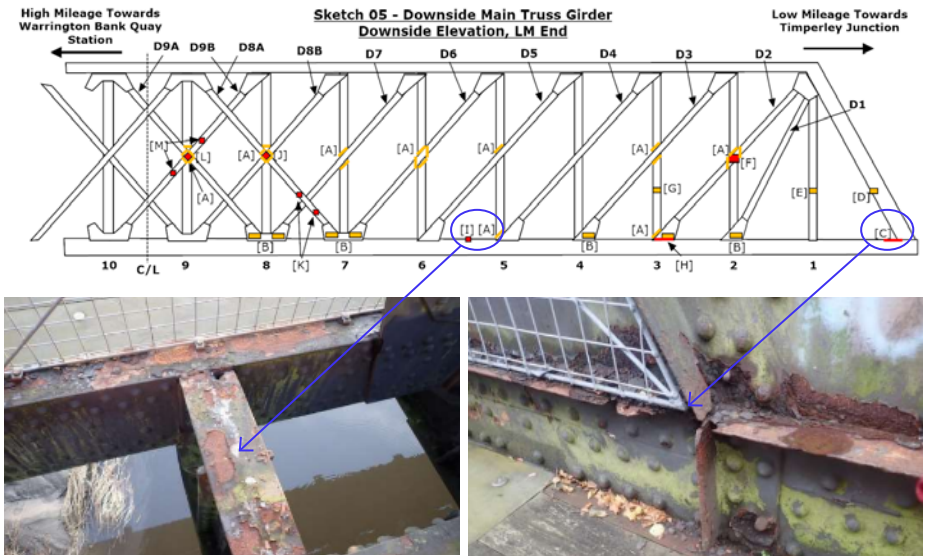

[A] [B]

FIGURE 5

LUSAS model indicating all losses were captured based on the IFA report findings

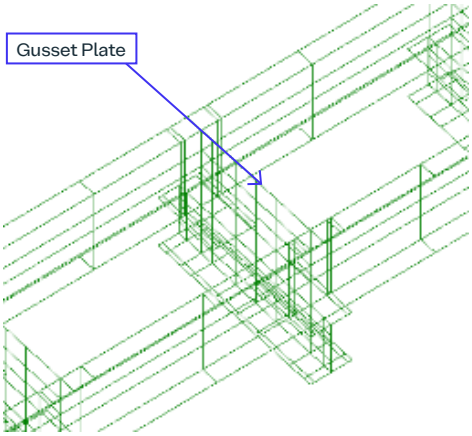

[A] Gusset plate top flange not modelled in LUSAS

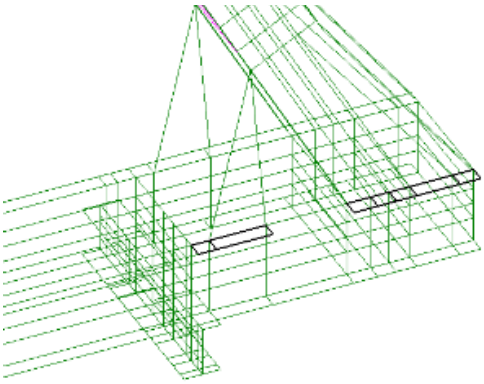

[C] Loss of section to bottom chord top flange 600 mm x 40 mm

The Inspection for Assessment Report highlights significant areas of corrosion and section losses to various elements throughout the structure. Based on these, corrosion has been applied to the structural members modelled as plates by reducing the thickness of plates and adjusting the eccentricity of the plate centroid from the plane of the surface which defines it.

FIGURE 6

Application of member thicknesses

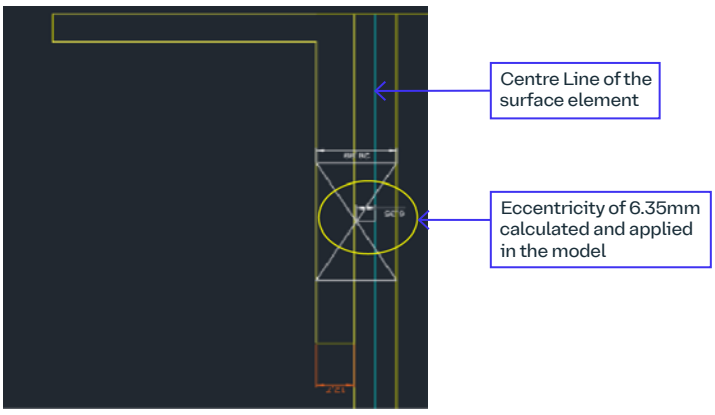

2. Assessment

2.1 METHODOLOGY FOR ASSESSMENT

The workflow for the assessment check included three critical stages outlined below.

Stage 1 - Linear Elastic Analysis was undertaken to investigate if the structural elements were susceptible to local and global buckling failure, highlighting potential problem areas for further analyses.

Stage 2 - Eigenvalue buckling analysis was undertaken to determine the tendency of the compression elements to buckle under the applied loads which had taken benefit of the increased structural restraint due to the overall interaction of the superstructure elements.

Stage 3 - Non-Linear Yield Analysis was performed to identify high stress/yield regions using Sx (Fx, My, Mz) for beam elements and resulting stress contours (SE) over shell elements. SLS checks were carried out.

2.2 MODELING OF THE SUPERSTRUCTURE

LUSAS analysis software (version 19.0) was used to analyse this bridge. Based on the available historical data and Inspection for assessment (IFA) report, the structure's geometry was modelled as precisely as possible. All the elements were modelled as thick shell elements (LUSAS element name Linear thick shell elements (QTS4)) except the wind bracings and bracings for vertical and diagonal members of the edge girders which were modelled as beam elements (LUSAS element name Thick beam element (BMI21)). 2 No. Main lattice girders – QTS4, 1 No. Central main girders – QTS4, 2 No. C-Section supporting – QTS4, 37 No. Transverse girders – QTS4, 4 No. Rail bearers – QTS4, Wind bracings – BMI21, and Bracings in lattice girders – BMI21.

FIGURE 7

QTS4 elements represented in green; BMI21 Elements in blue

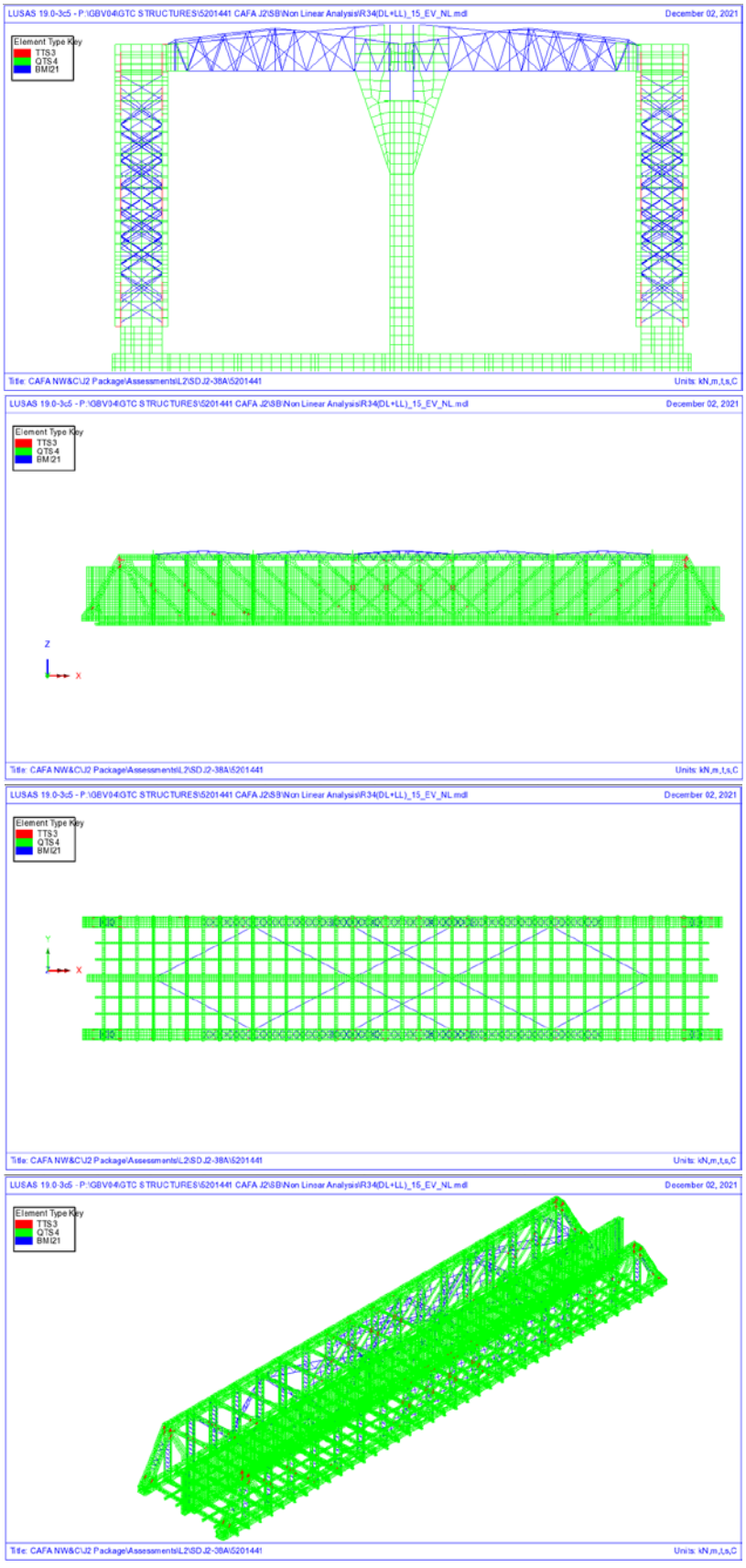

The two main lattice girders were modelled using plate elements. The lattice girder comprised of top and bottom chords connected by vertical and diagonal members by the gusset plate shown below (Figure 8).

FIGURE 8

Isometric view of the main lattice girder and its components

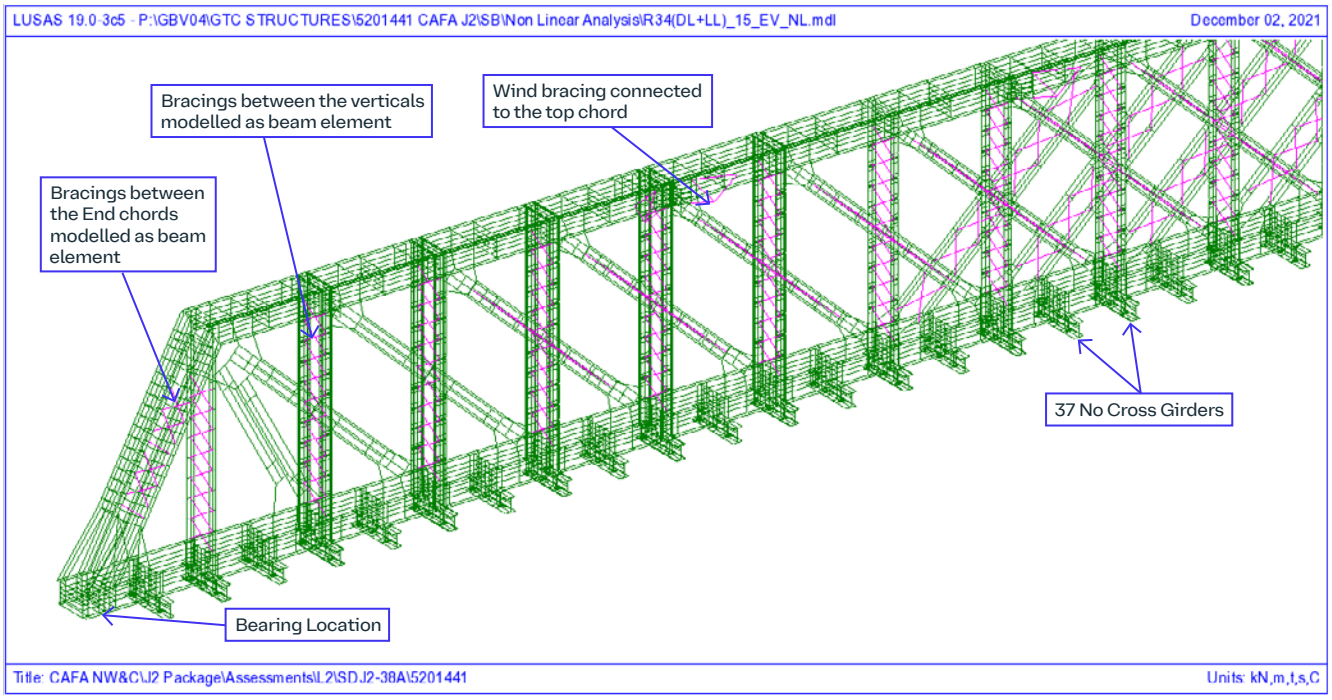

The wind bracings were modelled as a line beam and were connected to the lattice girder by gusset plates shown below.

FIGURE 9

Isometric view of wind bracings at the top modelled as beam element connected to the top chord of the main lattice girder at both the ends and connected to central box girder via stiffeners

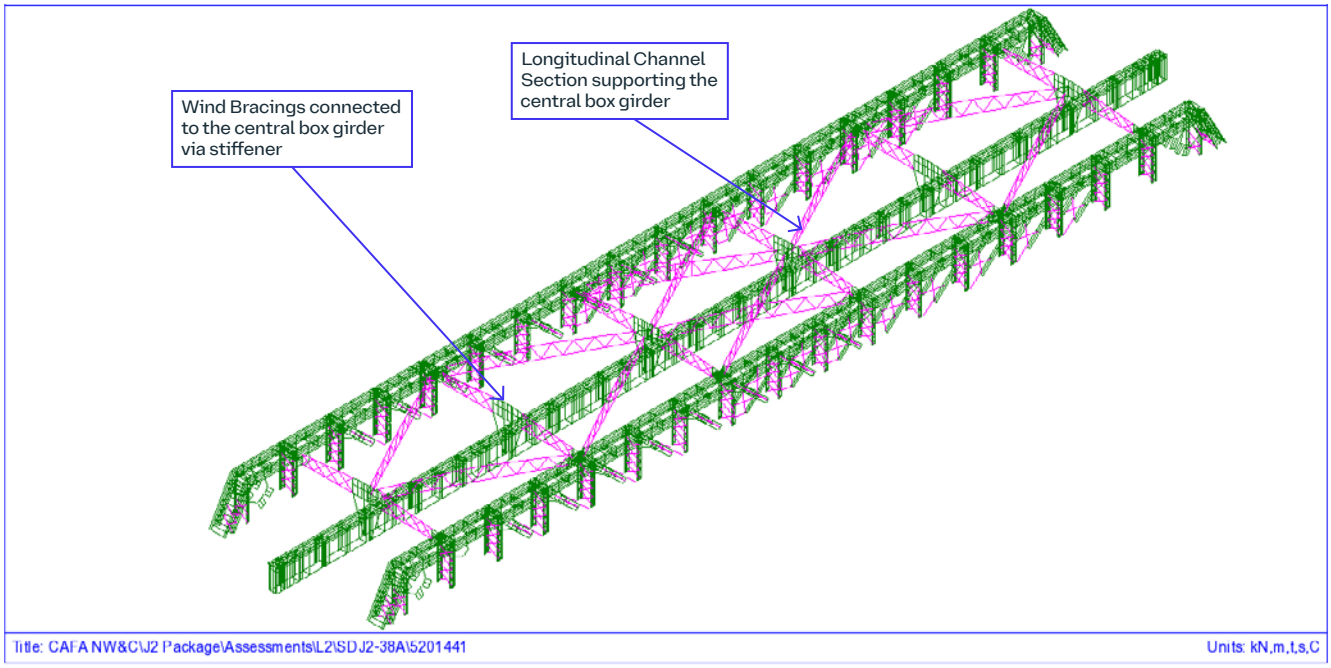

The central box girder along with the central channel section supporting the box portion were modelled as shell elements as shown below.

FIGURE 10

Isometric view of the central box girder and stiffener location

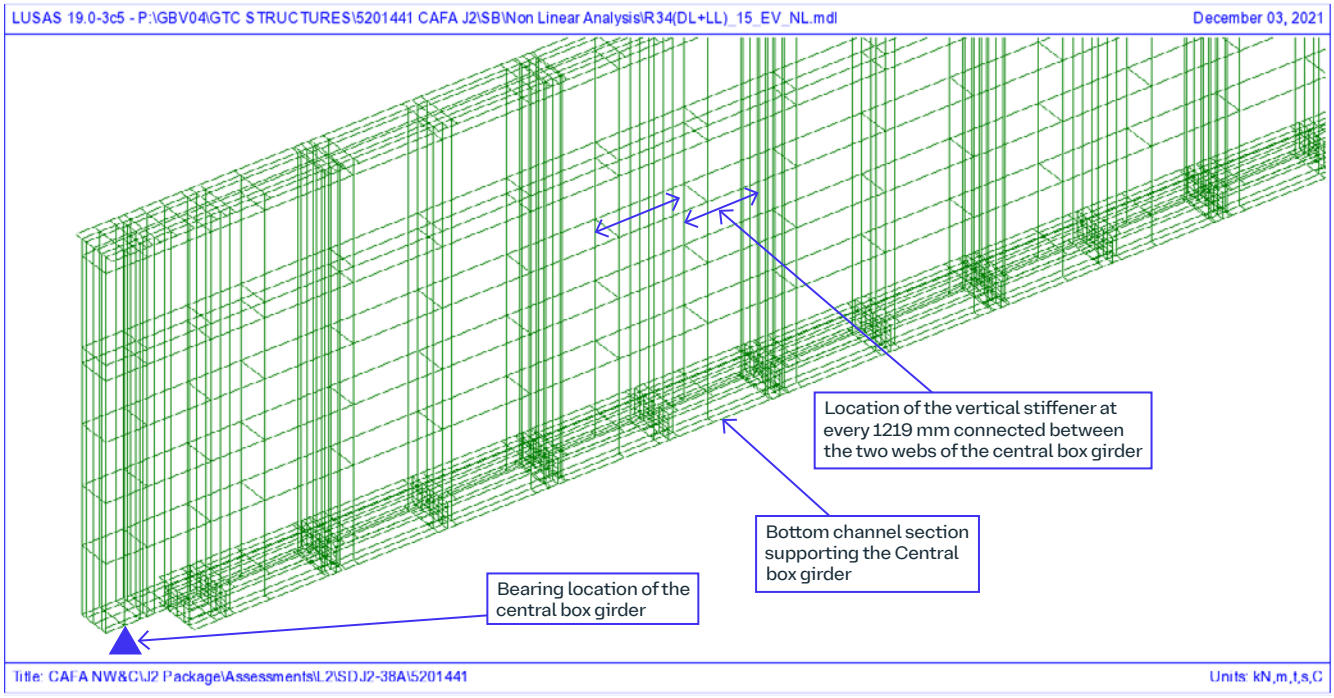

FIGURE 11

Plan view of the bridge showing bearing locations and wind bracings at the top

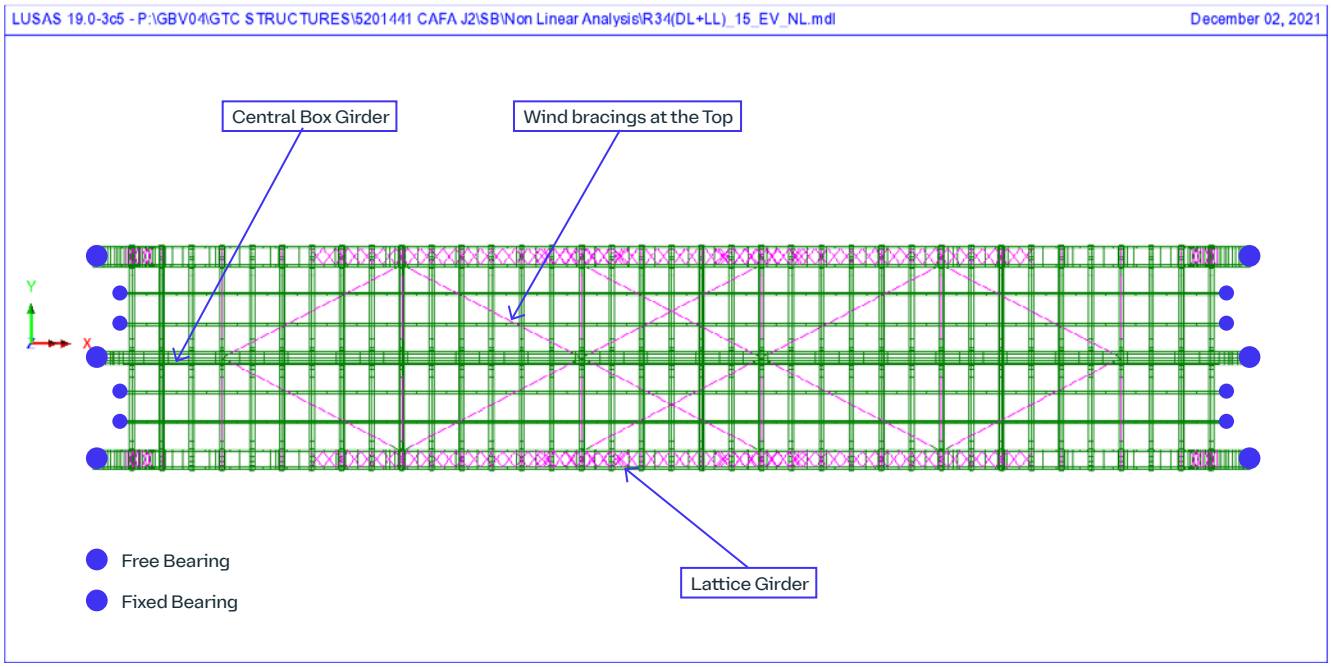

The mesh has been applied consistently, with all the elements being aligned in the same orientation where possible to ensure accurate load effects from the analysis. The shell elements within the model have been sub-divided to generate the most efficient mesh and obtain the most representative assessed capacity with the minimum mesh element size of 200 mm to a maximum of 400 mm. Accordingly, the mesh size of the BMI21 type of beam elements was decided and assigned.

In accordance with NR/GN/CIV/025, the characteristic yield strength of the superstructure steel and wrought iron elements has been adopted throughout as follows:

Wrought Iron, σ_y = 200 N/mm^2
Steel, σ_y = 230 N/mm^2

The factored yield stress values used within the non-linear model were therefore calculated as follows:

Factored Yield Stress = σ_y / (γ_m x γ_{f3})

Ultimate Limit State (ULS):
Allowable yield stress = σ_y / (γ_m x γ_{f3})
For Wrought Iron = 200 / (1.05 x 1.1) = **173.16** N/mm^2
For Steel = 230 / (1.05 x 1.1) = **199.14** N/mm^2

Serviceability Limit State (SLS):
Allowable yield stress = σ_y / (γ_m x γ_{f3})
For Wrought Iron = 200 / (1.0 x 1.0) = **200** N/mm^2
For Steel = 230 / (1.0 x 1.0) = **230** N/mm^2

A linear model has been used both for load optimization purposes and for an elastic linear buckling analysis. The support conditions applied to the model are summarized below:

- Lattice Girder (Low Mileage) – Fixed Bearing – X, Y & Z Restrained.
- Lattice Girder (High Mileage) – Free Bearing – Y & Z Restrained.
- Central Box Girder (Low Mileage) – Fixed Bearing - X, Y & Z Restrained.
- Central Box Girder (High Mileage) – Free Bearing - Y & Z Restrained.
- X indicates Longitudinal, Y indicates Transverse & Z indicates vertical.

2.3 MODEL LOADING

Steel and wrought iron dead loads have been directly applied in LUSAS as gravity load to the simulated parts. In the LUSAS model, the dead loads from the curve section at the top of the central box girder (made of cast iron), the RSJ, the deck plate, the base plate, and the walkway loads have all been manually computed and implemented. Additional 12% load was considered for mechanical fasteners and stiffeners as per code NR/GN/CIV/025 Cl. To verify the application of loads, reactions were checked against simple manual calculation.

Wind load was calculated as per NR/GN/CIV/025 cl 4.4.1 and applied as a pressure load to the truss lattice girder and central box girder using the patch load option in LUSAS.

The live loading has been applied following NR/GN/CIV/025 cl. 4.3.1.2 for 20 Units of RAI live loading. The loading was applied as a moving load projected onto the upside and downside track. The loading was optimized using the vehicle load optimization tool in LUSAS to create the worst case for bending moment and shear in both main girders and all other principal structural members. Dynamic factors have been applied to the live load following NR/GN/CIV/025 cl. 4.3.2. The short-length vehicle has been used for the assessment of cross girders and rail bearers.

FIGURE 12

20 Units of Type RAI Loading

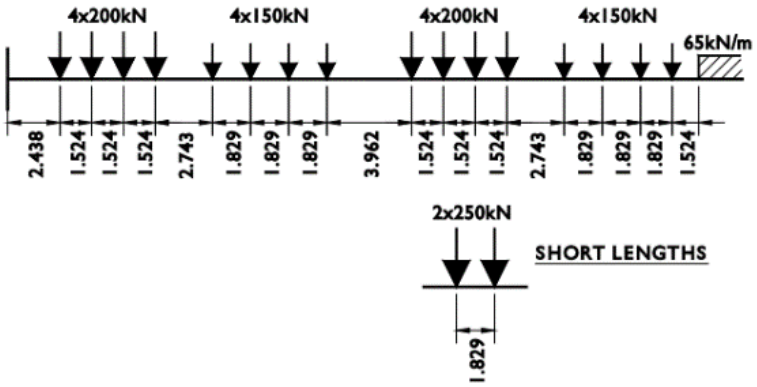

FIGURE 13

Isometric view of the Lusas model

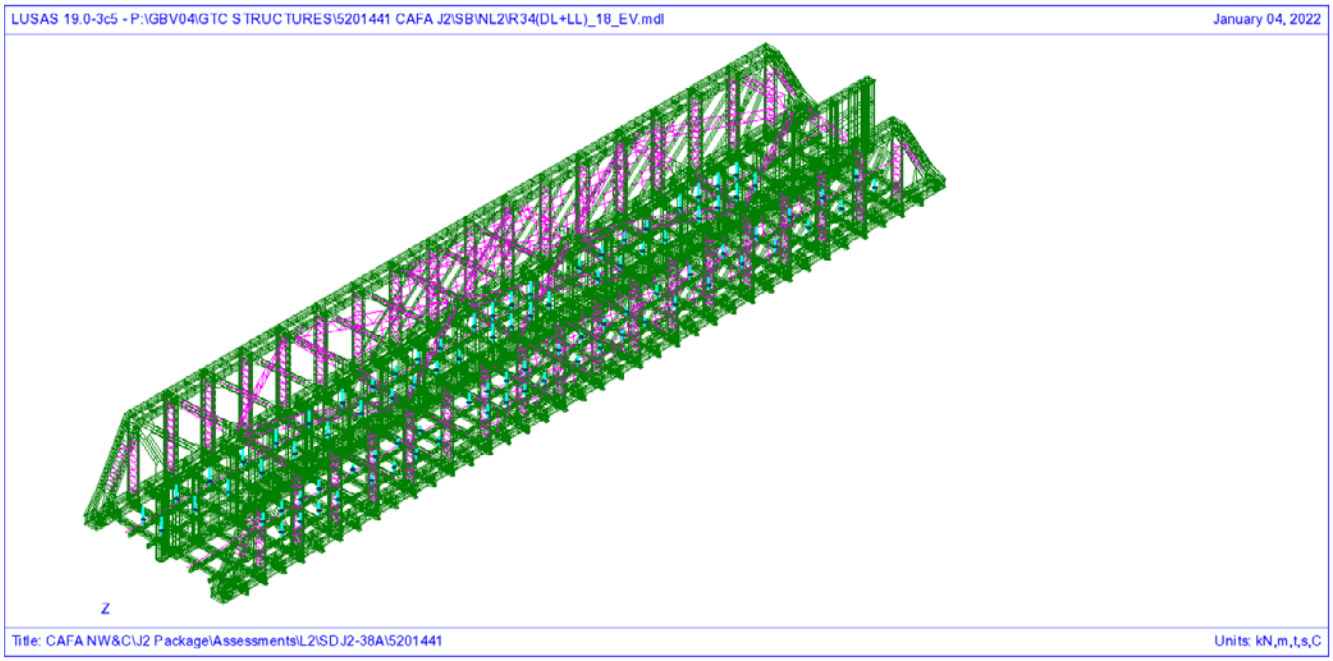

In the non-linear analysis LUSAS breaks the live loading down into a series of increments. These load increments were set to 0.1, with each increment representing a single change in RA number. The load case itself has been multiplied with dynamic factor for main girders. The results associated with the increments are the basis for determining element capacities based on stress or deflection criteria.

FIGURE 14

Rail Load Increment

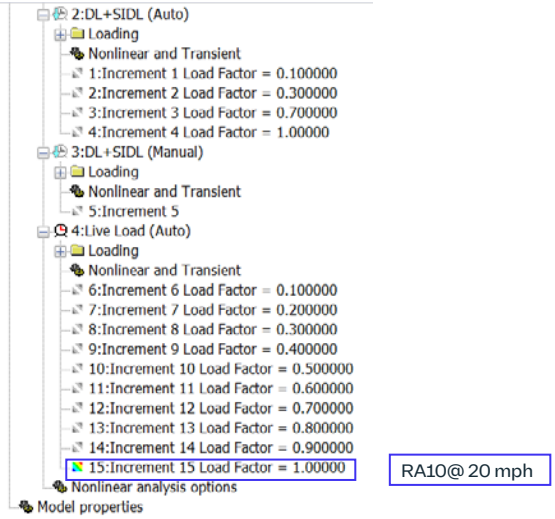

3. Results

3.1 LINEAR ANALYSIS – STATIC ANALYSIS

To investigate if any structural elements are theoretically susceptible to local and global buckling failure, thus highlighting potential problem areas for further analyses using the non-linear model.

3.2 LINEAR ANALYSIS – ELASTIC BUCKLING

An elastic premature buckling analysis was undertaken to investigate if the superstructure was theoretically susceptible to global buckling failure or local buckling failure. Elastic linear buckling analyses were undertaken as a useful starting point but however do not consider p-Δ effects.

From LUSAS: "A linear analysis which may be applied to relatively 'stiff' structures to estimate the maximum load that can be supported prior to structural instability or collapse."

Note: Eigenvalue = "one of the values of a certain parameter for which a differential or matrix equation has an eigenfunction. "In this case, the 'eigenfunction' is the 'linear buckling of the structure' hence the 'eigenvalue' is essentially a mathematical term used in LUSAS to identify the linear buckling modes of a structure. A model was created to check for linear buckling using load factors for ULS with dead load, superimposed dead load, and factored vertical live load applied.

The elastic analysis for this structure has been undertaken with the live loading optimized to produce maximum bending and shear effects in the structure under RAI Loading at ULS. 5 No.

Eigenvalues have been generated, representing the 5 No. buckling modes within the structure with the lowest factors of safety. It should be noted that in this assessment, the linear buckling analysis is only of limited applicability. This is because when using linear models there was no opportunity to separate the setup conditions for the application of live loading and permanent loading. Nevertheless, a linear buckling analysis has been undertaken to see which buckling modes are identified.

The figure highlighted below in Figure 15, represents the minimum load factors required to initiate the onset of buckling under the various modes. A minimum load factor of 0.44 x (ULS DL + SIDL + Rail LL of RA10), would need to be applied in order to cause theoretical buckling of the web of the central box girder (as shown in Figure 17). There were several iterations to find out the global buckling mode, but the global buckling mode was not achieved even with 75 mode shapes hence local buckling mode was identified to start the non-linear analysis.

FIGURE 15

Eigen Value/Load factors from Eigenvalue analysis

	Mode▲	Eigenvalue	Load Factor	Error norm
1	1	0.441903	0.441903	36.0073E-9
2	2	0.461848	0.461848	1.03465E-6
3	3	0.507363	0.507363	3.15178E-12
4	4	0.524496	0.524496	3.90047E-12
5	5	0.582945	0.582945	9.43744E-12

FIGURE 16

Eigen Value mode 1 – Local Buckling in the central Box Girder – MGI web plates

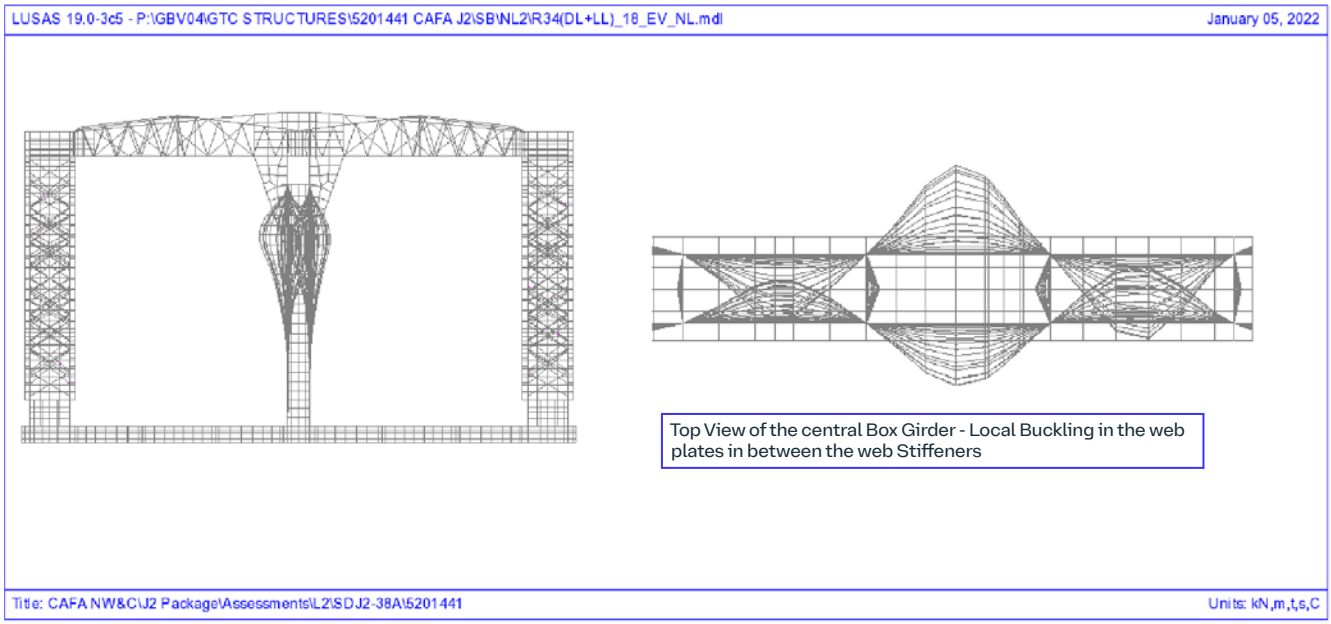

Following completion of the models, the structure was analyzed non-linearly as follows:

Non-linear Buckling Analysis – The non-linear buckling analysis provides an assessment of the buckling resistance of the main girders, considering $p\text{-}\Delta$ effects (geometric non-linearity), material plasticity (material non-linearity), and the overall interaction between the primary structural elements.

Non-linear Stress and Plastic Yield Analysis – Resultant stress contours (SE) over the shell elements were used to identify areas of theoretical over stress and yield within the structure.

A non-linear buckling analysis has been undertaken to investigate the buckling behavior of various elements of the structure. The position of the live loading (RA10 at 20 mph) has been optimized to produce maximum effects in model.

The following elements of the structure have been analysed for buckling behavior under the applicable applied live loading:

- Lattice Girder – MGE
- Central Box Girder – MGI
- Transverse Girders – XGE/XGI
- Channel section at bottom of Central Box Girder

Note: MGE (External Main Girder), MGI (Internal Main Girder), XGE/XGI (External/Internal Cross Girder), Bridge Condition Marking Index (BCMI) Annotation as per Network Rail Standard.

The non-linear buckling analysis provides an assessment of the buckling resistance of these members considering the benefit of the increased structural restraint provided by the overall interaction of the superstructure elements. Note that the results shown correspond to the load cases which were found to produce the most onerous load effects in each of the structural elements investigated.

The load-displacement relationship for each element checked is shown in the graphs. A tendency towards buckling behavior is indicated by a "flattening" of the gradient of the load deflection graph as the rate of movement increases with each applied load increment.

3.2.1 Central Box Girder

Figure 17 shows the lateral deformation contours (global lateral displacement, DY) of Central Box Girder – Downside Web under DL, SIDL and RA live loading, optimized to produce maximum midspan bending and shear effects at ULS. The selected load factor was 1.0, equivalent to RA10 Loading. The maximum lateral deflection was 14.54 mm.

Figure 18 shows the load-transverse displacement (global lateral, DY) relationship. No buckling behavior was observed under the applied loading. The web of the Central Box Girder (Downside) was therefore assessed as adequate for Permanent load + RA10 Live load at 20 mph at ULS with regards to buckling.

FIGURE 17

Central Box Girder
(DK1 MGI 1) – Displacement
DY (Downside web)

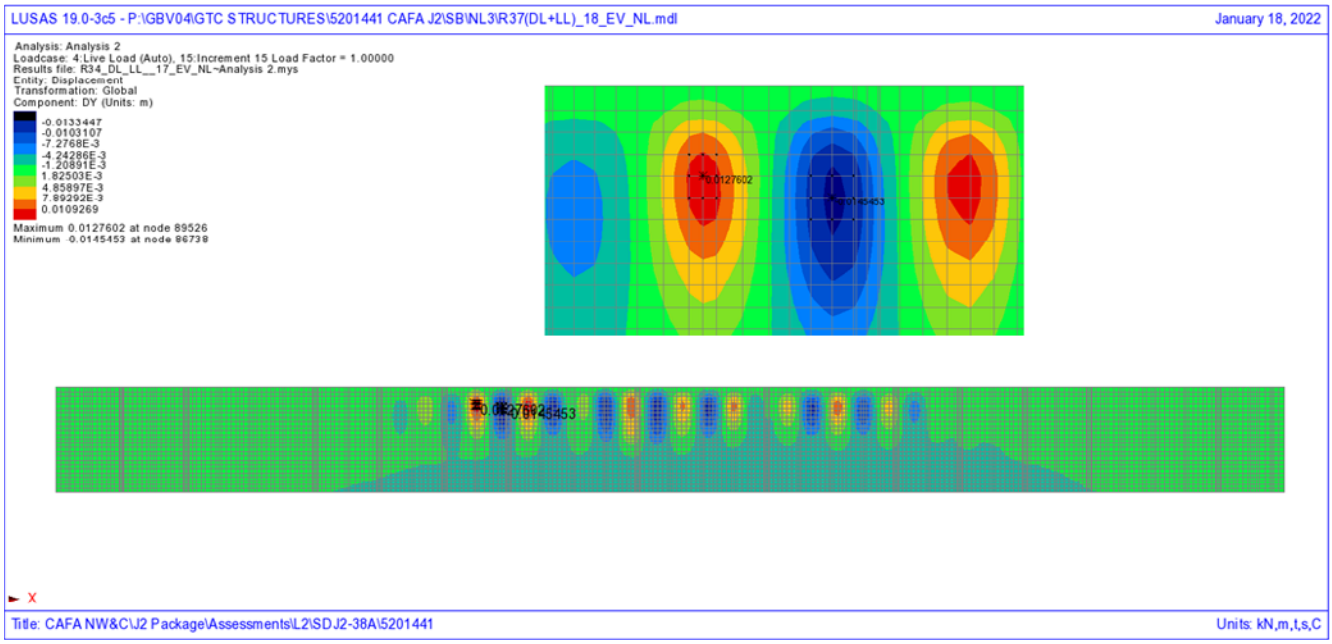

FIGURE 18

Load Factor vs displacement DY (Downside web)

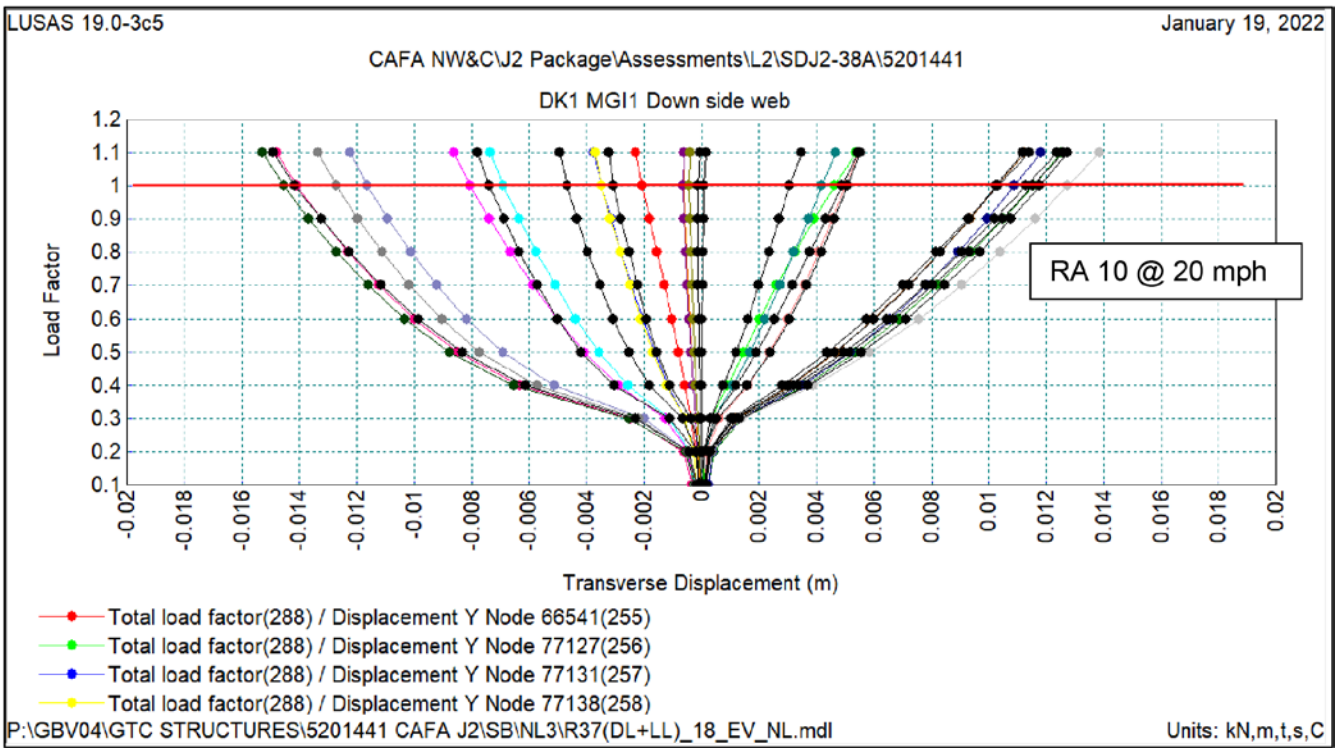

3.2.2 Lattice Girder 1 – MGE1

Figure 19 shows the lateral deformation contours (global lateral displacement, DY) of Lattice Girder 1 – Downside under DL, SIDL and RA live loading, optimized to produce maximum midspan bending and shear effects at ULS. The selected load factor was 1.0, equivalent to RA10 Loading. The maximum lateral deflection was 3.70 mm.

Figure 20 shows the load-transverse displacement (global lateral, DY) relationship. No buckling behavior was observed under the applied loading. The Lattice Girder (Downside) was therefore assessed as adequate for Permanent load + RA10 Live load at 20 mph at ULS with regards to buckling.

FIGURE 19

Lattice Girder
(MGE 1) Displacement
DY – Downside

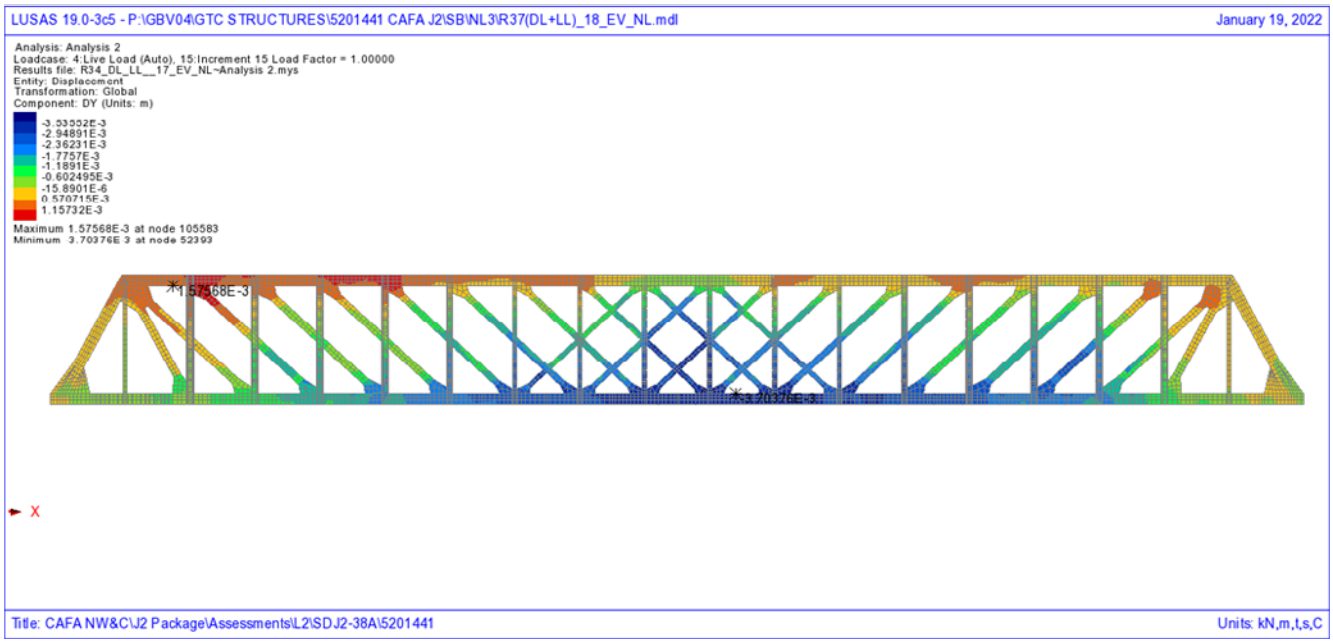

FIGURE 20

Load Factor vs
DY displacement
(Lattice Girder – Downside)

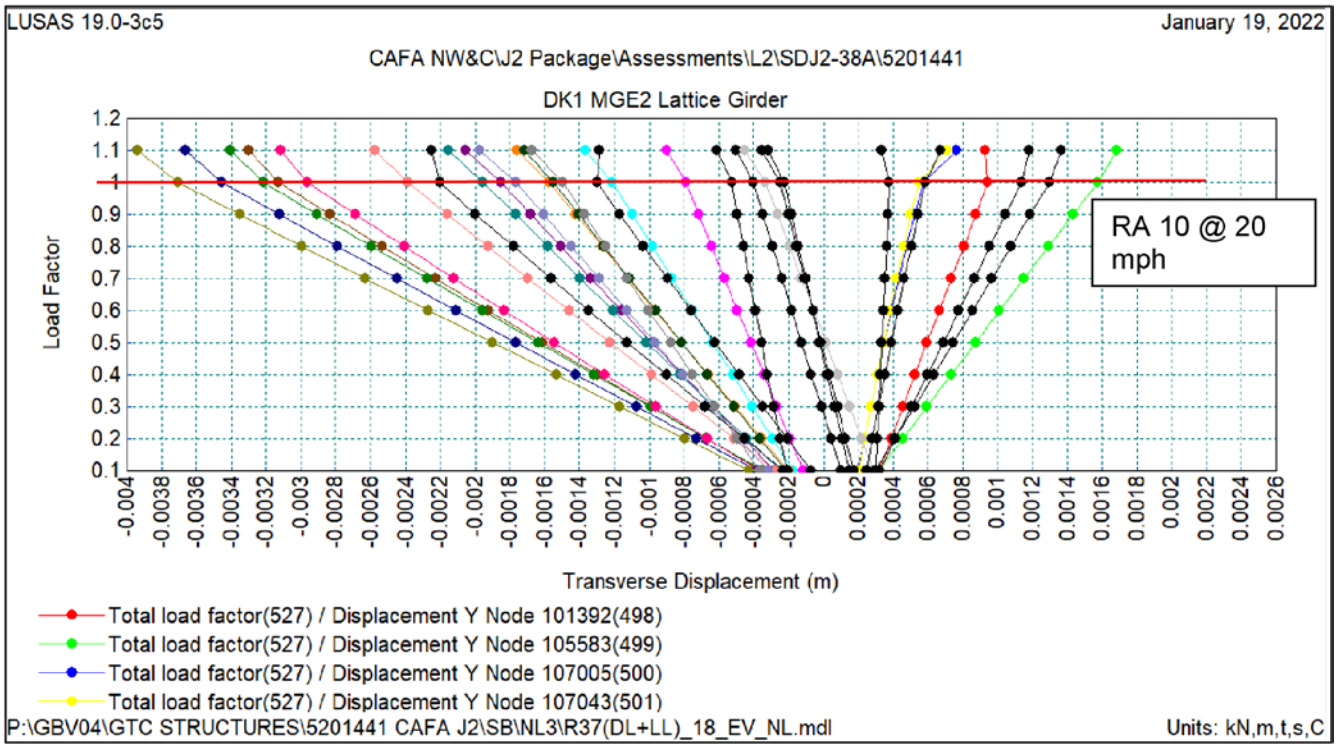

3.3 NON-LINEAR ANALYSIS – EQUIVALENT STRESS AND PLASTIC YIELD AT ULS

For the assessment of yield and stress levels within the structure, the following criterion had been adopted for the classification of failed elements:

At ULS, the limiting capacity was generally identified by extensive yield across a significant proportion of a section or the onset of non-linear geometric behavior to the main structural elements (i.e., Buckling), with strains being within the plasticity range of the material (i.e., no material rupture).

As with the non-linear buckling analysis, the position of the live loading has been optimized to produce maximum effects in the relevant element for each check, as required.

3.3.1 Lattice Girder 1 – DK1 MGE1

The ULS equivalent stress distribution and areas of material yield in the Lattice Girder 1, respectively, under the effects of permanent + RAI live loading. It was evident that areas of material yield (yield denoted by black asterisks) are summarized below.

Figures 21 and 22 indicate localized yield to connection point of the verticals and the diagonals as well as gusset points, but those were due to the modelling constraints as the plates were overlapping at those areas and not getting connected (see Figures 21 and 22). Under a Load factor of 1.0, corresponding to RA10 at 20mph loading. This was deemed to be too localized/ not significant enough to limit capacity. Therefore, Lattice Girder 1 – DK1 MGE1 was adequate for Permanent load + RA10 Live load at 20 mph at ULS.

FIGURE 21

ULS stress distribution and predicted yield under RA10 loading in Lattice Girder - DK1 MGE1 (verticals, diagonals, and gusset plates) HM Side

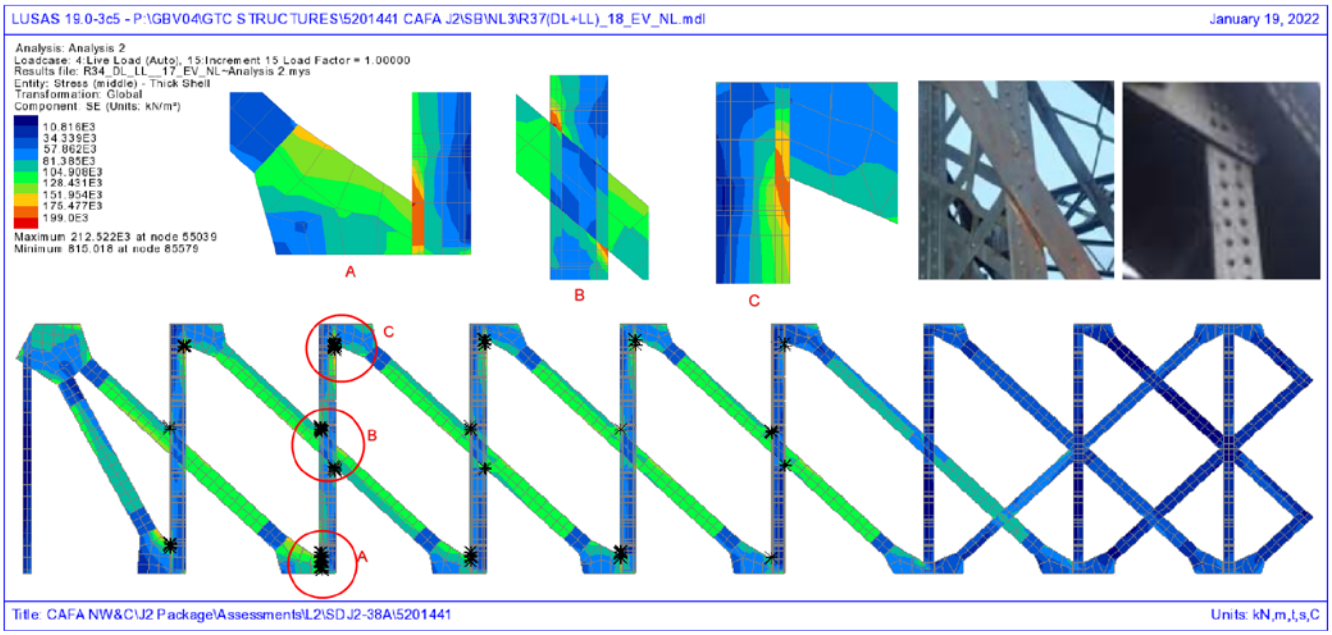

FIGURE 22

ULS stress distribution and predicted yield under RA10 loading in Lattice Girder - DK1 MGE1 (verticals, diagonals, and gusset plates) LM Side

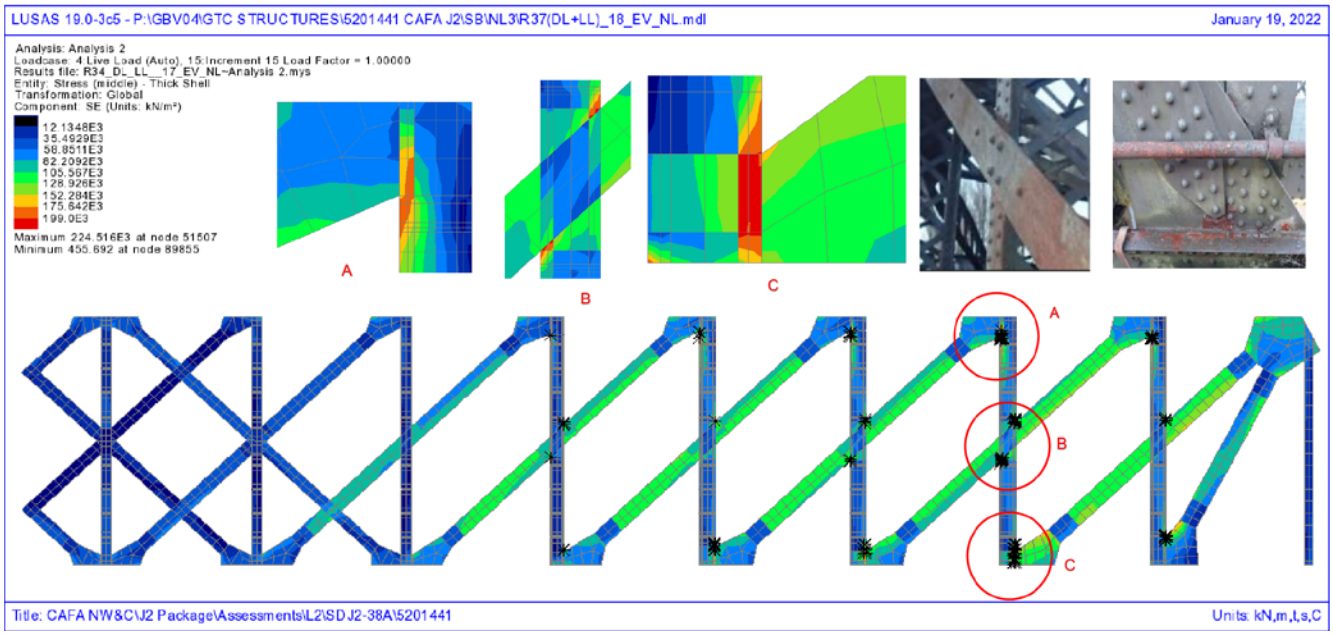

FIGURE 23

Summery Table

Elements	BCMI	Failure Mode	Level 2 Assessment (ULS)	Level 2 Assessment (SLS)
Main Lattice Girder (Down side)	DK1 MGE1	Yield	RA10	RA10
		Buckling	RA10	RA10
Main Lattice Girder (Up side)	DK1 MGE2	Yield	RA10	RA10
		Buckling	RA10	RA10
Central Box Girder	DK1 MGI1	Yield	RA10	RA10
		Buckling	RA10	RA10
Internal Transverse Girder	DK1 XGE	Yield	RA10	RA10
		Buckling	RA10	RA10
External Transverse Girders	DK1 XGI	Yield	RA10	RA10
		Buckling	RA10	RA10
Rail Bearers	DK1 LSI	Yield	RA10	RA10
		Buckling	RA10	RA10

The Level 2 Assessment subsequently found the structure to be able to accommodate the current Route Availability of RA8 at the current line speed of 20 mph at ULS in accordance with NR/GN/CIV/025. Based on observations made during IFA (December 2020), abutments and wing walls have been assessed qualitatively in accordance with NR/GN/CIV/025. The abutments and wing walls were in generally fair condition and are thus considered to be adequate for current levels of loading.

4. Comparison Between Linear and Non-Linear Analysis

During the initial stage of the assessment programme, a linear static analysis was performed to study the stress distribution throughout the model. It was observed that there were sudden increases in stress values near the joints and connection points. To normalize the stress values, a non-linear analysis was performed. It produced significantly better results than the static analysis, particularly near the joints and connection points. A brief comparison of linear and non-linear analysis briefed in Figures 24 and 25, and Table 1.

FIGURE 24

Static Analysis - ULS stress distribution under RA10 loading in Lattice Girder - DK1 MGE1 (verticals, diagonals, and gusset plates) HM Side

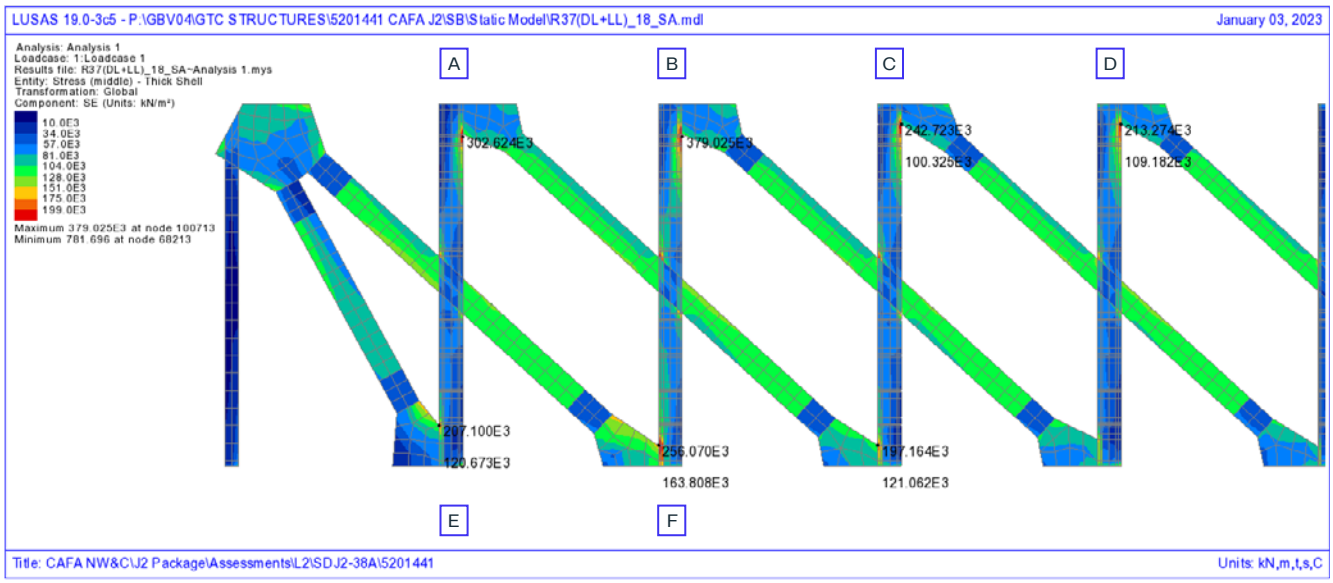

FIGURE 25

Non-linear Analysis - ULS stress distribution under RA10 loading in Lattice Girder - DK1 MGE1 (verticals, diagonals, and gusset plates) HM Side

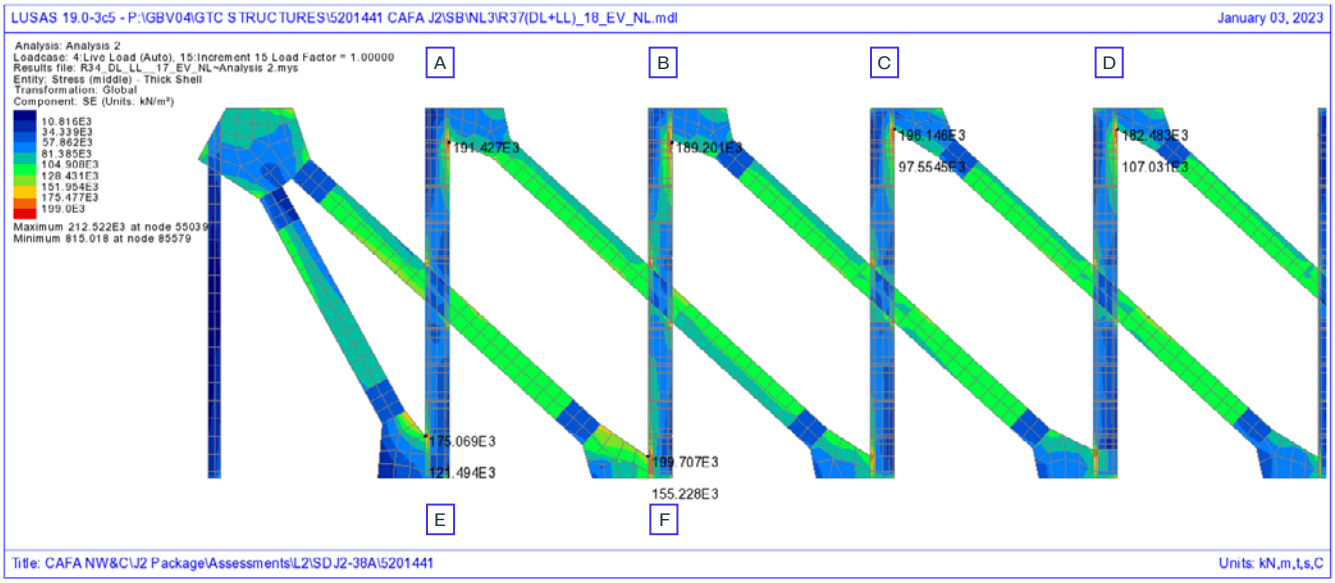

TABLE 1

Result variation between linear and non-linear analysis in percentage

Gusset Plate connection Point	Static Analysis (Stresses) N/mm²	Non-Linear Analysis (Stresses) N/mm²	Percentage variation
A	303.62	191.42	37%
B	379.02	189.20	50%
C	242.72	196.14	19%
D	213.27	182.48	14%
E	207.10	175.06	15%
F	256.07	199.70	22%

5. Conclusions

5.1 RECOMMENDATIONS FOR FURTHER ASSESSMENT

In terms of further assessment, no further analysis was required for the structure as the structure has been found to be safe for the published route availability (RA8) at the maximum permissible speed of 20 mph. The current Level 2 Assessment has adopted a high level of detail, being representative of the full superstructure. As such, the Level 2 Assessment, using LUSAS Finite Element Analysis, has utilized all the available theoretical assessment capacity within the structure.

5.2 RECOMMENDATIONS FOR MONITORING

Due to aggressive corrosion at the connection point between the central box girder base plate and channel section attached to it and in the diagonals of the lattice girder, consideration may be given to monitoring of these areas until any temporary or long-term mitigation measures are developed and implemented. The development and implementation in a targeted monitoring regime was therefore recommended. Furthermore, due to defects on the substructure, consideration should be given to monitoring of these areas until any temporary or long-term mitigation measures are developed and implemented. Several fractures, open joints and water staining leachate areas were noted during the inspection for assessment. The development and implementation of a targeted monitoring regime was therefore recommended.

5.3 RECOMMENDATIONS FOR STRENGTHENING

Consideration should be given to strengthening with additional over-plating and/or the addition of other localized retrofitting measures on the diagonal bracings present in between the diagonals in both lattice girders and diaphragm top flange which connects both the channels in the bottom chord lattice girders.

5.4 RECOMMENDATIONS FOR MAINTENANCE/REPAIRS

The Inspection for Assessment carried out by ATKINS (now AtkinsRéalis) found the bridge to be in generally fair condition with localized areas of corrosion throughout on various superstructure elements. The following maintenance measures are therefore recommended with respect to the findings of the Inspection for Assessment as part of a programme of preventative maintenance to ensure the ongoing serviceability and longevity of the structure.

Consideration should be given to the replacement of any of the defective rivets in the girders with HSFG fasteners or similar approved. Due to high section loss and missing nuts at several locations, high priority should be given to replacement of the bolts between the central box girder base plate and the channel section attached to it.

Local over-plating to arrest further deterioration in areas of heavy corrosion (Bracing in between the diagonals in both lattice girder – DK1 – MGE1 and MGE2), notching and any apertures in the structure. To be connected with HSFG fasteners or approved similar.

Acknowledgements

The authors would like to acknowledge Network Rail (NR) for their support and permission to publish this paper.

The author would like to extend appreciation to Harpreet Singh (Contractor's responsible engineer for SDJ2_38A), Jon Wang (Lead accessor for SDJ2_38A), Tiju Zachariah, and Abani Kumar Satapathy for their valuable input and fruitful technical discussions.

Originally presented and published as: "Assessment of River Mersey Steel Truss Bridge Using Non-Linear Finite Element Analysis". IABSE Symposium Istanbul 2023: Long Span Bridges, April 26-28, 2023, Istanbul, Turkey. Available at: https://www.iabse.org/Sys/Store/Products/339186

References

NR/L2/CIV/035 Issue 2 June 2019 – Management of structures.

NR/L2/CIV/035/MOD01 Issue 2 June 2019 – Management of Structural Assessment.

NR/L2/CIV/035/MOD02 Issue 1 December 2017 – Carry out Structural Assessment.

NR/GN/CIV/025 Issue 3 June 2006 – The structural assessment of Underline bridges.

NR/L3/CIV/023 Issue 1 March 2018 – Assessment of Footbridge.

LUSAS Finite Element Analysis (2021), LUSAS, Kingston upon Thames, UK.

AtkinsRéalis

Contact Information
Dorothy Gartner
Sr Librarian
Office of the COO, Group Quality
& Knowledge Management
dorothy.gartner@atkinsrealis.com

atkinsrealis.com